

NASA CONTRACTOR REPORT

NASA CR-1037



NASA CR-1037

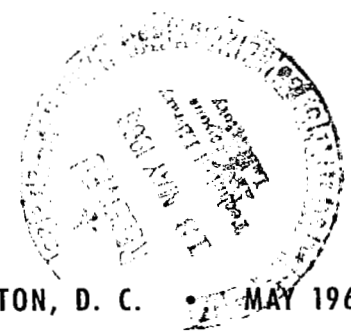


LOAN COPY: RETURN TO
AFWL (WLIL-2)
KIRTLAND AFB, N MEX

STUDY OF RADIATION HAZARDS TO MAN ON EXTENDED MISSIONS

by S. B. Curtis and M. C. Wilkinson

Prepared by
THE BOEING COMPANY
Seattle, Wash.
for





STUDY OF RADIATION HAZARDS TO MAN ON EXTENDED MISSIONS

By S. B. Curtis* and M. C. Wilkinson

Distribution of this report is provided in the interest of information exchange. Responsibility for the contents resides in the author or organization that prepared it.

* Consultant, Lawrence Radiation Laboratory

Prepared under Contract No. NASw-1362 by
THE BOEING COMPANY
Seattle, Wash.

for

NATIONAL AERONAUTICS AND SPACE ADMINISTRATION



ABSTRACT

This study attempts to identify the particle types and energies which are important in the evaluation of the radiation hazard on long manned missions outside the magnetosphere. Important areas where information is presently lacking are identified. Spectra of the various components of the galactic cosmic radiation have been compiled from experimental data gathered during the period of minimum solar activity. These spectra, as well as typical solar particle spectra, have been used to determine depth-dose curves and differential particle and dose spectra behind typical shielding thicknesses. From this analysis, the important energies for various thicknesses and various spectra have been determined. In general, low energy particles (below 100 MeV) appear to be the most important at the dose point in solar particle events. From the biological standpoint, very low energy particles are important only for very steep spectra. The high energy heavy component of the galactic cosmic rays is of considerable importance for thin shielding and it appears that low energy heavy particles may continue to be important at thicker shielding, although secondary production data are not available for a thorough analysis.



FOREWORD

This report is submitted to the National Aeronautics and Space Administration, Headquarters Branch, Washington, D. C., in accordance with the requirements set forth in NASA contract NASw-1362. The work herein reported was performed by M. C. Wilkinson of the Space Physics Group, Space Division, The Boeing Company, and by Dr. Stanley B. Curtis of the Lawrence Radiation Laboratory, consultant to The Boeing Company. This work was done under the supervision of J. A. Barton and Dr. R. V. Hanks.

CONTENTS

	<u>Page</u>
Introduction	1
The Natural Radiation Environment	2
Galactic Cosmic Rays	2
Time Variations of the GCR	3
Heliocentric Intensity Gradients of the GCR at Solar Minimum	5
Solar Particle Events	6
General Considerations	6
Solar Cosmic Rays	8
Energetic Storm Particles	9
Recurrent Energetic Storm Particles	9
Summary of Solar Particle Activity	10
Energy Deposition Studies	11
General Considerations	11
Galactic Cosmic Rays	13
Dose from Galactic Protons	14
Dose from Heavy Ions	15
Solar Cosmic-Ray Dose Calculations	16
Depth-Dose Characteristics	16
Importance of Various Particle Energies	17
Importance of Various Proton Energies in Producing Secondary Doses	19
Conclusions	20
Energetic Storm Particle Doses	22
Biological Considerations	22
Biologically Weighted LET Spectra	25
Conclusions	27
Acknowledgements	32
References	33



LIST OF FIGURES

1. Differential Energy Spectrum of Galactic Protons
2. Differential Energy Spectrum of Galactic He Nuclei
3. Differential Energy Spectrum of Galactic L-Nuclei
4. Differential Energy Spectrum of Galactic M-Nuclei
5. Differential Energy Spectrum of Galactic LH-Nuclei
6. Differential Energy Spectrum of Galactic VH-Nuclei
7. Differential Spectra of Protons at Different Times in the Solar Cycle
8. Differential Spectra of Helium Nuclei at Different Times in the Solar Cycle
9. Comparison of Boeing Secondary Code and Oak Ridge NTC Protons with Incident Exponential Rigidity Spectrum Having Characteristic Rigidity 100 MV.
10. Galactic Cosmic-Ray Protons in Aluminum - Depth Dose Curves
11. Heavy Particle Galactic Depth Dose Curves
12. 40 MV Proton Spectrum - Depth Dose
13. 100 MV Proton Spectrum - Depth Dose
14. 160 MV Proton Spectrum - Depth Dose
15. Depth-Dose Plots for 40, 100, and 160 MV Rigidity Incident Alpha Spectrum
16. Differential Dose Distributions for 100 MV Rigidity Spectra Protons Incident on Aluminum
17. Differential Dose Distributions for 40 and 160 MV Rigidity Spectra Protons Incident on Aluminum
18. Differential Dose Distributions for Galactic Cosmic-Ray Protons
19. Dose Per Unit Logarithmic Interval for Helium, Nitrogen (M), Magnesium (LH) and Cobalt (VH)
20. Penetrating Proton Number - Energy Spectrum in Various Depths of Aluminum - 40 MV Spectrum Incident
21. Penetrating Proton Number - Energy Spectrum in Various Depths of Aluminum - 160 MV Spectrum Incident
22. Penetrating Proton Number - LET Spectrum - 40 MV Spectrum Incident
23. Penetrating Proton Number - LET Spectrum - 160 MV Spectrum Incident
24. Number - LET Spectrum - 100 MV Alpha Spectrum
25. Number - LET Spectrum - 160 MV Alpha Spectrum

26. Primary Dose - 1 gm/cm^2 AL
27. Primary Dose - 5 gm/cm^2 AL
28. Primary Dose - 10 gm/cm^2 AL
29. Secondary Proton Dose - 1 gm/cm^2 AL
30. Secondary Proton Dose - 5 gm/cm^2 AL
31. Secondary Proton Dose - 10 gm/cm^2 AL
32. Secondary Proton Dose - 20 gm/cm^2 AL
33. Neutron Dose - 1 gm/cm^2 AL
34. Neutron Dose - 5 gm/cm^2 AL
35. Neutron Dose - 10 gm/cm^2 AL
36. Neutron Dose - 20 gm/cm^2 AL
37. Neutron Dose - 30 gm/cm^2 AL
38. Neutron Dose - 50 gm/cm^2 AL
39. Differential Secondary Proton Dose Per Unit Incident Proton Energy
40. Differential Neutron Dose Per Unit Incident Proton Energy
41. Depth-Dose Profiles for 10, 20, and 30 Mv Rigidity Events
42. Penetrating Proton Number - LET Spectrum 20 Mv Spectrum Incident
43. LET Spectrum for Galactic Cosmic-Rays Under 0.2 g/cm^2 Water Shielding
44. Lower Limits for the Number of Thin-Down Hits Per cm^3 -day Neglecting Secondaries
45. Solar Particle Event LET Spectrum for Penetrating Protons $P_0=20\text{Mv}$ for Various Thicknesses of Aluminum
46. Solar Particle Event LET Spectrum for Penetrating Protons $P_0=160\text{MV}$ for Various Thicknesses of Aluminum
47. Solar Particle Events LET Spectrum for Penetrating He Ions $P_0=160\text{Mv}$ for Two Thicknesses of Aluminum
48. Solar Particle Event LET Spectrum for Penetrating He Ions $P_0=100\text{Mv}$ for Two Thicknesses of Aluminum

LIST OF TABLES

1. Radial Intensity Gradients From Mariner II Data
2. Characteristics of Different Types and Classes of Solar-Particle Events
3. Free Space Dose Rates From the Various Components of the Galactic Cosmic Rays at Solar Minimum

INTRODUCTION

As the goals of manned space missions expand beyond the Apollo lunar landing, the astronaut will find himself on extended earth-orbital trips, extended visits to the moon, and eventually on missions to Mars and Venus, lasting on the order of a year or longer. The problem of radiation and its effects on performance and health will grow in importance as the total dose and the probability for encountering large solar particle fluxes increase. The purpose of this study is first to summarize our knowledge to date (early 1967) on the natural radiation environment beyond our magnetosphere. Secondly, the radiation spectra will be used to calculate the spectra of various components of the radiation dose behind a variety of shielding thicknesses. Thirdly, we will attempt to evaluate, with the available knowledge of biological effects, the relative importance of the energies and types of particles found in space. It is hoped that this evaluation and the specification of the limitations in our knowledge will be helpful in directing future experimental efforts so that the necessary information for a more accurate evaluation will eventually become available.

THE NATURAL RADIATION ENVIRONMENT

It is convenient to divide the radiation environment outside the magnetosphere into two parts: that arising from the galactic cosmic rays (GCR) and that arising from the solar emissions, the solar cosmic rays (SCR) and energetic storm particles (ESP). The GCR originate outside our solar system and are characterized by rather low, fairly steady isotropic fluxes which vary over the eleven-year solar cycle by about a factor of three or four and reach maximum during or soon after the period of minimum solar activity. The solar activity cycle modulates the lower energy portion of the GCR spectra. The SCR occur in association with solar flares, and such fluxes can be many orders of magnitude higher than the GCR fluxes during the occurrence of a giant solar particle event. Typically, such events last two or three days, with the flux rising to a maximum within 24 hours and then decaying more slowly through the rest of the event. The ESP arrive in the vicinity of the earth about 24 hours after the onset of the solar flare. These low energy particles are of concern only for EVA activity, or very thinly shielded spacecraft. A thorough discussion of the physical characteristics of solar particle events has appeared in the literature (1,2), and only a synopsis of these results will be presented here.

GALACTIC COSMIC RAYS

Recent well-instrumented experiments on satellites are yielding good data on the identity and energy spectra of the various components of the GCR. Spectra have been measured of particles with atomic numbers (i.e., charges) up through $z=28$. There is a definite preponderance of particles with even z over those with odd z . It is convenient to divide the heavier ions into groups

with similar charge. Our designation will be:

L-particles: $3 \leq z \leq 5$

LH-particles: $10 \leq z \leq 14$

M-particles: $6 \leq z \leq 9$

MH-particles: $15 \leq z \leq 25$

VH-particles: $26 \leq z \leq 28$

A compilation of GCR data obtained during the most recent period of the quiet sun (1964-1965) is given in Figures 1-6 for protons, He ions, and the particle groups listed above (3-9). One group, the MH-particles, has been omitted because good data on the spectral shape are not presently available. It is known, however, that the flux of these particles is low compared with that of the LH- and VH-particles, and their exclusion will not affect the conclusions to be discussed below.

Time Variation of the GCR

Solar activity and the resultant solar wind emission and disturbances in the solar magnetic field configuration cause a decrease in the GCR fluxes during the height of the activity cycle. The decrease occurs only in the lower energy portions of the GCR spectra. Recent comparisons of data obtained near the minimum of the solar cycle (6, 10) lead to the conclusion that for particles with energies greater than 100 MeV/nucleon, the modulation mechanism has a rigidity dependence $\exp(-K/P\beta)$ where K is constant for any given time and P is the rigidity and β the velocity relative to the velocity of light. This means that the spectrum near the orbit of the Earth can be written

$$\frac{dJ}{dT} = \frac{dJ}{dT} \Big|_{\infty} \exp(-\eta(t)/P\beta) \text{ for } T > 100 \text{ MeV/nucleon}^*$$

*Note added: The restriction to higher energies for this analytic form has been suggested by very recent work (G. Gloeckler and J. R. Jokipii, Astro. J. 148, L41 (1967)).

where $\left. \frac{dJ}{dT} \right|_{\infty}$ is the spectrum outside the influence of the solar magnetic field and $\eta(t)$ depends on time but not on particle rigidity or velocity. It appears that during solar minimum, the low energy portion of the spectrum varies considerably over a few months' time. Such variations will cause variations in the free space (no shielding) GCR dose, and thus the accuracy of free space dose calculations is limited by our lack of knowledge of the very low energy portion of the spectra.

There have appeared in the literature studies of the correlation of spectral shape with ground level neutron monitor readings. The correlation is good enough so that the shape of the GCR spectra in the rigidity region around 1 GV can be roughly inferred from a knowledge of ground-level neutron fluxes. Thus a rough idea of the shape of the GCR spectrum can be obtained at any time during the solar cycle if the ground-level neutron rate is known. Results of two studies (11, 12) are shown in Figures 7 and 8. In the two studies, different values of the Mt. Washington neutron monitor counting rate were used as the baseline value. To find the shape of the proton or He ion spectrum for any time during the solar cycle (i.e., for any neutron counting rate), the percentage difference between the neutron rate at the time of interest and the baseline value (labelled N in the graphs) is calculated. Then the desired curve is found by interpolation on the appropriate graph. This is admittedly a crude estimate and gives no information on the critical low energy portion. Other more accurate descriptions of the variation of the spectral shapes with time will undoubtedly be available soon as more is learned about the modulation mechanism and its time dependence.

Heliocentric Intensity Gradients of the GCR at Solar Minimum

The dependence of the GCR flux on distance from the sun is of interest for missions to Mars and Venus. Recent data from Mariner IV (10) indicate that the radial dependence is measurable between the Earth and Mars. The gradient appears to be linear and is given in Table I for protons and He ions of various energies as measured on Mariner IV between 1.0 and 1.6 a.u. (astronomical units). The overall proton flux is about 6% higher at Mars (1.56 a.u.) than at the Earth during solar minimum. Also, the He ion flux between 100 and 300 MeV/nucleon is increased 36% and between 300 and 420 MeV/nucleon is increased 31%. The proton flux between 1 and 15 MeV rises by less than a factor of three.

TABLE I (From Ref. 10)

Particle	Kinetic Energy (MeV/nucleon)	Radial Intensity Gradient (per cent/a.u.)
Protons	Mean energy ~ 6000	+ 9.6 ± 0.9
Protons	1-15	< + 500
He Ions	100-300	+ 65 ± 8
He Ions	300-420	+ 55 ± 5

SOLAR PARTICLE EVENTS

General Considerations

Although the characteristics of the galactic cosmic radiation have been recognized and investigated for many years, only in the past ten years have the particulate emissions of the sun been studied in detail. The recognition that these emissions, or solar particle events, occurred more frequently than previously supposed focused attention on the radiation hazard they might pose to manned space travel.

The aspects of solar particle events which are of greatest importance in determining their potential radiation hazard are:

- 1) Particle type (or charge composition) of the ejected particles.
- 2) The time dependent intensity and energy spectra of the emitted particles.
- 3) The angular distribution of the particles at the spatial regions of interest.
- 4) The predictability of the particle events.

Conclusions From Solar Cycle 19 Data

It was soon recognized that protons formed the bulk of the particulate emissions, although significant fractions of helium and heavy ions were occasionally present. The determination of the time dependent energy spectrum of the solar particle events proved a major problem, and not until the exponential rigidity spectrum representation was proposed by P. S. Freier and W. R. Webber (13) did one have available a reasonably accurate analytic representation of the solar particle energy spectrum which could be used over an energy range sufficiently large (30-100 MeV) to be useful for shielding studies.

The ground-based observational techniques available during solar cycle 19 indicated that the solar particles were nearly isotropic in angular distribution in the vicinity of the earth. Marked anisotropies were felt to be associated with the high-energy particles and with the effects of the earth's magnetic field. Predictability of the large solar particle events was unreliable.

Anticipated Results from Cycle 20

Due to advances in observational techniques, chiefly from satellites, we can expect a great deal of improvement in our information on the solar particle events. We can expect to obtain more accurate time dependent spectral and intensity measurements, extending over a wider energy range than were available in cycle 19. The angular dependences of the particle fluxes are being measured directly. The limited results available at this time (7,14) indicate that there are strong angular dependences in the proton fluxes, and that this anisotropy is important for low energy protons, that is for energies less than 80 MeV.

The major questions to be answered during solar cycle 20 are:

- 1) Is the exponential rigidity representation of the particle energy spectra adequate, or must it be modified?
- 2) How strong are the angular dependences of the proton events, and can this dependence be predicted in advance from a knowledge of the interplanetary magnetic field configuration?
- 3) What will be the intensity of solar proton activity during cycle 20, and how will the characteristics of the events observed in cycle 20 compare with cycle 19?

4) How well can the larger particle events be predicted?

These points all bear heavily on our ability to predict the radiation hazards to man on extended missions.

SOLAR COSMIC RAYS (SCR)

This class of particles is characterized by spectra in which an appreciable fraction of the particles have energies above 20 to 30 MeV. The time dependence of the SCR intensity can be expressed as a rapid quasi-exponential rise from onset. The characteristic onset time depends on the location of the source flare on the solar disk and on the condition of the interplanetary magnetic field. Typical onset times range from 2 times the rectilinear earth-sun travel time for west-limb flares to 10 times for east-limb flares.

After maximum intensity is reached, for any given energy, the particle flux decays slowly in an exponential-like fashion. The typical decay times may be greater than the onset times by factors of from 10 to 100. During this decay time, the spectrum typically steepens considerably; i.e., the percentage of high energy particles decreases. The incidence of these SCR events has been relatively infrequent in the recent sunspot minimum, but during the past several months, a number of larger SCR events have occurred. These recent events, corresponding to the increasing solar activity of cycle 20, were observed by a number of satellites and should provide more information on the SCR events. The available data on cycle 19 has been tabulated by Webber (1, 2).

ENERGETIC STORM PARTICLES (ESP)

Beginning about 1962, nearly continuous measurements of particle fluxes down to energies of about 1 MeV confirmed the presence of a large low-energy flux of particles associated with the solar particle events. This population of particles does not begin to arrive in appreciable numbers until about 24 hours after the onset of the solar cosmic rays. It is found that most SCR events are accompanied by energetic storm particles (ESP), although the correlation between the size of the SCR and its associated ESP is not understood.

The ESP particle population is characterized by a much steeper energy spectrum than the SCR. Best estimates for the ESP characteristics associated with cycle 19 are given in Reference 2.

RECURRENT ENERGETIC STORM PARTICLES

These particles constitute that phase of an SCR event which tends to recur with the 27-day solar rotation period. This series is started by a solar particle event and continues with a succession of ESP events. The duration of the individual events is 1 to 2 days with the intensity increasing and decreasing more or less symmetrically in time about the time of peak intensity. The particles causing the event are presumably contained in a rather highly ordered magnetic field "bottle" that sweeps through interplanetary space, anchored to the active region on the sun. These events have the typically steep spectra of the prompt ESP events but the intensity is down by a factor of from 1000 to 10,000 from the original ESP event.

SUMMARY OF SOLAR PARTICLE ACTIVITY

In summary, the integral spectrum of each class of solar particle event (i.e., SCR or ESP) is thought to be best described at the present time by an exponential form in rigidity: $J(P) = J_0 \exp(-P/P_0)$, where the steepness of the spectrum is determined by the characteristic rigidity, P_0 , and the total intensity of particles of a particular class is determined by J_0 . The behavior of P_0 and J_0 during the course of a typical solar particle event is shown in Figure 1 of Reference 2. Typical values of these parameters are shown in Table 2.

TABLE 2

CHARACTERISTICS OF DIFFERENT CLASSES OF SOLAR-PARTICLE EVENTS

<u>Class</u>	<u>P_0 (MV)</u>	<u>J_0 (cm⁻² sec⁻¹)</u>
Solar Cosmic	40-200	10^2 to 10^4
Energetic Storm Particles	5 to 20	10^5 to 10^7
Recurrent Events	5 to 20	10 to 10^3
Thermal Plasma	1 to 2	10^8 to 10^9

The thermal plasma, or solar wind, is included for completeness.

As will be shown in the shielding analysis, some SCR particles are of sufficient energy to penetrate any reasonable space-vehicle shielding, while the ESP events present a threat only to very thinly shielded vehicles, or during extra-vehicular activity.

ENERGY DEPOSITION STUDIES

GENERAL CONSIDERATIONS

When the incident particle types and energy spectra have been determined or specified in some manner, the next step in the radiation hazard evaluation process is to determine the energy deposition distribution in the body of the space traveler. The logical program to follow in making this calculation is first to determine the particle energy spectrum at each dose point of interest and then determine the energy deposited at the dose point. This straight-forward approach is complicated by several major difficulties, the most severe of which are the complexity of the complete angle and energy dependent transport equations, the multiplicity of particles resulting from the interactions of high-energy particles with nuclei, and the lack of accurate and complete nuclear production cross section data for the complete range of particle types and energy regions of interest.

In an effort to advance the dose calculational capability for the high energy protons encountered in space travel, the Neutron Physics Division of the Oak Ridge National Laboratory has engaged for several years in research efforts to provide the cross section data needed for such work. In addition, a series of Monte Carlo transport codes utilizing these data has been developed. These computer codes provide the most accurate theoretical calculations available of the dose distributions from incident protons. The Boeing Company has developed shielding codes for the determination of the radiation dose received by space travelers in the complex shielding configurations of actual space vehicles. In order to make these calculations of manageable length, it is necessary to simplify the calculations as much as possible. The Boeing codes which evaluate

the dose from incident protons and heavier charged particles have been described in detail (15), and a complete description of the theory and assumptions will not be presented here. The major assumptions made in the calculations, however, will be briefly summarized below.

In the proton secondary dose code:

- 1) The range-energy and stopping power data of Barkas and Berger (16) are used, augmented at low energies by the work of Northcliffe (17).
- 2) Range and path length of the particles are assumed the same, and multiple coulomb scattering and straggling are neglected.
- 3) Nuclear interaction data of Bertini and Dresner (18) are used.
- 4) The straight-ahead approximation is used throughout.
- 5) Only first-generation cascade and evaporation particles are treated.
- 6) The neutron transport is estimated by removal theory, and the dose from the high energy neutrons is calculated by the energy removal cross sections of W. Gibson (19).

In the heavy particle dose code, nuclear interactions are neglected. In these computer codes and throughout this report, the doses calculated are in tissue rads. The primary proton dose is defined as the ionization dose resulting from incident protons which have not been involved in nuclear interactions. It is assumed that the rate at which energy is being lost by the proton through ionization of the atoms in the tissue at a point is the sole contributor to the dose at that point. The secondary proton dose is defined in the same way as the primary proton dose, but nuclear interactions are not assumed to attenuate the secondary proton flux. The neutron dose is calculated by assuming that for high neutron energies, all the neutron energy involved in nuclear interaction is

deposited at the point of the interaction. At low energies, the first collision dose-conversion values of Snyder and Neufeld are used. The nuclear recoil dose is defined as the ionization dose resulting from the recoiling nuclei caused by the nuclear interactions of the incident proton flux. For the alpha and heavier particles, secondaries from nuclear interactions are neglected and only the primary ionization dose is calculated.

To check the various approximations used in these codes, a comparison was made between the Boeing code and the Oak Ridge Monte Carlo codes. The results are shown in Figure 9. It is felt that these results indicate a good agreement. Significant differences were noted in a previous comparison before the nuclear cross section data of Bertini were incorporated in the Boeing code (20).

GALACTIC COSMIC RAY DOSE CALCULATIONS

The characteristics of the galactic cosmic ray spectra cause several problems in determining their ionization dose. First of all, the galactic cosmic-ray energy spectra extend to at least 10^{20} electron volts, and the resulting nuclear and electromagnetic interactions are of sufficient complexity to occupy the attention of a sizeable portion of the physics community. As the nuclear cascade calculations available to us at the present time are restricted to the energy region between 25 and 400 MeV, no estimate is made of the secondary dose resulting from incident protons of greater than 400 MeV in our calculations. In addition, the nuclear cascades which result from the incident helium and heavier nuclei present in the galactic particles are not amenable to the same theoretical treatment as is used for incident protons. Consequently, no estimate is made in this report of their secondary dose contributions. In future work it is hoped

to extend our estimates of the secondary dose to higher energy protons as the Oak Ridge work in the energy region from 400 to 2000 MeV is made available.

DOSE RATE FROM GALACTIC PROTONS

Figure 10 shows the dose rate that results from the galactic cosmic-ray proton spectrum normally incident on a slab shield of aluminum. The primary proton dose is defined as the dose resulting from proton-electron collisions in a small volume of tissue. The further transport of energy by delta rays is neglected, and the electrons are assumed to deposit their energy locally. The dose presented is from protons of energies between 1 MeV and 10 GeV at the dose point. On the assumption that the actual galactic cosmic-ray proton spectrum can be extrapolated to higher energies by taking the differential energy spectrum, dJ/dT , to be proportional to $1/(T+m_p)^{5/2}$, it is found that protons above 10 GeV contribute approximately an additional 10% to the total primary ionization dose.

The secondary dose components shown are the secondary proton dose, the neutron dose, and the dose resulting from recoiling nuclei. These secondary dose components are calculated only for interacting primary protons with less than 400 MeV energy. The secondary dose components are shown by dotted lines to indicate that they include only part of the total secondary dose. An estimate is made of the nuclear recoil dose resulting from protons of up to 10,000 MeV, and this curve is shown as solid. The secondary proton dose is calculated in the same manner as the primary proton dose except that nuclear interactions are neglected. The neutron dose is calculated using removal theory and the dose conversion values of Gibson (19). The nuclear recoil dose is calculated by the use of the Monte Carlo results of the Oak Ridge nucleon transport code.

DOSE RATES FROM INCIDENT HEAVY IONS

In Figure 11 are shown the dose rates resulting from incident He, M, LH and VH ions incident on a slab shield of aluminum. In these calculations, M-particles were all assumed to have $Z=7$, LH-particles, $Z=12$, and VH-particles, $Z=27$.

Only the primary ionization dose from these ions is calculated. The solid lines show the dose rate estimates neglecting nuclear interactions entirely. The dashed lines indicate the dose rate from those ions surviving to the dose point without undergoing a nuclear interaction, assuming interaction mean free paths independent of ion energy. The true depth-dose rate curves will fall somewhere between these curves.

Clearly, the dose from the secondary particles resulting from nuclear interactions is important, and it would be highly desirable to evaluate this dose contribution.

At zero depth, the dose rates from the various components can be read from the figures and are as accurate as the spectral measurements allow. Converted into rads/yr, they are presented in Table 3.

TABLE 3

FREE SPACE DOSE RATES FROM THE VARIOUS COMPONENTS OF THE GALACTIC COSMIC RAYS
AT SOLAR MINIMUM (≤ 10 GeV)

<u>Particle</u>	<u>Dose Rate (Rads/Yr)</u>
Protons ($Z = 1$)	4.6
He Ions ($Z = 2$)	3.5
M Ions ($6 \leq Z \leq 9$)	1.9
LH Ions ($10 \leq Z \leq 14$)	1.3
VH Ions ($26 \leq Z \leq 28$)	<u>1.3</u>
Total	12.6 rads/yr

SOLAR COSMIC-RAY DOSE CALCULATIONS

Depth-Dose Characteristics

The representation of the solar cosmic-ray particle spectra as exponential in rigidity allows a convenient method of presenting the resulting depth-dose profiles parametrically. Figures 12 through 14 present depth-dose profiles for incident rigidity spectra with characteristic rigidities of 40, 100 and 160 MV. In each case, the primary ionization dose from protons of between 1 and 400 MeV is calculated, assuming the incident proton flux is attenuated by nuclear interactions. The neutron, secondary proton, and nuclear recoil doses are calculated with the same assumptions as in the galactic cosmic ray proton dose calculation. As the energy spectra fall off much more rapidly than the GCR spectra, the 400 MeV cutoff is of less importance, particularly for the low rigidity event. Several observations on the relative importance of the various dose components are of interest. First, the ionization dose from the primary protons is the dominant dose contribution to thicknesses of several tens of g/cm^2 of Al shielding. The thickness at which the secondary radiation rivals the primary dose is dependent on the characteristic rigidity of the incident proton spectrum, with the lower rigidities resulting in a secondary dose contribution which becomes significant for thinner shielding. The rad dose from the recoiling nuclei remains low relative to the other dose components at all shielding thicknesses. It should be noted that the neutron dose, calculated by the energy removal cross section of Gibson actually contains some fraction of the total nuclear recoil dose. Figure 15 presents the depth-dose profiles of incident alpha particles. Nuclear interactions are neglected.

A word of caution is in order when using the rigidity representation for thick shields. The results shown depend strongly on the validity of the exponential rigidity representation above proton energies that can penetrate to the dose point of interest. For large shielding thicknesses, greater than 10 g/cm^2 , it may well be that the prompt spectrum from certain particle events determines the spectral shape at high energies, and the average rigidity for the entire event may not represent this energy region adequately. This is certainly true of the great event of February 23, 1956. Its prompt spectrum seems best fit by a much higher characteristic rigidity (perhaps near 700 MV) than is obtained by consideration of the total fluence only. This will strongly affect the dose rates at great shielding thicknesses.

Importance of Various Particle Energies

If we fix attention on any particular dose point in the aluminum slab, we find an energy distribution of proton and neutrons which are producing dose at the point in question. The ionization dose from the protons can be expressed in the approximations used as:

$$D = K \int_{E_{\min}}^{E_{\max}} \phi_p(E) S(E) dE$$

where: $\phi_p(E)$ is the proton differential energy spectrum in protons ($\text{cm}^2 - \text{MeV}$) at the point;

$S(E)$ is the stopping power, in $\text{MeV cm}^2/\text{gm}$;

K is the conversion factor to convert the dose to rads.

The differential dose resulting from protons of energy between E and $E+dE$ is

$$dD = K \phi_p(E) S(E) dE.$$

Thus the importance of protons with energies between E and $E+dE$ in providing dose can be evaluated from a knowledge of the proton energy spectrum at the point and the stopping power. We find, as a typical result, that the lowest energy protons at the dose point are the most important in producing dose, when judged in a dose per unit energy basis. This result holds generally for all solar particle spectra and shield thicknesses. This result can be deceptive, however, unless one realizes that the fraction of the total dose deposited by low energy protons is not large. Perhaps a clearer way to present the importance of the various proton energies is to plot the differential dose per unit logarithmic interval. The reason for presenting the curves in this way is because the energy range of interest extends over several orders of magnitude. Since it is convenient to plot the results using a logarithmic scale in energy, it is instructive to plot the dose distributions for linear intervals along the abscissa, i.e., per logarithmic energy interval. In this way, equal distances along the abscissa have equal weights for the evaluation of the importance of different energy ranges in contributing to the dose. Thus, we write the differential dose element $dD = K\phi_p(E)s(E)Ed(\ln E)$. The quantity plotted in this case is $K\phi_p(E)S(E)E$. In this way the importance of the higher energy protons, which contribute less dose per unit energy but span a much larger energy range is more clearly presented. We see in Figures 16 and 17 that it is in fact these higher proton energies (up to 100 MeV) which can contribute a large fraction of the total dose. In Figures 18 and 19 the differential dose distributions for the galactic particles are also shown.

One additional way to view the importance of the various particle energies is to examine the differential particle energy spectrum at the dose point. Figures 20 and 21 show the number-energy spectrum of protons present from proton spectra with characteristic rigidities of 40 and 160 MV at various depths in aluminum. One can also show the number of particles present as a function of the stopping power, or LET, of the particle, and Figures 22 through 25 show the results of typical proton and alpha particle rigidity spectra incident on aluminum.

It is also of interest to examine the importance of the various incident proton energies in producing dose at an interior point. If we examine first the dose from penetrating protons, it is apparent that for any given shield thickness, x , only those incident protons with range equal or greater than x can deliver dose at the depth x . Thus we have an energy cutoff, E_0 , below which the protons cannot reach the dose point. In Figures 26 through 28 we show the fraction of the total dose delivered by protons of incident energy greater than E at various thicknesses of aluminum for three typical solar proton rigidity spectra. We see that the higher characteristic rigidity spectra cause the curves to fall off more slowly with increasing incident proton energy than do the lower rigidity events. This is another way of stating the fact that high incident energies are more important for flat spectra than for steep spectra.

Importance of Various Proton Energies in Producing Secondary Doses

Next, let us examine the secondary doses from the incident protons. In Figures 29 through 38, we present the fraction of the secondary proton and neutron dose delivered as a result of nuclear interactions which involve

incident protons of greater than initial energy E. For the secondary protons, we have a similar cut-off effect as with the primary dose since the secondary protons are less than or equal to the energy of the primary interacting proton. In addition, it is of interest to examine the importance of the nuclear interactions initiated by protons above particular energies in producing neutron and secondary proton dose. This gives one a feeling for the importance of an accurate knowledge of these cross sections at the various energies of interest. These results are shown as dashed lines in Figures 29 through 38.

Finally, we present the normalized differential dose distributions of the secondary proton and neutron dose as a function of incident proton energy in Figures 39 and 40. Results are presented for three typical characteristic rigidities at a depth in aluminum of 10 g/cm^2 .

Conclusions

Certain general conclusions can be drawn from the data presented. We note that for any given shielding thickness, the fraction of the total secondary dose resulting from protons of initial energy greater than E increases with increasing characteristic rigidity. Also, we find as the shielding thicknesses increase, the lower incident proton energies contribute less to the total secondary dose. When we compare the incident proton energy cutoff curves with the reacting energy cutoff curve for a given spectral shape, we find that they gradually approach at higher energies. We now present three specific illustrations of the use of the data. First, what incident proton energies are most important in producing secondary proton and neutron dose under 10 g/cm^2 of aluminum? Figure 39 shows that for secondary proton dose, they are those protons that

have energies just slightly greater than necessary to reach the dose point. Only the 160 MV differential dose spectrum peaks at a slightly higher energy (130 MeV) than the cutoff energy for this case (100 MeV). The neutron dose, on the other hand, shows a strong dependence on the incident spectral characteristic rigidity. The 40 MV differential dose plot shown in Figure 40 peaks at an incident proton energy of 35 MeV, the 100 MV spectrum peaks at 65 MeV, while the 160 MV spectrum shows a very broad peak from 150 to 260 MeV. Second, let us estimate the importance of the low energy cross sections used in the calculations. At 10 g/cm^2 in aluminum, we note from Figure 35 that 30 percent of the neutron dose resulting from the 40 MV spectrum is contributed by reactions involving protons of less than 25 MeV. Cross sections in this region are extrapolations of Bertini's data and could contain large errors. The 100 and 160 MV spectra, however, show that less than 10 and 5 percent, respectively, of the neutron dose comes from the low energy proton interactions. It appears unlikely that a knowledge of the proton reaction cross sections below 25 MeV is critical for evaluating the neutron doses resulting from most SCR events. Thirdly, assuming some type of exterior cutoff in proton energy is operating, such as a magnetic shield or the earth's magnetosphere, how does the secondary dose under 10 g/cm^2 of aluminum compare with that which would be received from the complete spectrum? Figure 35 tells us, assuming a 100 MeV cutoff, that 65%, 45% and 4% of the neutron dose would be received from 160 MV, 100 MV and 40MV rigidity spectra, respectively.

ENERGETIC STORM PARTICLES DOSES

In Figure 41, we present depth-dose plots for three characteristic rigidities thought to be representative of the energetic storm particles: 10, 20, and 30 MV. No secondary dose estimates are given here, as the results depend completely on the low energy proton reaction cross sections below 25 MeV, which are not adequately known. Figure 42 presents the LET spectrum associated with these typical characteristic rigidities. Tables 131 and 132 of Reference 2 give the total dose estimates which have resulted from the events of cycle 19. For the shielding thickness shown, the secondary doses should be negligible.

BIOLOGICAL CONSIDERATIONS

At this point, it is considerably easier to identify the important problems to be tackled in radiobiology in order to better evaluate the radiation hazard than it is to speculate on the various important effects and enumerate which particles and energies are important for a given effect. It appears that two distinct kinds of hazards present themselves. First, we consider the problem of a massive dose from a giant solar particle event. Here the danger will differ considerably depending on whether the astronaut is caught in extra-vehicular activity (that is, in a low shielding situation) or has the time and shielding available to retire to an area where say 10 to 15 g/cm² or more of shielding is between him and the incident flux. In the first case, relatively low fluxes may constitute a hazard and the most critical area will be the skin and perhaps the eyes if they are not well shielded. The reason for this is that the body itself provides considerable shielding to the internal organs for the rather steep spectra which typically occur in solar particle events. The shielding

provided by the Lunar Module in which the astronauts will first touch down on the moon is in the category of thin shielding, where the dose to the skin will be the important consideration. The most important particles here will be the ESP and low energy SCR particles. If the anisotropy recently measured (7,14) is a typical characteristic of large events with steep spectra, it would definitely be of help to orient the craft so that the area of thinnest shielding is pointed in the minimum flux direction. According to data (7) received on Pioneer 6 from the solar event of 30 December 1965, low energy protons (13-20 MeV) were highly anisotropic over the period of peak flux. The direction of minimum flux (for a 2-hour period) was around 150° from the sun-spacecraft line. The ratio of maximum to minimum flux in opposite directions was about 3 to 1 over this period. It was also noted that this direction of peak intensity was highly variable over periods of 10 minutes or so.

If the astronaut has with him enough shielding to effectively absorb the low energy component, then the event must be a large one for him to be in serious danger. In this case the skin ceases to be a critical organ since the body self-shielding is less effective and the doses to the intestinal tract and marrow become important. The prodromal syndrome of nausea, vomiting, anorexia, and fatigue could cause trouble inside a spacecraft. The particles most responsible for this have initial energies whose range is the order of the shielding thickness available. Thus events with flat spectra (high P_0 's) become important. The most important particles would be the penetrating protons and the secondaries caused by those which interacted. Alpha particles and the heavier components would not contribute substantially to the dose.

Recovery is an important consideration here since it has been noted that there is a tendency for several giant events to occur within several days. Thus if recovery and repair from the first event are not complete when the second event occurs, the resultant biological damage at the end of the second event could be considerably greater than if it had been an isolated one. Unfortunately, repair mechanisms in humans and the recovery capacity of the body involve complex processes. It is known that repair is less likely for damage caused by the highly ionizing components - recoil protons and heavy recoils. Thus it is possible that damage to certain organs in which cells are not replaced, such as the retina, might accumulate over a period of time and eventually cause a problem. In this regard, the GCR may play a significant role. Figure 43 shows the LET spectrum of the GCR at a depth of 0.2 g/cm^2 of water. The upper curves give the LET spectra multiplied by QF (see next section). Because of the high energies involved, this basic spectrum does not change significantly as the shielding is increased, except that the higher dE/dx components are attenuated faster than the proton component.

One glaring gap in our knowledge is the lack of information on the secondary production cross sections from He and heavier ions. It is of interest, however, to calculate the number of stopping GCR heavy ions (sometimes called "thin-down hits") per cm^3 -day as a function of depth assuming only particle removal from the flux due to nuclear interactions, but neglecting the secondaries caused by the fragmentation of heavier ions. The results of such a calculation are shown in Figure 44 for the M-, LH-, and VH-particles. The VH-particle calculation is probably quite accurate (assuming a correct interaction mean free path);

but the LH- and M-particle curves are certainly lower limits, since secondaries in those classes that arise from interactions of heavier ions are neglected entirely. Even so, it is interesting to note that the number of M-particle thin-down hits at 15 cm is still 30% of that at 1 cm, and the number of LH-particle thin-down hits at 15 cm is 25% that at 1 cm.

BIOLOGICALLY WEIGHTED LET SPECTRA

In general, large uncertainties are involved in making quantitative calculations using biological effectiveness factors (RBE's) to obtain "rem" values which might or might not have significance to the spacecraft situation of mixed radiations, low dose rates and steep depth-dose curves. Therefore, only crude estimations have been made to indicate trends. A few LET spectra under various shielding thicknesses for protons and He ions in typical solar particle events and for the galactic cosmic radiation behind thin shielding have been calculated and are shown in Figures 43 and 45 through 47. In addition, these spectra were multiplied by the QF recommended by the ICRP (21) as the biological effectiveness factor for use with radiations of varying dE/dx to give a rough idea of the biological importance of various dE/dx 's in a hazard evaluation. As stated by the Commission, such a factor is probably conservatively high and so the areas between the two curves are shaded in the figures. All that can be concluded at present is that the "true" curve lies somewhere between these two extremes. The curves will vary for different shielding thicknesses and body depths.

It is clear that the high dE/dx component of the GCR is the most biologically important portion for thin shielding. At the present time it is impossible to treat accurately the situation for thicker shielding because of the lack of data on secondary production by the heavier ions and by protons above 400 MeV.

CONCLUSIONS

From the above considerations it has been possible to make several conclusions concerning the nature of the radiation, the properties of the radiation behind various shielding thicknesses, the areas where physical and biological data are lacking, and the problems which need immediate attention in order to improve our evaluation capability. Several of these conclusions have been discussed in the text, but it might be helpful to list the major ones again here.

1. Experimental data on the radiation environment are being supplied by well-instrumented satellites. There are several areas, however, in which more detailed information is needed. Experimental errors on the data points for spectra of the heavier ions in the GCR are still large, and for completeness the shape of the MH-particle spectrum should be obtained. The spectra at very low energies are important in determining the free space dose at solar minimum; therefore, the accuracy of free space dose calculations suffer from the lack of information in this low energy region. The rather rapid variation of the low energy portion of the proton and He ion spectra near solar minimum implies that the free space GCR dose also varies throughout this period. An explicit form for the temporal and spatial dependence of the modulation mechanism is necessary for a complete description of the spectra and therefore for an accurate estimation of the dose.

2. Secondary production data for protons of energy greater than 400 MeV are necessary for a proper treatment of the dose behind typical shielding thicknesses from the galactic protons, and also from solar particle spectra with large characteristic rigidities (≥ 160 MV). Secondaries from protons in this energy region were omitted in the present treatment and the depth-dose curves for the GCR are consequently too low. Data in this energy region will soon be available from Oak Ridge National Laboratory.
3. Secondary production from heavier ions was neglected in all energy regions. Little is known about the mean free paths or production cross sections for high energy heavy ions in light elements, and one may have to await the construction of a high-energy heavy-ion accelerator to obtain the necessary data for an accurate evaluation. It may be possible, however, to arrive at crude estimates by making certain simplifying assumptions as to the character of the primary interactions between the heavy ion and a complex nucleus. The proper inclusion of all secondaries from the various heavy ion nuclear interactions in an absorber for the different spectra of the GCR heavy particles and the resultant calculation of a dose would undoubtedly involve the development of a computer code of some complexity.
4. The rigidity representation for the solar particle spectra should be critically evaluated as the data on particle events accumulate in the present cycle to ascertain whether all large events can be adequately described in this manner. The presence of low energy anisotropies at the time of peak flux is an important new experimental result and has an obvious bearing on spacecraft operational procedures during the course of an event.

5. Regarding the calculations, reasonable agreement has been obtained between the results of the code used in this study and the more comprehensive codes developed at Oak Ridge National Laboratory. Excellent agreement was obtained for the primary doses. Somewhat less good agreement was obtained for the secondary doses due to the approximations involved in the present code. The agreement is felt to be adequate for meaningful conclusions to be drawn.

6. The detailed calculations show that, in general, protons of energies between 10 and 100 MeV at the dose point are the most important in contributing dose from solar particle events. Thus, the most important incident energy of the primary proton is that energy such that the proton arrives at the dose point in the above energy range. For instance, behind 1 g/cm^2 , protons of initial energy between 28 MeV (the cutoff energy) and 40 MeV account for 85%, 65% and 57% of the primary dose for spectra with characteristic rigidities of 40 MV, 100 MV and 160 MV, respectively. One consequence of this is that if another type of shielding (such as a magnetic field or plasma shield) is used in conjunction with static shielding, the energies most important to be swept away are those just above the static shielding cut-off energy (the energy of a particle with a range equal to the shielding thickness). Higher proton energies become more important for flatter spectra and for thicker shielding. For secondary protons the situation is not so clear cut. Behind 1 g/cm^2 , protons of initial energy between 28 MeV and 40 MeV account for 50%, 20% and 15% of the secondary proton dose for spectra with characteristic rigidities of 40 MV, 100 MV and 160 MV, respectively. In the case of secondary neutrons, proton energies below

the cutoff energy are important. The percentages of the dose from protons with initial energies below 40 MeV are 70%, 30%, and 20% for the three spectral shapes. As another example for the secondary particles, at 10 g/cm^2 of aluminum shielding the most important initial proton energy for the secondary proton dose is slightly greater than 100 MeV (the cut-off energy) for the spectra with characteristic rigidities of 40 MV and 100 MV. The most important energy moves out to 130 MeV for the spectrum of 160 MV characteristic rigidity. For the cases of the neutron dose at the same depth, the most important initial proton energies are 35 MeV for the spectrum with characteristic rigidity of 40 MV, and 65 MeV for the spectrum with characteristic rigidity of 100 MV. For the spectrum with 160 MV characteristic rigidity, the maximum is very broad and initial proton energies between 100 and 300 MeV are important. Also, since the calculation requires this curve to go to zero at 400 MeV, the lack of secondary data for primaries greater than 400 MeV is affecting the results for this spectrum.

Finally, the curves indicating the fraction of the dose produced by protons greater than various energies show that in events with low characteristic rigidity, a significant fraction of the dose is produced by nuclear reactions involving protons with energies less than 25 MeV where the neutron production cross sections can only be roughly estimated since few experimental data are available. Thus, in these cases the conclusions must be treated with caution.

7. Although biological effects are difficult to quantify at this stage, certain general conclusions can be made concerning the biological importance of the various particles. For the solar particle events, it is clear from the LET spectra that the low energy particles at the dose point (≤ 10 MeV) are the most important for low characteristic rigidity events behind thin shielding. Higher energies become increasingly important as the characteristic rigidity increases. However, for the GCR, at least for low shielding, there is an interesting reversal. Although the high dE/dx components are particularly important biologically, the higher energy heavy particles, i.e., the ones near minimum ionization, are the most important. This is due, of course, to the very different shapes of the GCR and SCR energy spectra. The GCR spectra all have maxima in the range of several hundred MeV/nucleon, while the SCR spectra peak at very low energies! Also of interest is the slow drop-off of thin-down hits/cm³-day as a function of shielding thickness. Certainly, considerable research is necessary on the effects of heavy ions to interior body organs, both by stopping ions as well as by those penetrating through the body. Finally, work on recovery and repair from chronic, low-level radiation with special emphasis on accumulated damage from multiple exposures to both high and low dE/dx particles is important to be able to improve our evaluation capability for extended missions.

ACKNOWLEDGEMENT

Dr. R. G. Alsmiller, Jr., of the Oak Ridge National Laboratory, assisted us greatly by providing, before publication, much of the nuclear data used in our calculations and the results of the Oak Ridge Nucleon Transport Code. Dr. W. R. Webber, a consultant to Boeing from the University of Minnesota, provided much of the information on solar particle events presented in this report. His assistance in defining the galactic cosmic-ray environment was also most helpful.

REFERENCES

1. W. R. Webber, "An Evaluation of the Radiation Hazard due to Solar-Particle Events", Boeing Document D2-90469, December 1963
2. W. R. Webber, "An Evaluation of Solar-Cosmic-Ray Events During Solar Minimum", Boeing Document D2-84274-1, June 1966
3. F. B. McDonald and G. H. Ludwig, "Measurement of Low-Energy Primary Cosmic-Ray Protons on IMP-1 Satellite", Phys. Rev. Lett. 13, 783 (1964)
4. P. S. Freier and C. J. Waddington, "Electrons, Hydrogen Nuclei, and Helium Nuclei Observed in the Primary Cosmic Radiation During 1963", J. Geophys. Res. 70, 5753 (1965)
5. C. Y. Fan, G. Gloeckler and J. A. Simpson, "Cosmic Radiation Helium Spectrum Below 90 MeV per Nucleon Measured on IMP-1 Satellite", J. Geophys. Res. 70, 3515 (1965)
6. G. Gloeckler and J. R. Jokipii, "Low-Energy Cosmic-Ray Modulation Related to Observed Interplanetary Magnetic Field Irregularities", Phys. Rev. Lett. 17, 203 (1966)
7. C. Y. Fan, J. E. Lamport, J. A. Simpson and D. R. Smith, "Anisotropy and Fluctuations of Solar Proton Fluxes of Energies 0.6-100 MeV Measured on the Pioneer 6 Space Probe", J. Geophys. Res. 71, 3289 (1966)
8. S. M. Comstock, C. Y. Fan and J. A. Simpson, "Abundances and Energy Spectra of Galactic Cosmic-Ray Nuclei Above 20 MeV/Nucleon in the Nuclear Charge Range $2 \leq Z \leq 26$ ", Astrophys. Journ. 146, 51 (1966)
9. W. R. Webber, to be published
10. J. J. O'Gallagher and J. A. Simpson, "The Heliocentric Intensity Gradient of Cosmic-Ray Protons and Helium During Minimum Solar Modulation", Astrophys. Journ. 147, 819 (1967)
11. W. R. Webber, "Time Variations of Low-Rigidity Cosmic-Rays During the Recent Sunspot Cycle", Progress in Elementary Particle and Cosmic Ray Physics, Vol. VI, 75 (1962)
12. P. S. Freier and C. J. Waddington, "The Helium Nuclei of the Primary Cosmic Radiation as Studied Over a Solar Cycle of Activity Interpreted in Terms of Electric Field Modulation", Space Science Reviews 4, 313 (1965)

13. P. S. Freier and W. R. Webber, "Exponential Rigidity Spectrums for Solar Flare Cosmic-Rays", J. Geophys. Res. 68, 1605 (1963)
14. W. C. Bartley, R. P. Bukata, K. G. McCracken and U. R. Rao, "Anisotropic Cosmic Radiation Fluxes of Solar Origin", J. Geophys. Res. 71, 3297 (1966)
15. J. A. Barton and B. W. Mar, "Computer Codes for Space Radiation Environment and Shielding", Technical Documentary Report No. WL TDR-64-71, Vol. I. Air Force Weapons Laboratory, August 1964
16. W. H. Barkas and M. J. Berger, "Tables of Energy Losses and Ranges of Heavy Charged Particles", NASA SP-3013, 1964
17. L. C. Northcliffe, "Passage of Heavy Ions Through Matter", Annual Review of Nuclear Science, Vol. 13, p. 67 (1963)
18. R. G. Alsmiller, Jr., M. Leimdorfer, and J. Barish, "Analytic Representation of Nonelastic Cross Sections and Particle-Emission Spectra From Nucleon-Nucleus Collisions in the Energy Range 25 to 400 MeV", Oak Ridge National Laboratory Report ORNL-4046, April 1967
19. W. A. Gibson, "Energy Removed From Primary Proton and Neutron Beams by Tissue", Oak Ridge National Laboratory Report ORNL-3260, 1962
20. W. Wayne Scott and R. G. Alsmiller, Jr., "Comparison of Results Obtained with Several Proton Penetration Codes", to be published.
21. "Report of the RBE Committee to the ICRP and ICRU", Health Physics 9, 357 (1963)

- ⊕ PIONEER 6 - C. Y. FAN, J. E. LAMPORT, J. A. SIMPSON AND D. R. SMITH:
JOURN. GEOPHYS. RES. 71, 3289 (1966)
- ▲ V. K. BALASUBRAHMANYAN AND F. B. McDONALD; JOURN. GEOPHYS.
RES. 69, 3289 (1964)
- P. S. FREIER AND C. J. WADDINGTON; JOURN. GEOPHYS. RES. 70, 5753 (1965)
- IMP-I - F. B. McDONALD AND G. H. LUDWIG; PHYS. REV. LET. 13, B, 783 (1964)
- V. K. BALASUBRAHMANYAN, D. E. HAGGE, G. H. LUDWIG AND F. B. McDONALD;
PROC. INT. CONF. COSMIC RAYS 1965, 417 (1966)

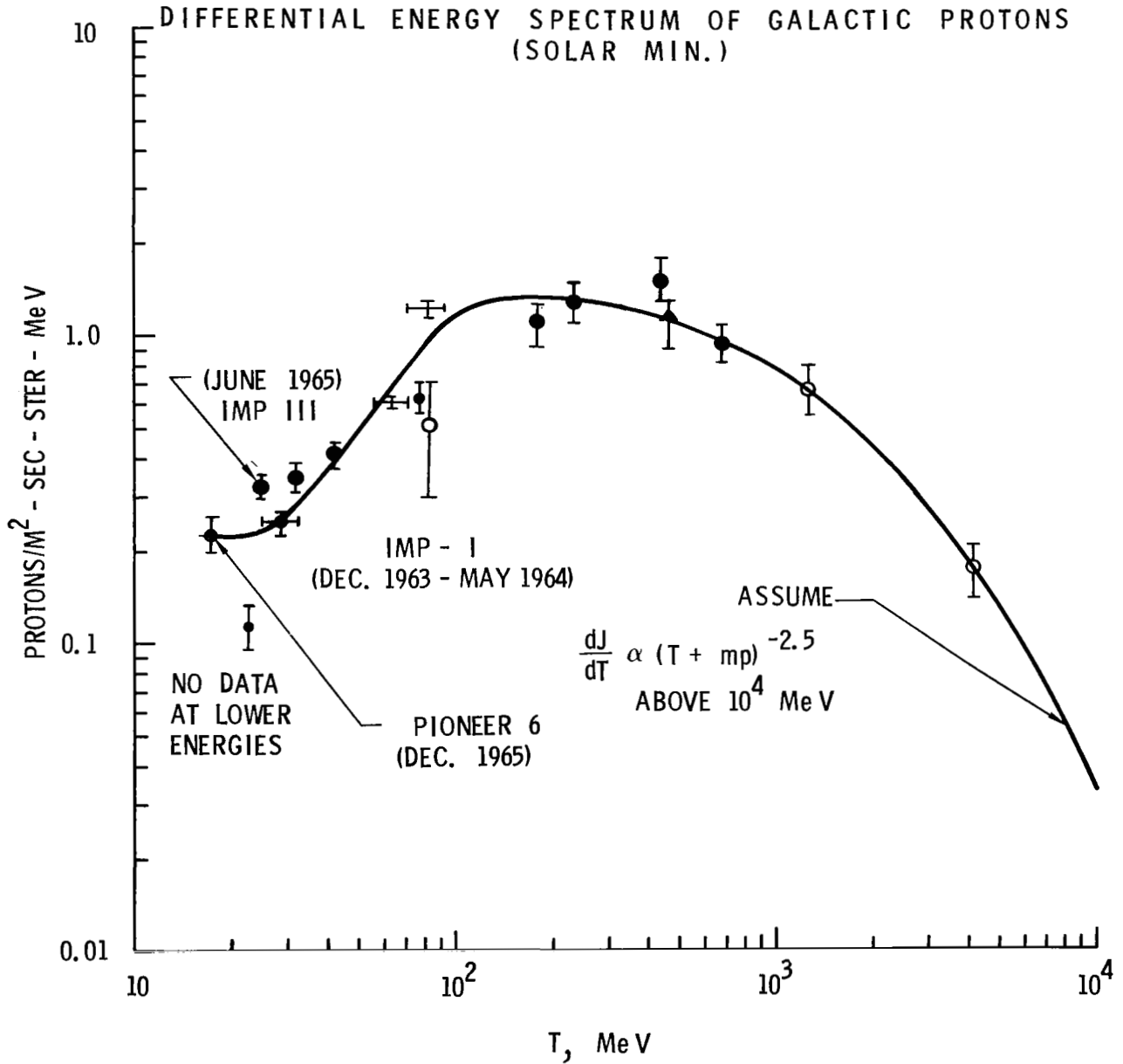






FIGURE 1

- 
 IMP III - G. GLOECKLER AND J. R. JOKIPU: PHYS. REV. LETT. 17,
 203 (1966)
- 
 V. K. BALASUBRAHMANYAN, D. E. HAGGE, G. H. LUDWIG AND F. B.
 McDONALD; PROC. INT. CONF. COSMIC RAYS 1965, 427 (1966)
- 
 P. S. FREIER AND C. J. WADDINGTON: JOURN. GEOPHYS. RES. 70,
 5753 (1965)
- 
 IMP I - C. Y. FAN, G. GLOECKLER AND J. A. SIMPSON: JOURN.
 GEOPHYS. RES. 70, 3515 (1965)

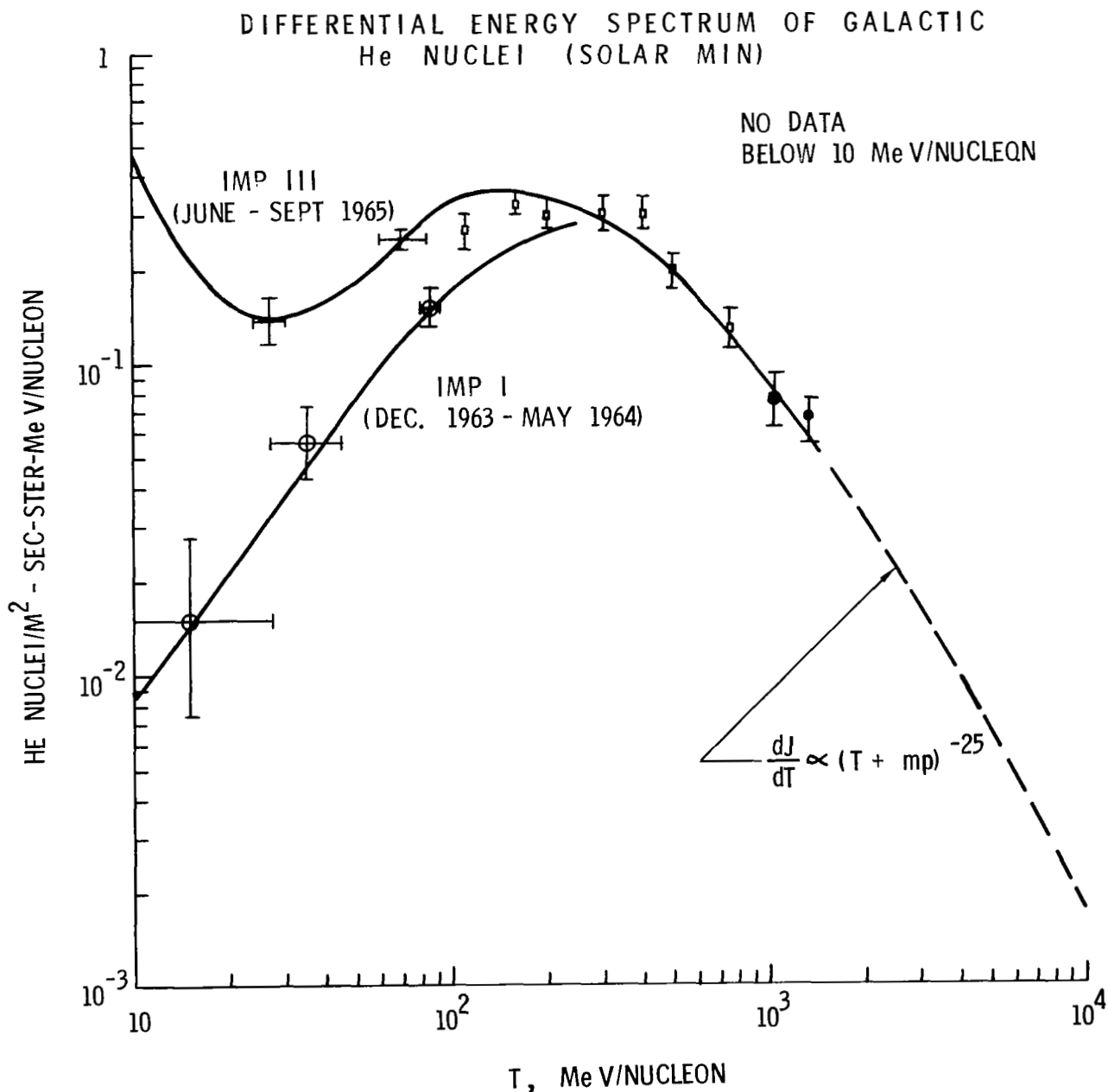


FIGURE 2

✚ S. M. COMSTOCK, C. Y. FAN AND J. A. SIMPSON, ASTROPHYSICS
 JOURN. 146, 51 (1966)
 ✚ BISWAS
 ✚ FICHEL AND REAMES

DIFFERENTIAL ENERGY SPECTRUM OF GALACTIC
 L - NUCLEI ($3 \leq Z \leq 5$) (SOLAR MIN.)

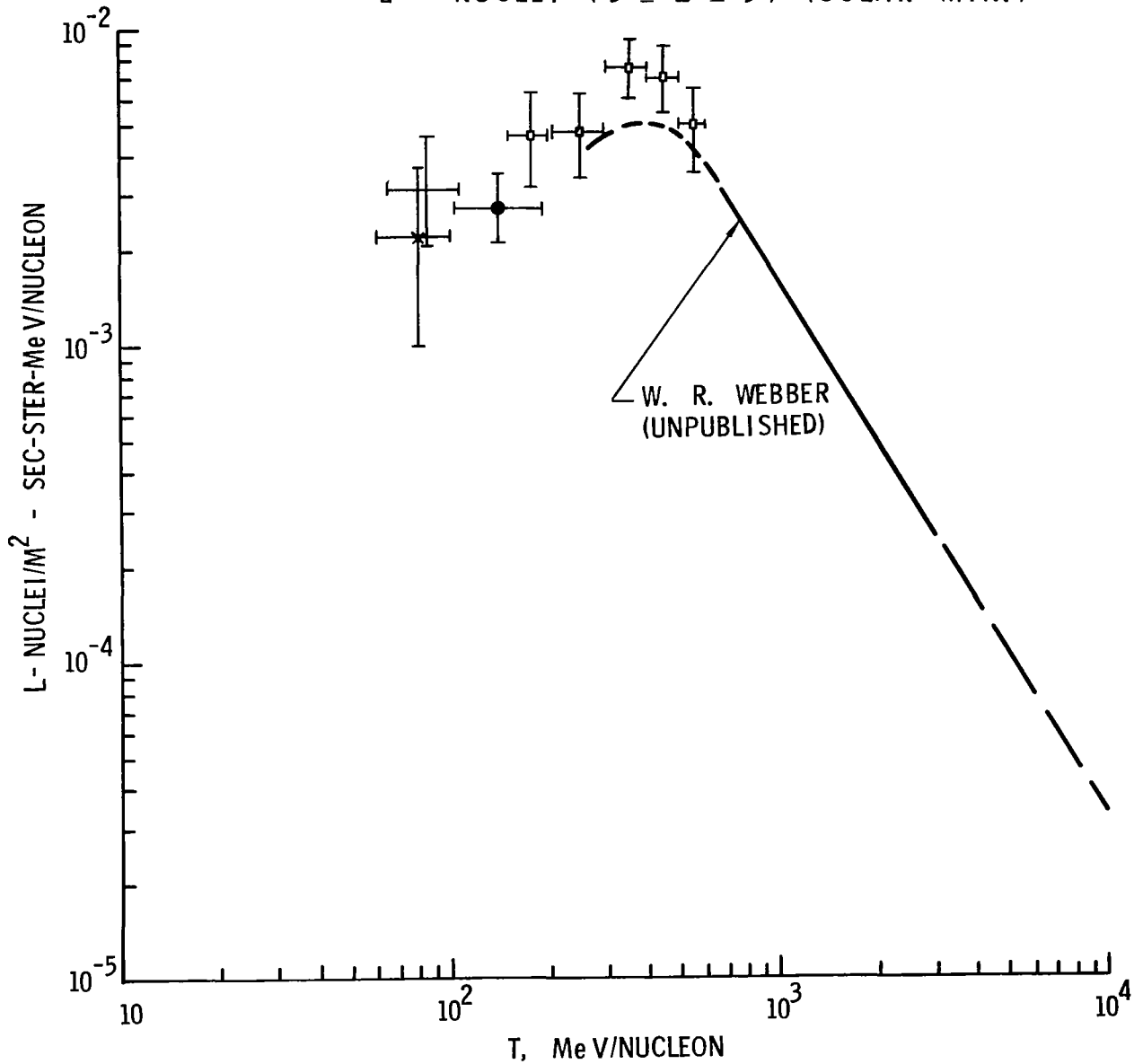
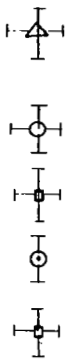


FIGURE 3



- G. M. COMSTOCK C. Y. FAN AND J. A. SIMPSON; ASTROPHYS. JOURN. 146 51 (1966)
- C. F. FICHEL D. E. GUSS K. A. NEELAKANTAN AND D. V. REAMES: PROC. INT. CONF. COSMIC RAYS 1965 400 (1966)
- Y. K. LIM AND K. FUKUI; JOURN. GEOPHYS. RES. 70 4965 (1965)
- D. E. EVANS; NUOVO CIM. 37 394 (1963)
- S. BISWAS AS QUOTED BY W. R. WEBBER

DIFFERENTIAL ENERGY SPECTRUM OF GALACTIC M - NUCLEI ($6 \leq Z \leq 9$) (SOLAR MIN.)

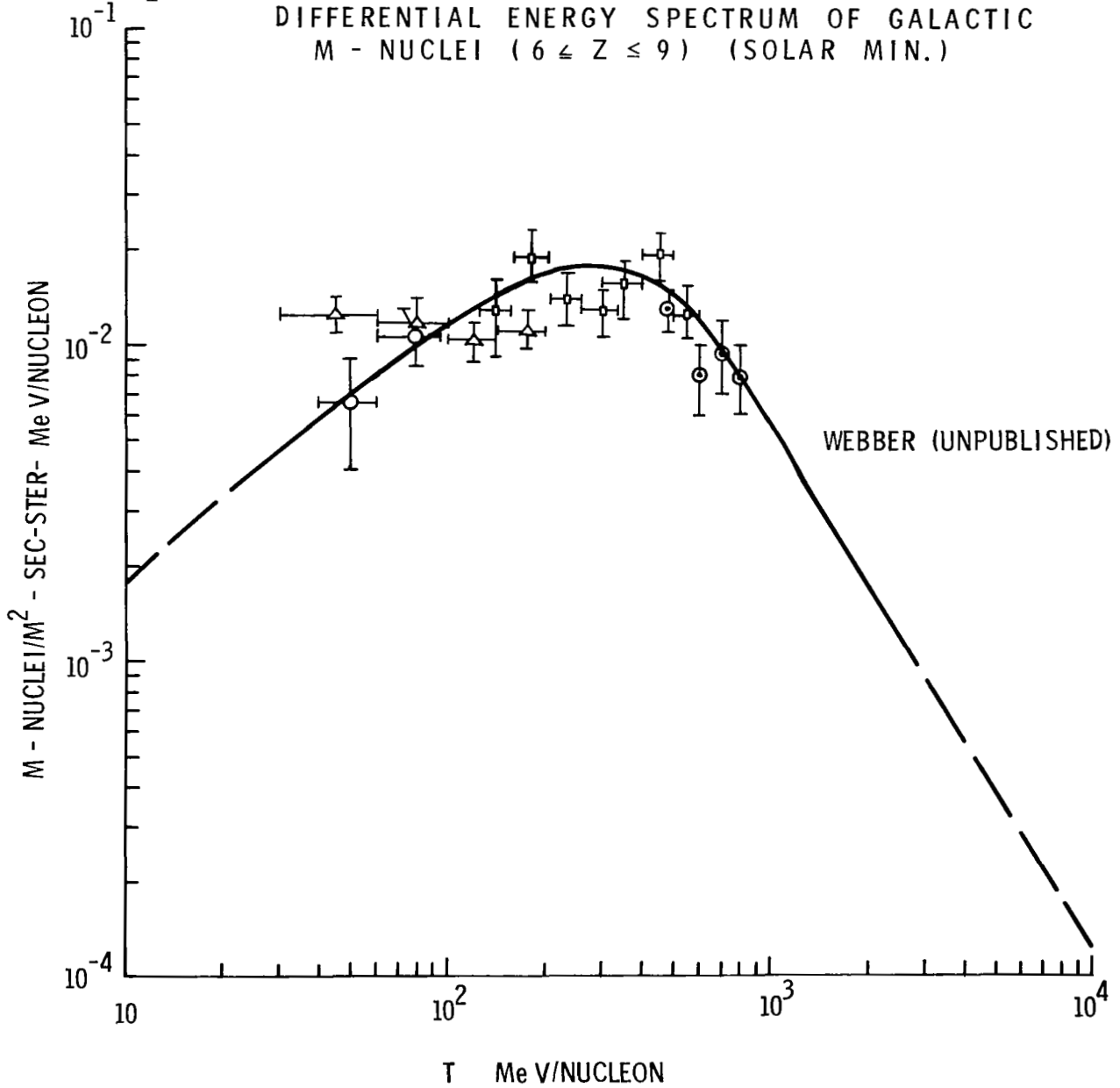


FIGURE 4

⊕ G. M. COMSTOCK, C. Y. FAN AND J. A. SIMPSON: PROC. INT. CONF.
COSMIC RAYS 1965, 383 (1966)

⊙ Y. K. LIM AND K. FUKUI

⊕ BISWAS

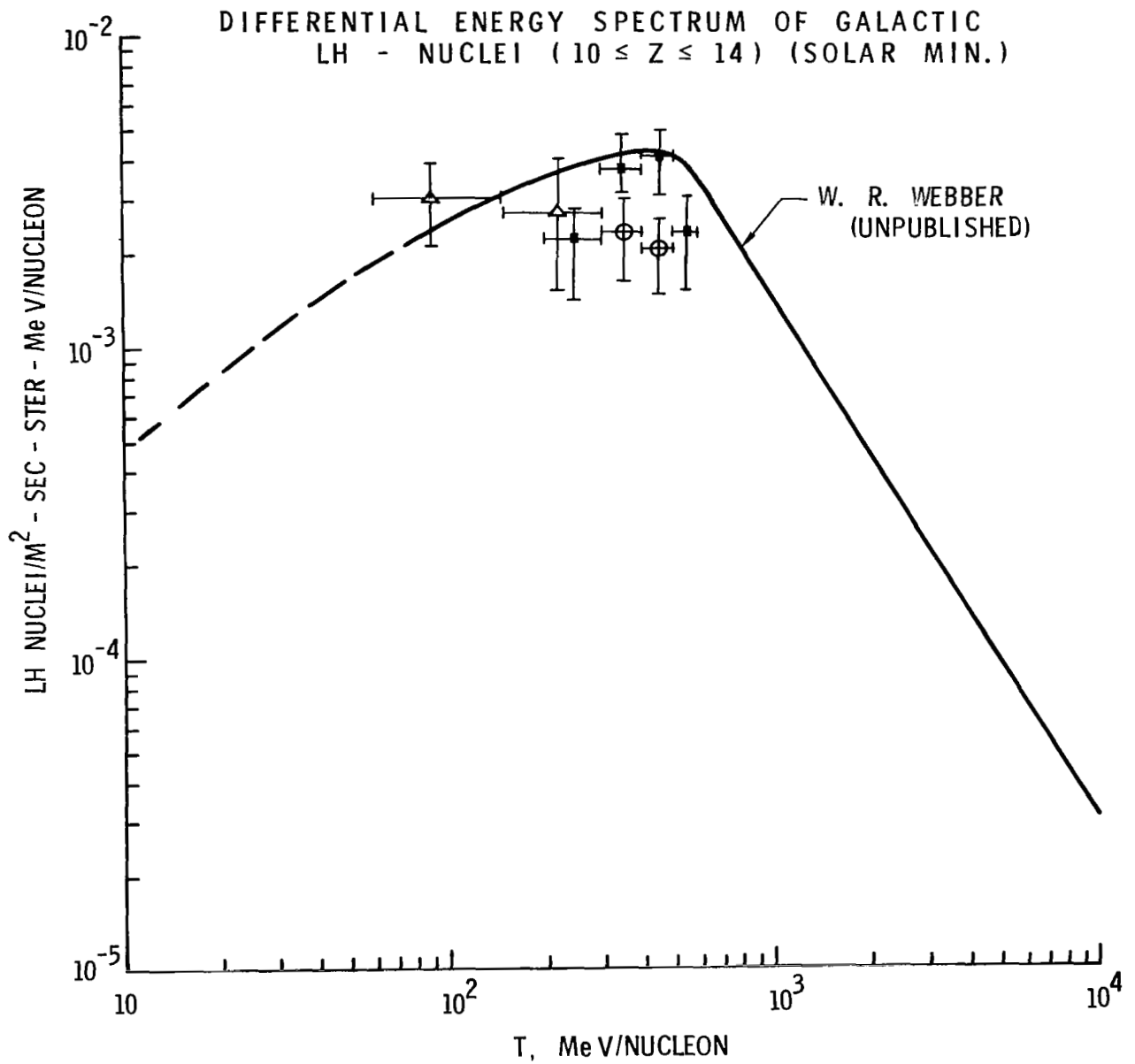


FIGURE 5

✚ G. M. COMSTOCK, C. Y. FAN AND J. A. SIMPSON;
ASTROPHYS. JOURNAL 146 51, (1966)

DIFFERENTIAL ENERGY SPECTRUM OF GALACTIC
VH - NUCLEI ($26 \leq Z \leq 28$) (SOLAR MIN.)

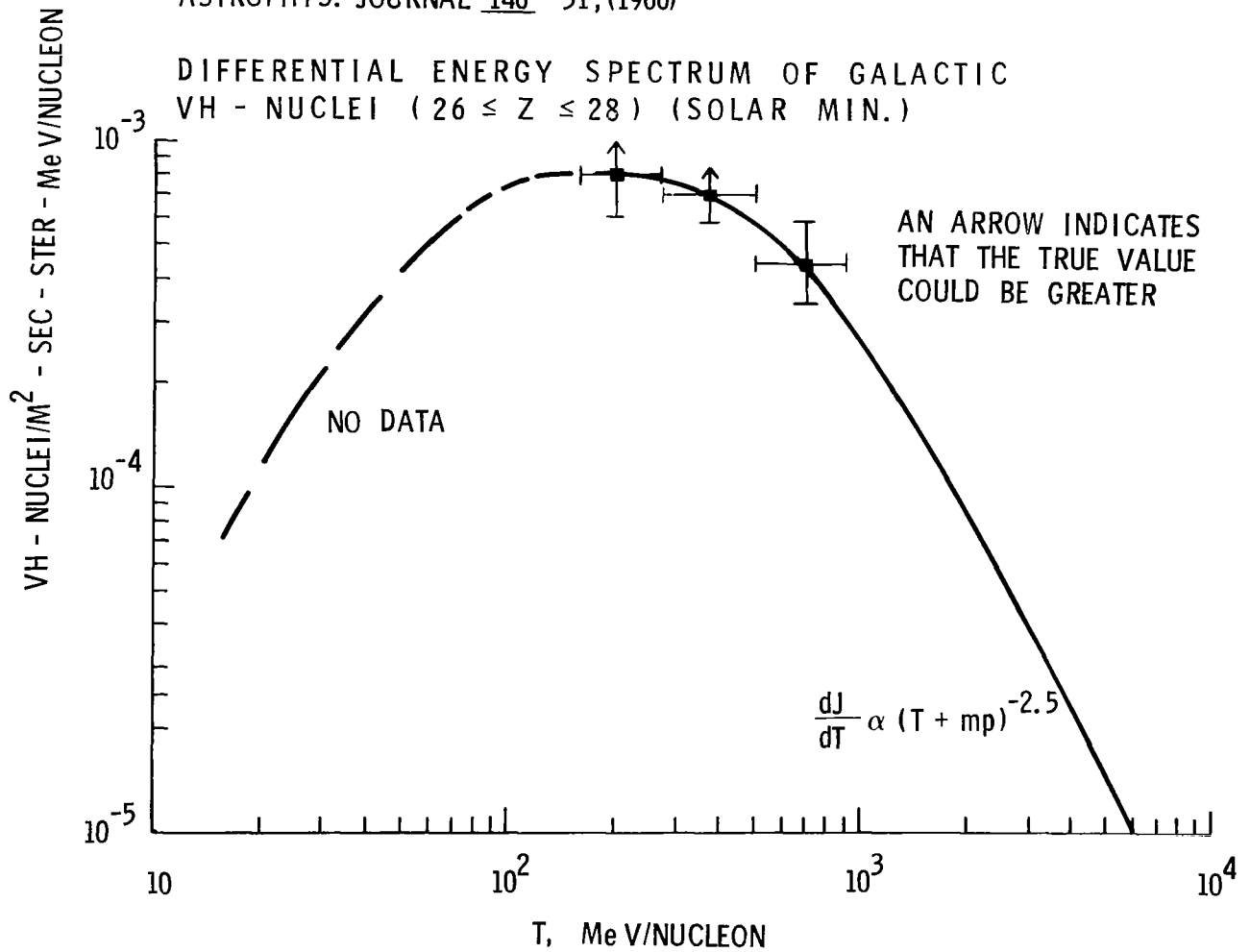


FIGURE 6

DIFFERENTIAL RIGIDITY SPECTRA OF GALACTIC PROTONS
 AT DIFFERENT TIMES DURING THE SOLAR CYCLE
 (FROM REF. 11)

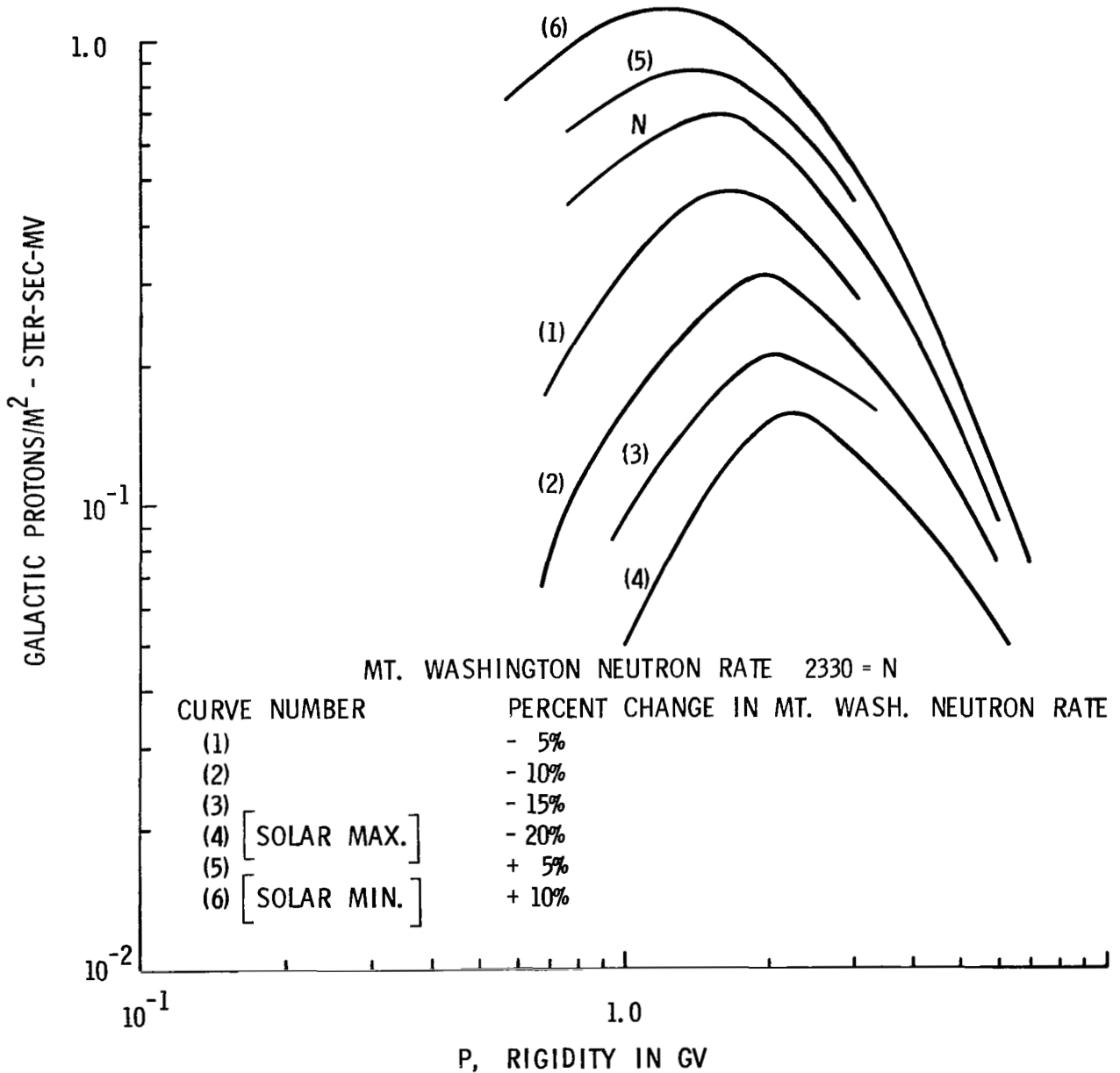


FIGURE 7

DIFFERENTIAL RIGIDITY SPECTRA OF GALACTIC HELIUM IONS AT DIFFERENT TIMES DURING THE SOLAR CYCLE
(FROM REF. 12)

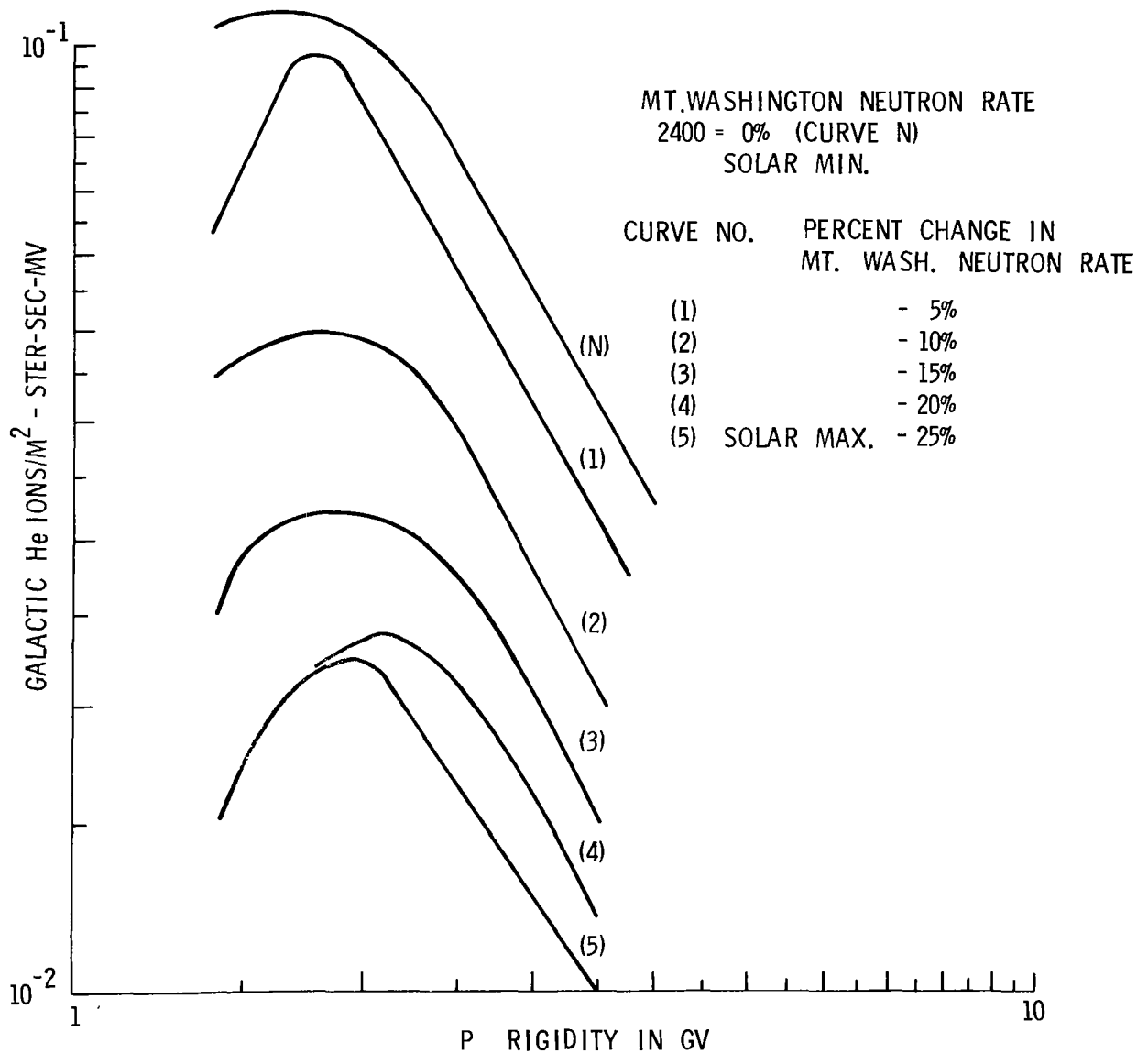


FIGURE 8

OAKRIDGE NTC

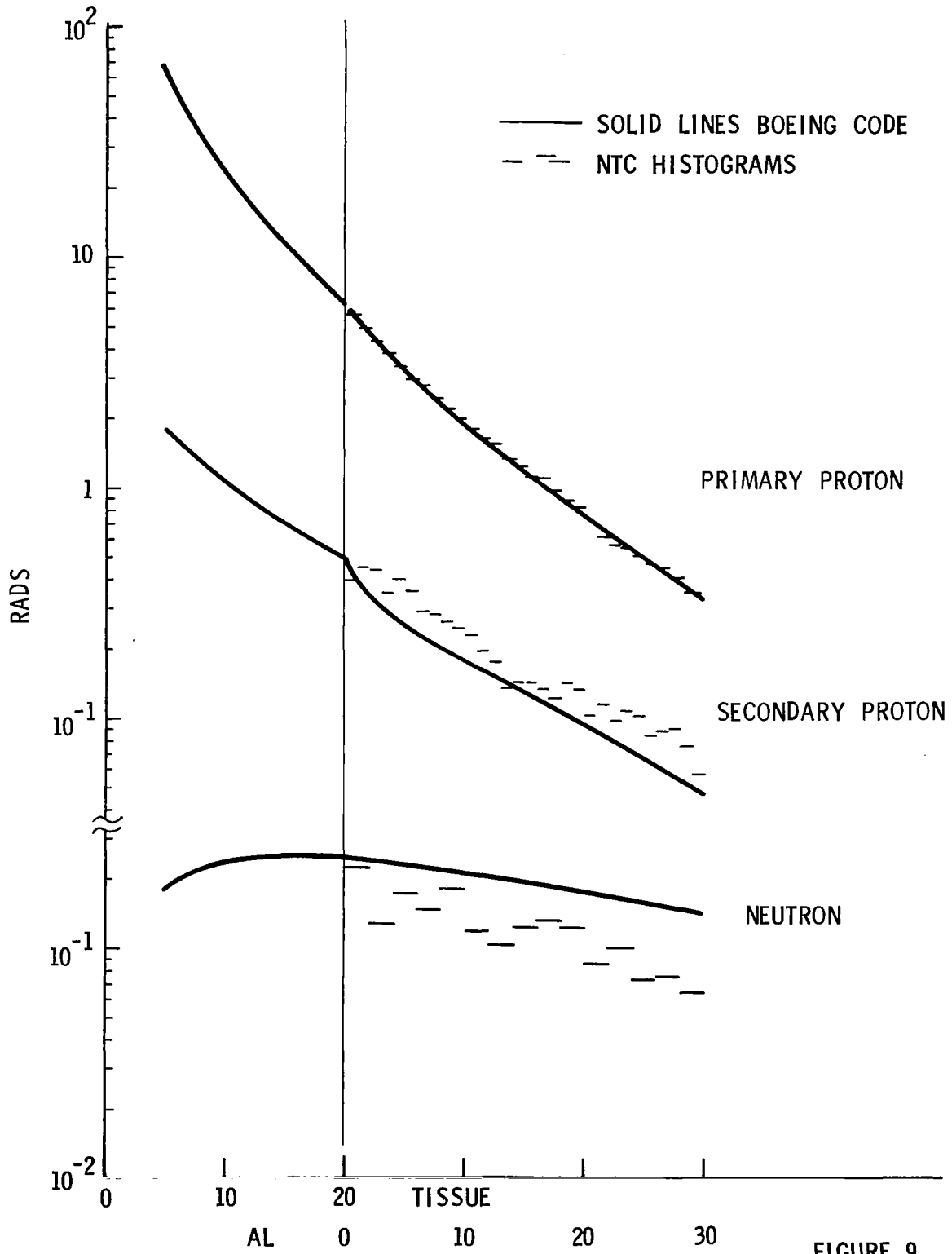


FIGURE 9

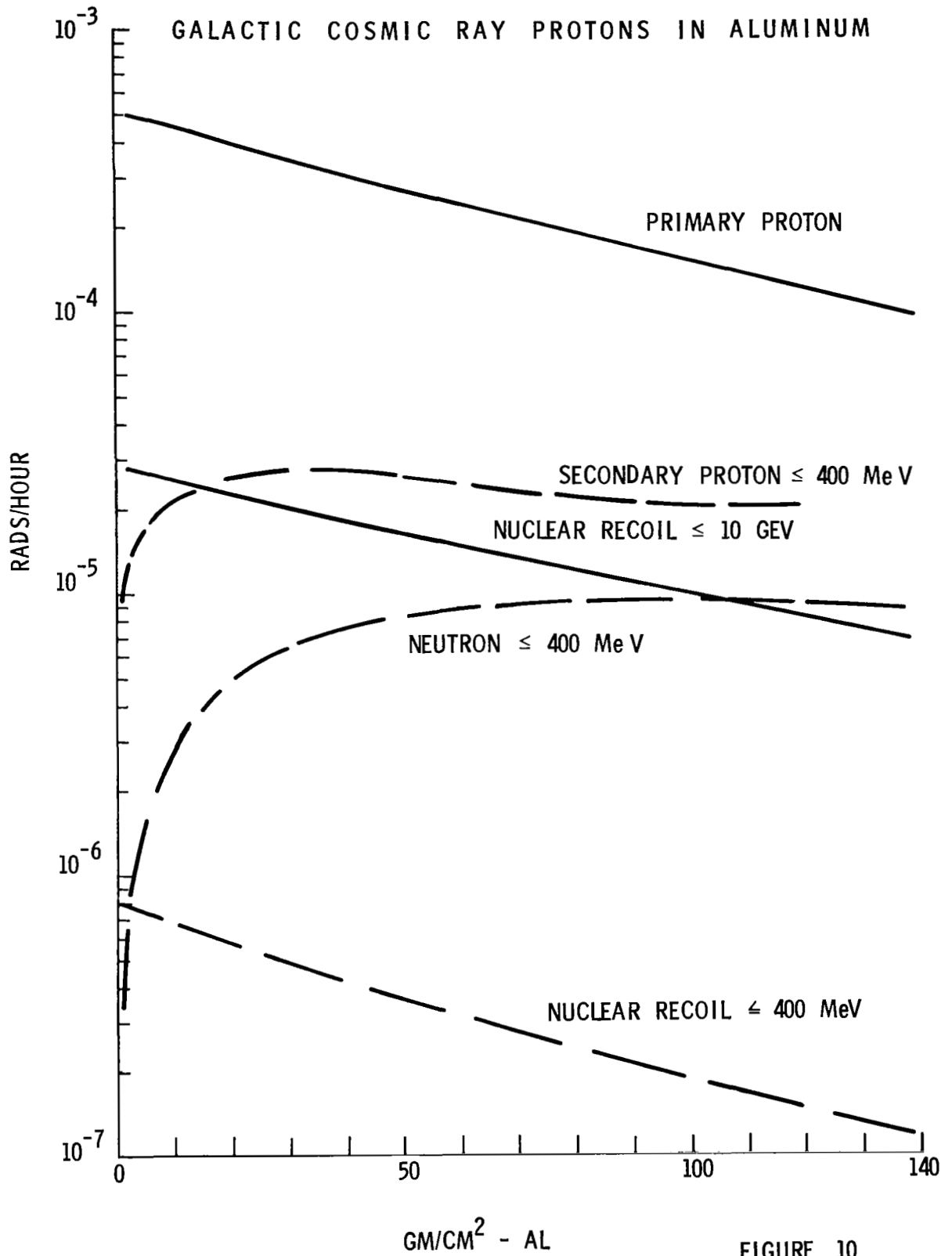
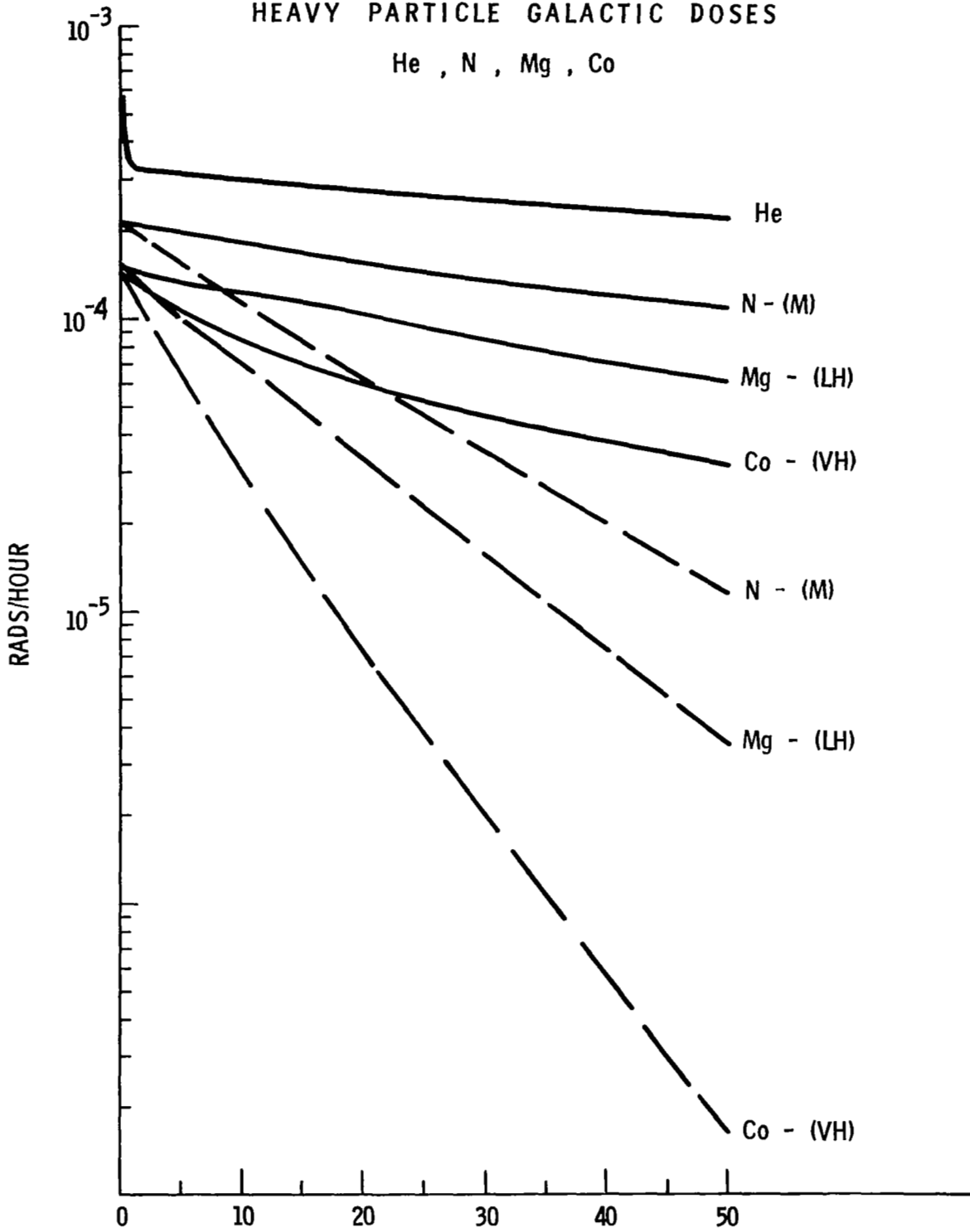


FIGURE 10

HEAVY PARTICLE GALACTIC DOSES

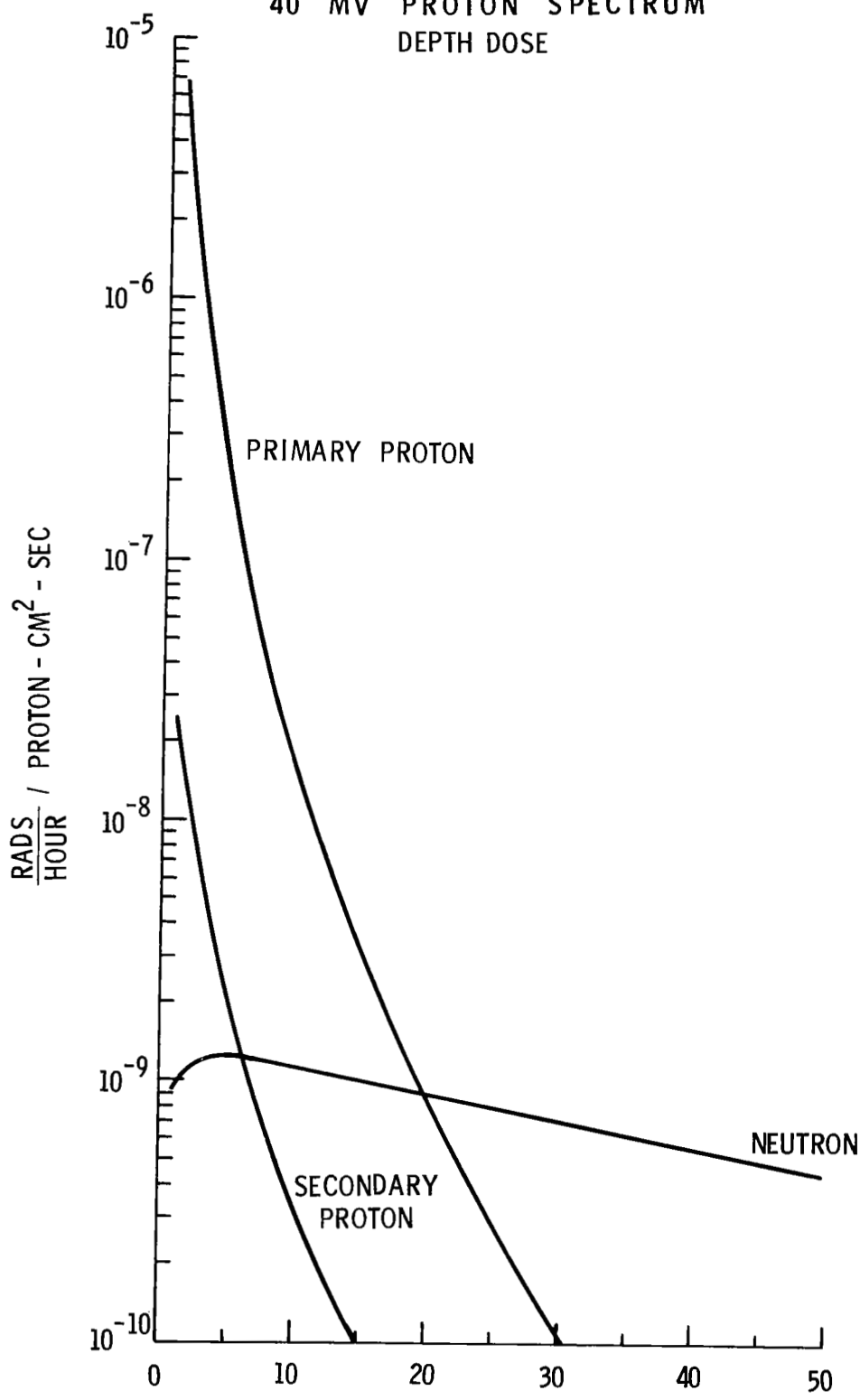
He , N , Mg , Co



GM/CM² - AL

FIGURE 11

40 MV PROTON SPECTRUM
DEPTH DOSE



GM/CM² ALUMINUM
FIGURE 12

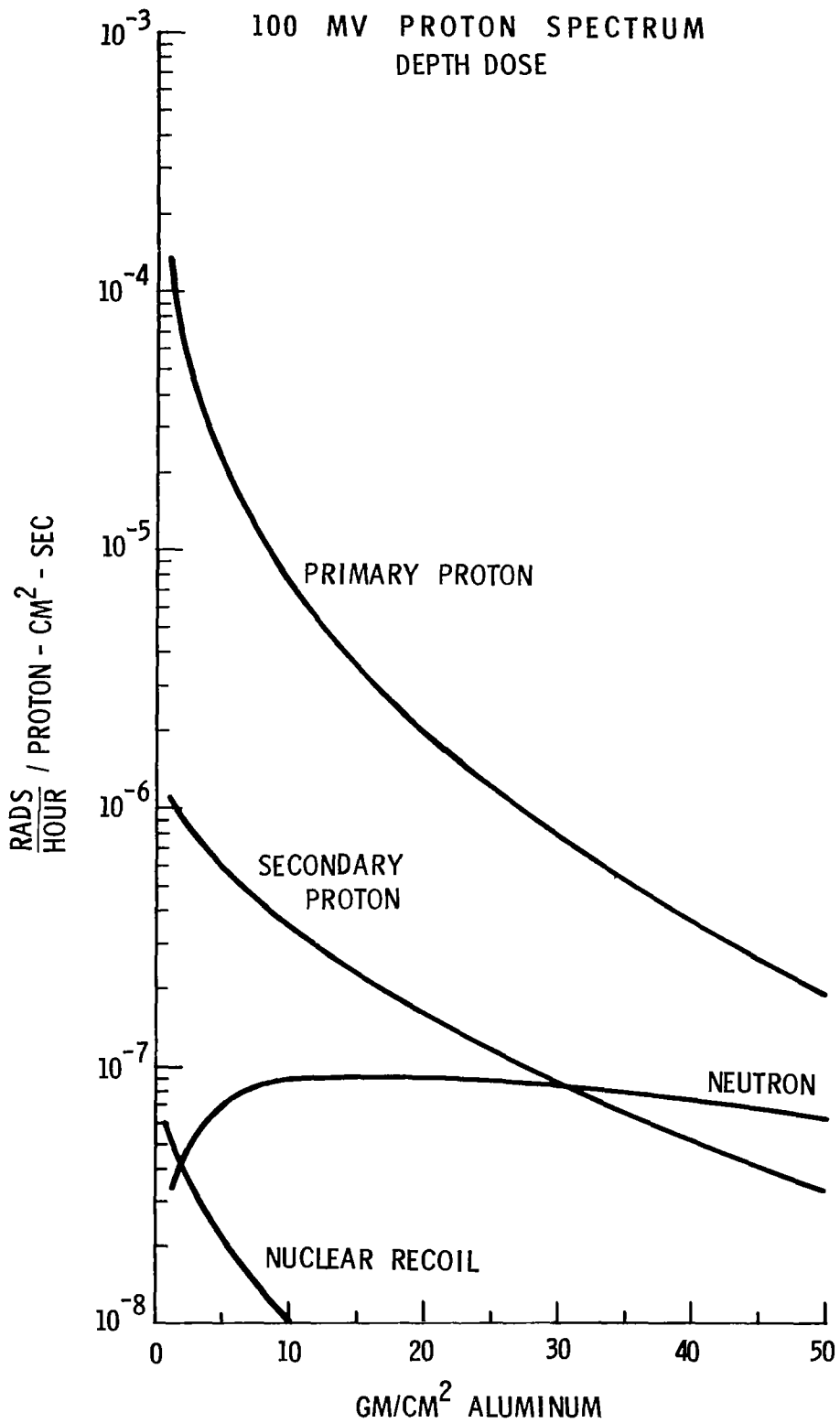


FIGURE 13

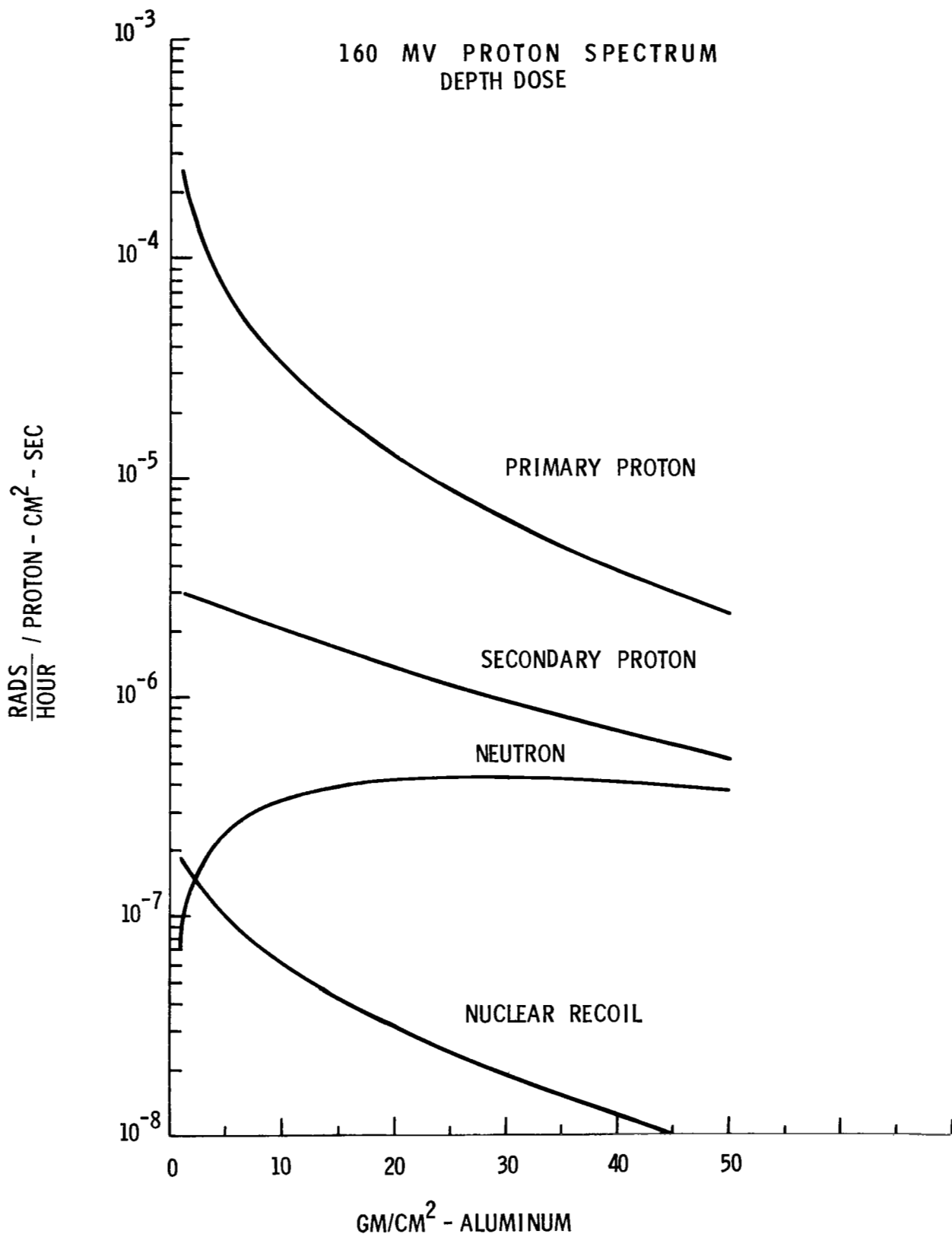


FIGURE 14

DEPTH - DOSE PLOTS FOR 40, 100, & 160 MV
RIGIDITY INCIDENT ALPHA SPECTRUM

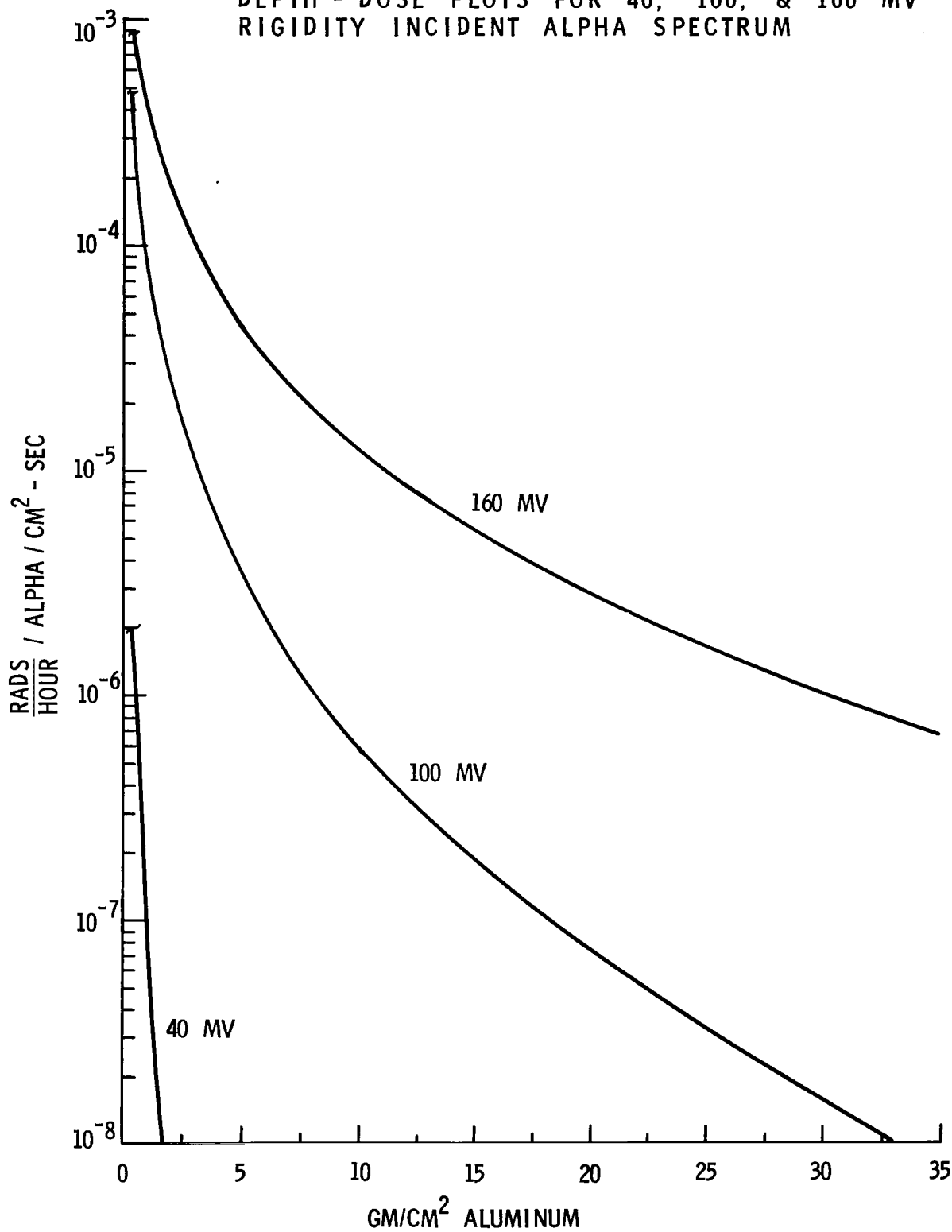
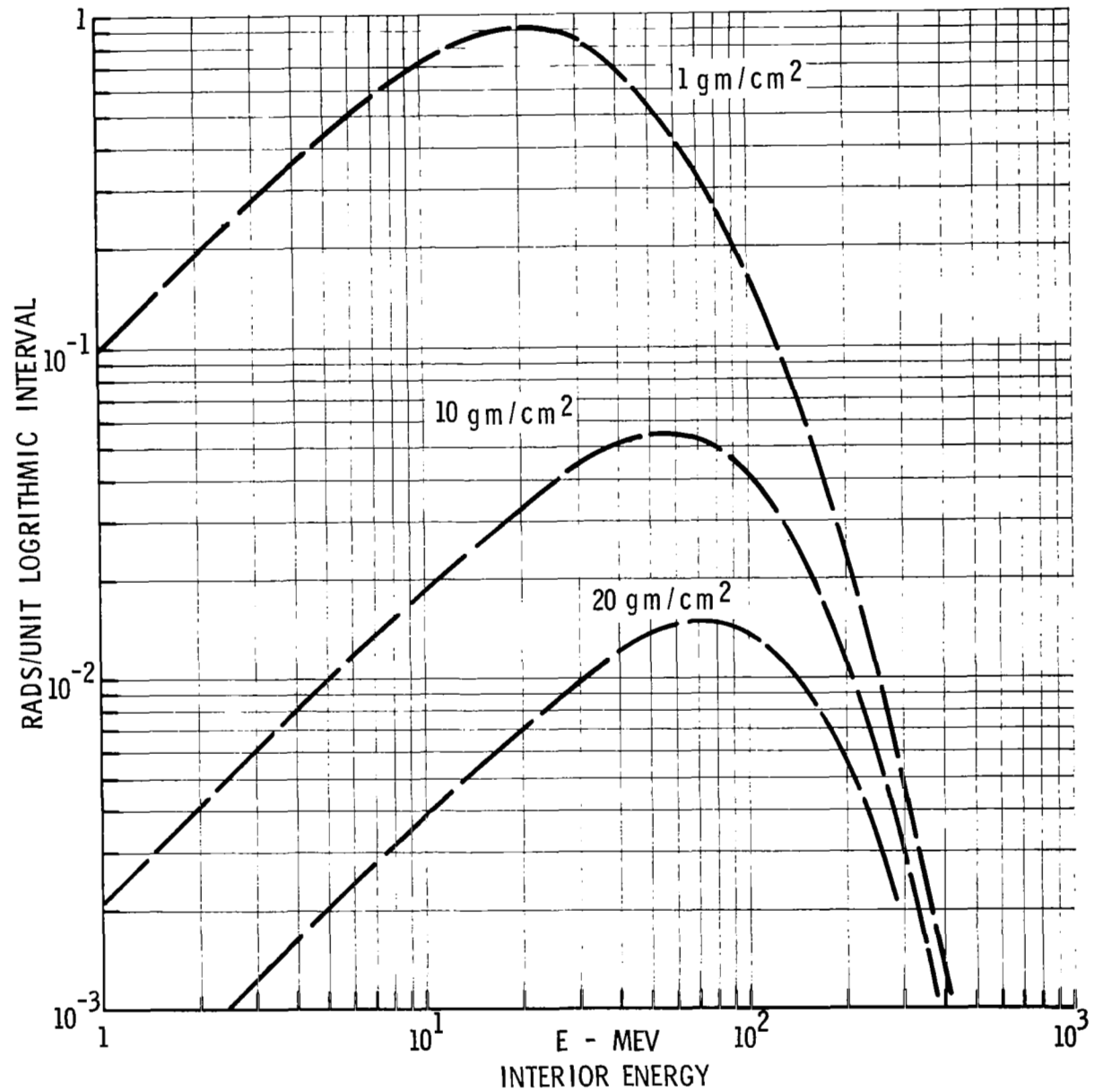


FIGURE 15

DIFFERENTIAL DOSE
DISTRIBUTIONS
FOR 100 MEV
RIGIDITY SPECTRA
PROTONS INCIDENT
ON ALUMINUM

FIGURE 16



DIFFERENTIAL DOSE DISTRIBUTION FOR 40 AND 160 MV RIGIDITY SPECTRA PROTONS INCIDENT ON ALUMINUM

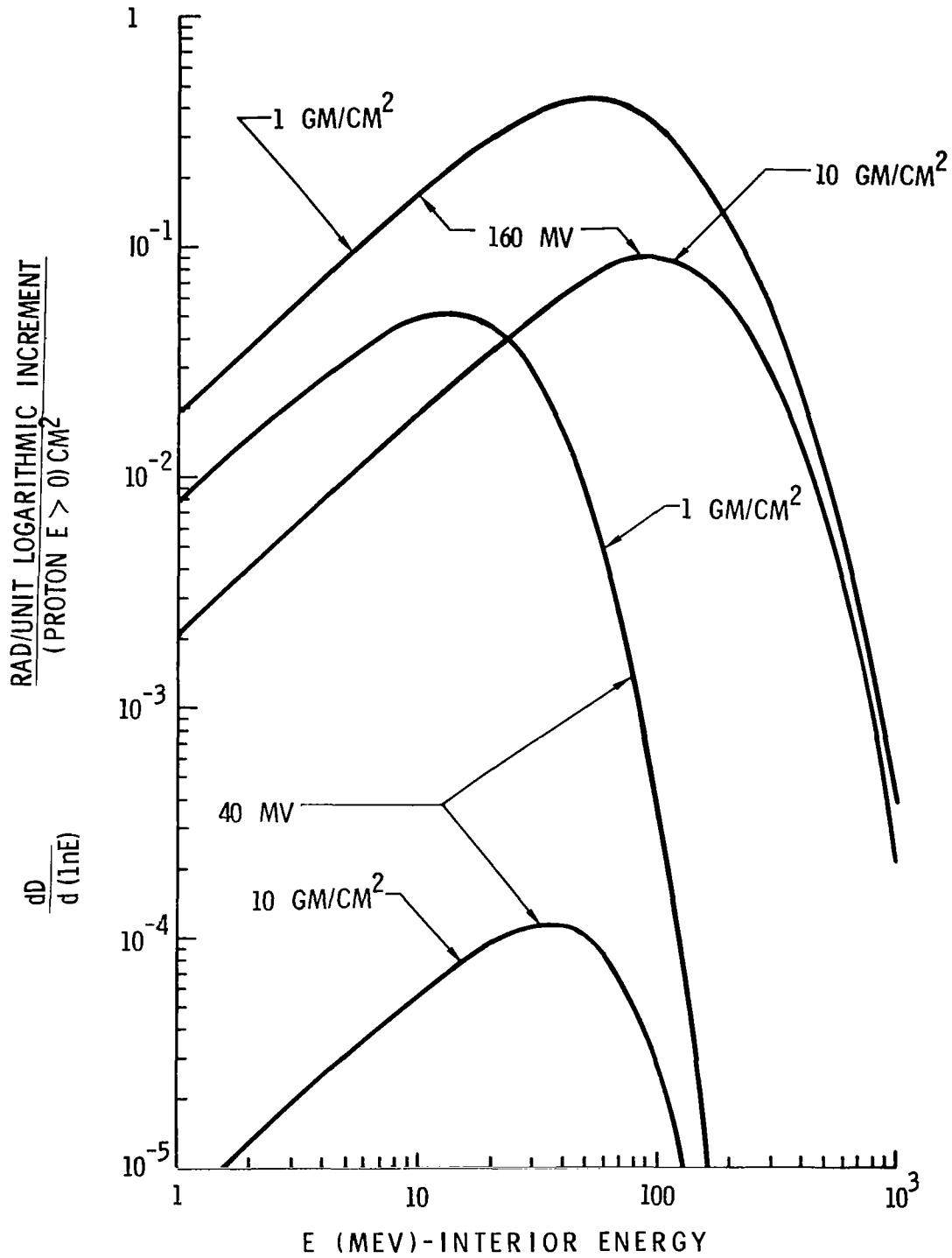


FIGURE 17

DIFFERENTIAL DOSE DISTRIBUTION FOR GALACTIC
COSMIC - RAY PROTONS

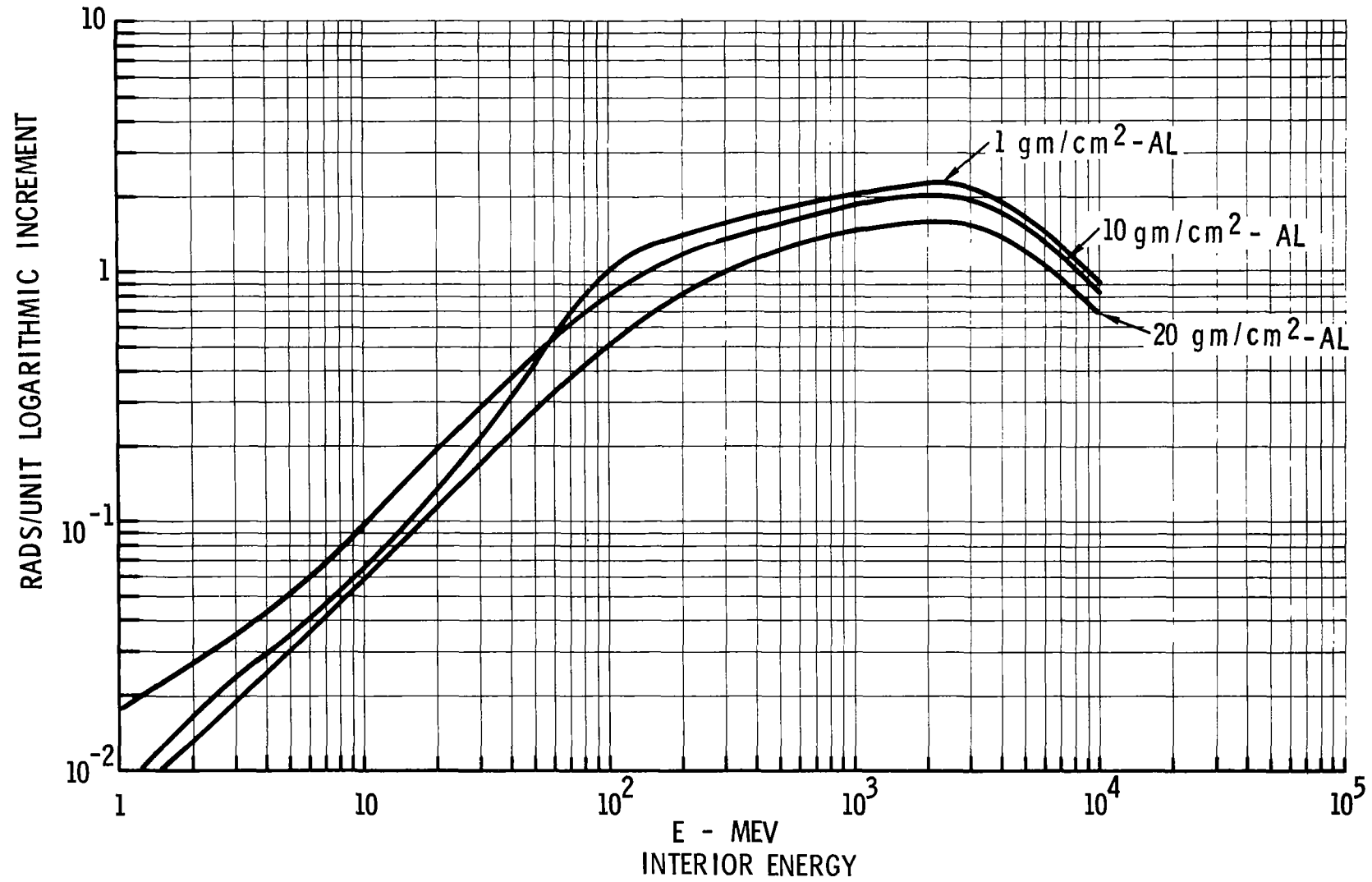


FIGURE 18

DOSE PER UNIT LOG INTERVAL FOR HELIUM,
NITROGEN (M), MAGNESIUM (LH), AND COBALT (VH)

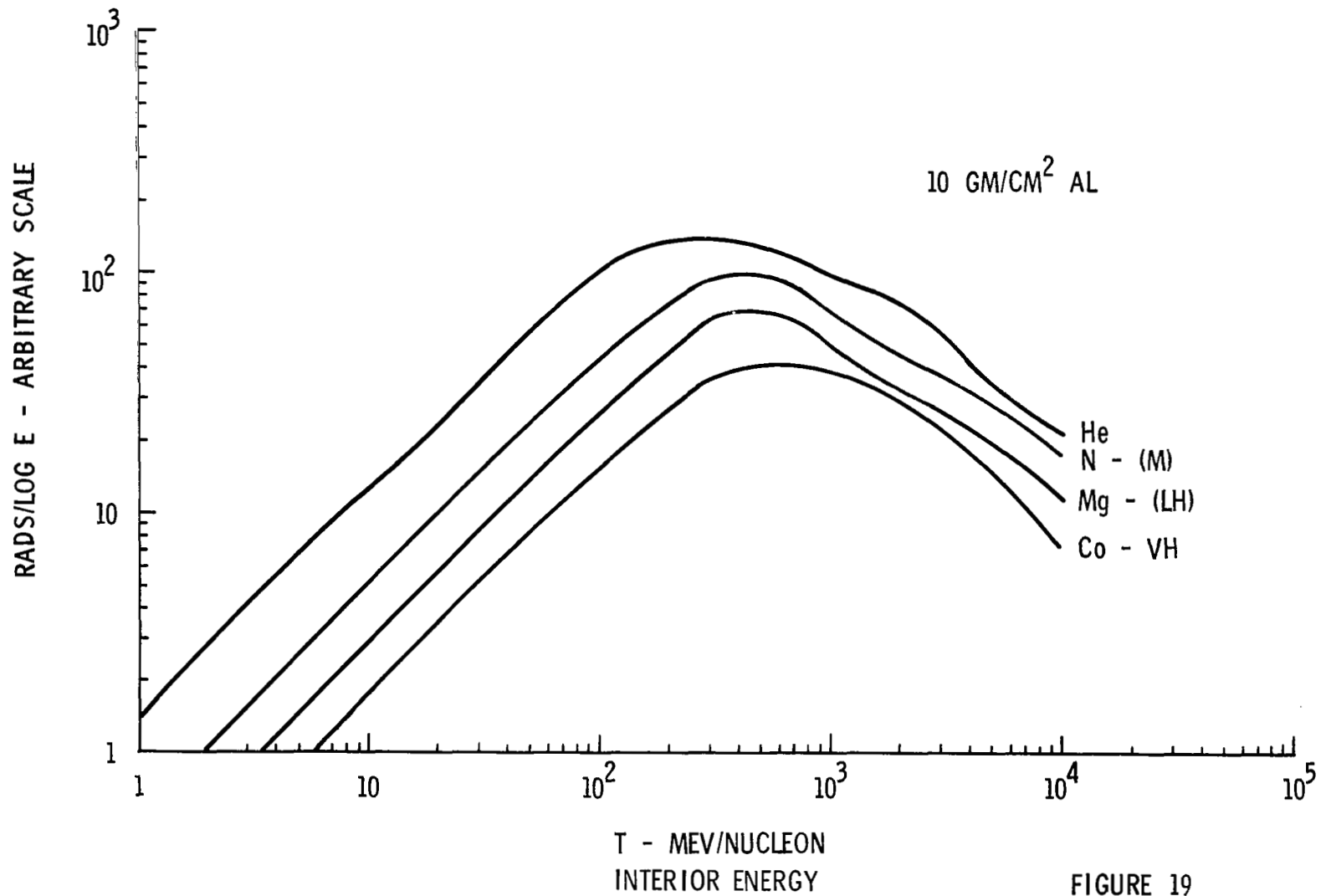


FIGURE 19

PENETRATING PROTON NUMBER-ENERGY SPECTRUM
IN VARIOUS DEPTHS OF ALUMINUM
40 MV SPECTRUM INCIDENT

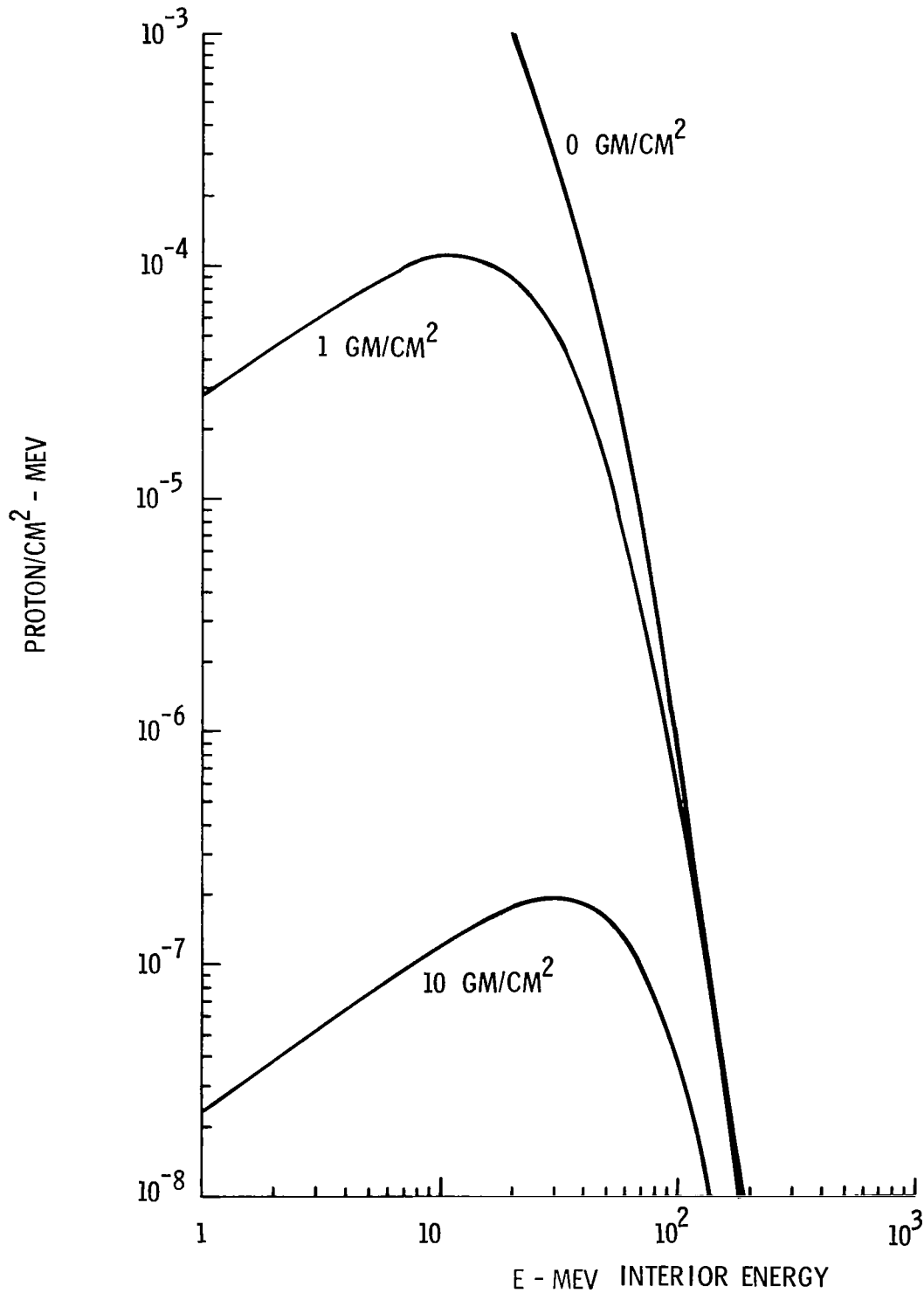
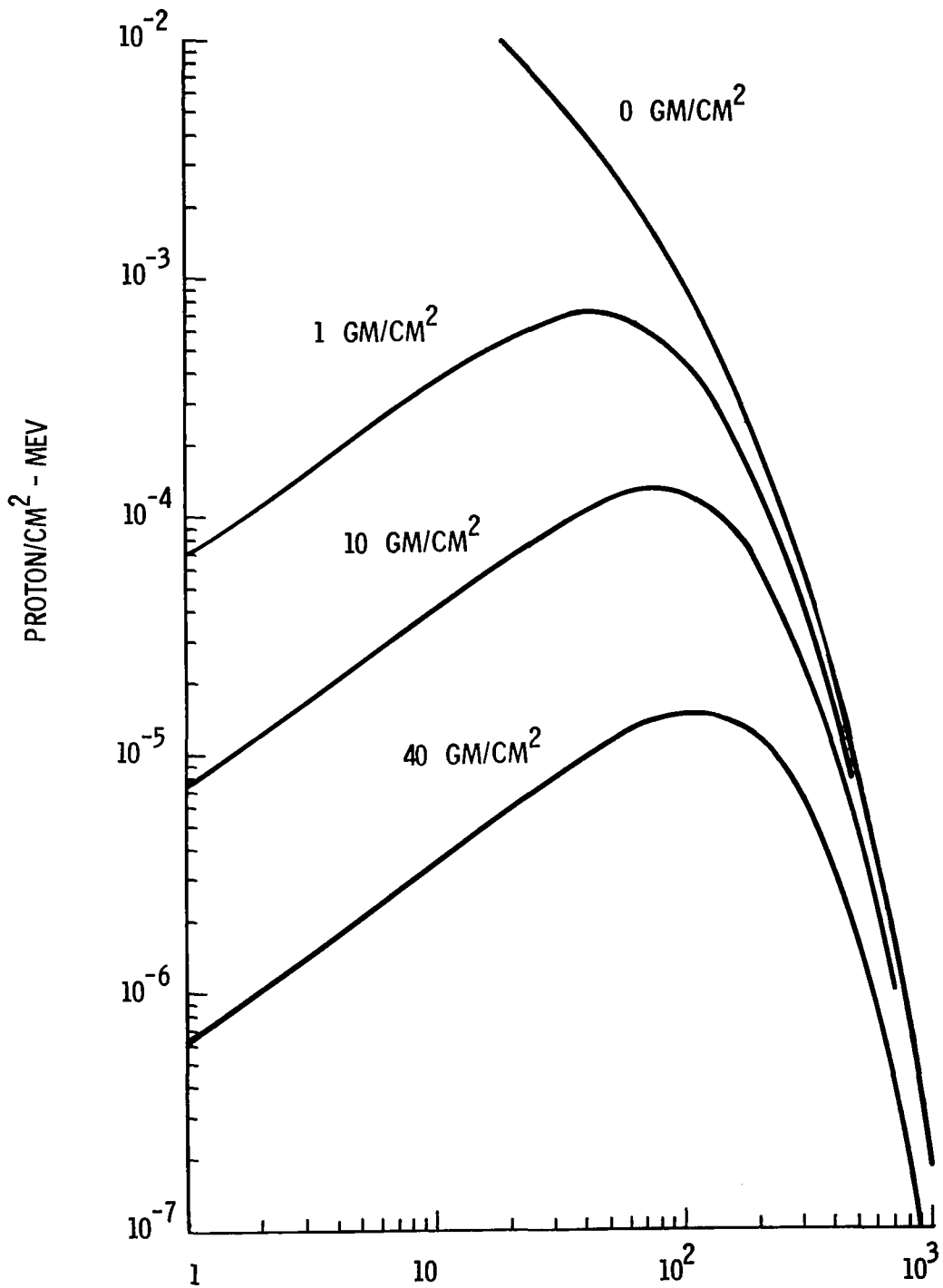


FIGURE 20

PENETRATING PROTON NUMBER-ENERGY SPECTRUM IN
VARIOUS DEPTHS OF ALUMINUM
160 MV SPECTRUM INCIDENT



E - MEV INTERIOR ENERGY

FIGURE 21

PENETRATING PROTON NUMBER-LET SPECTRUM 40 MV
SPECTRUM INCIDENT

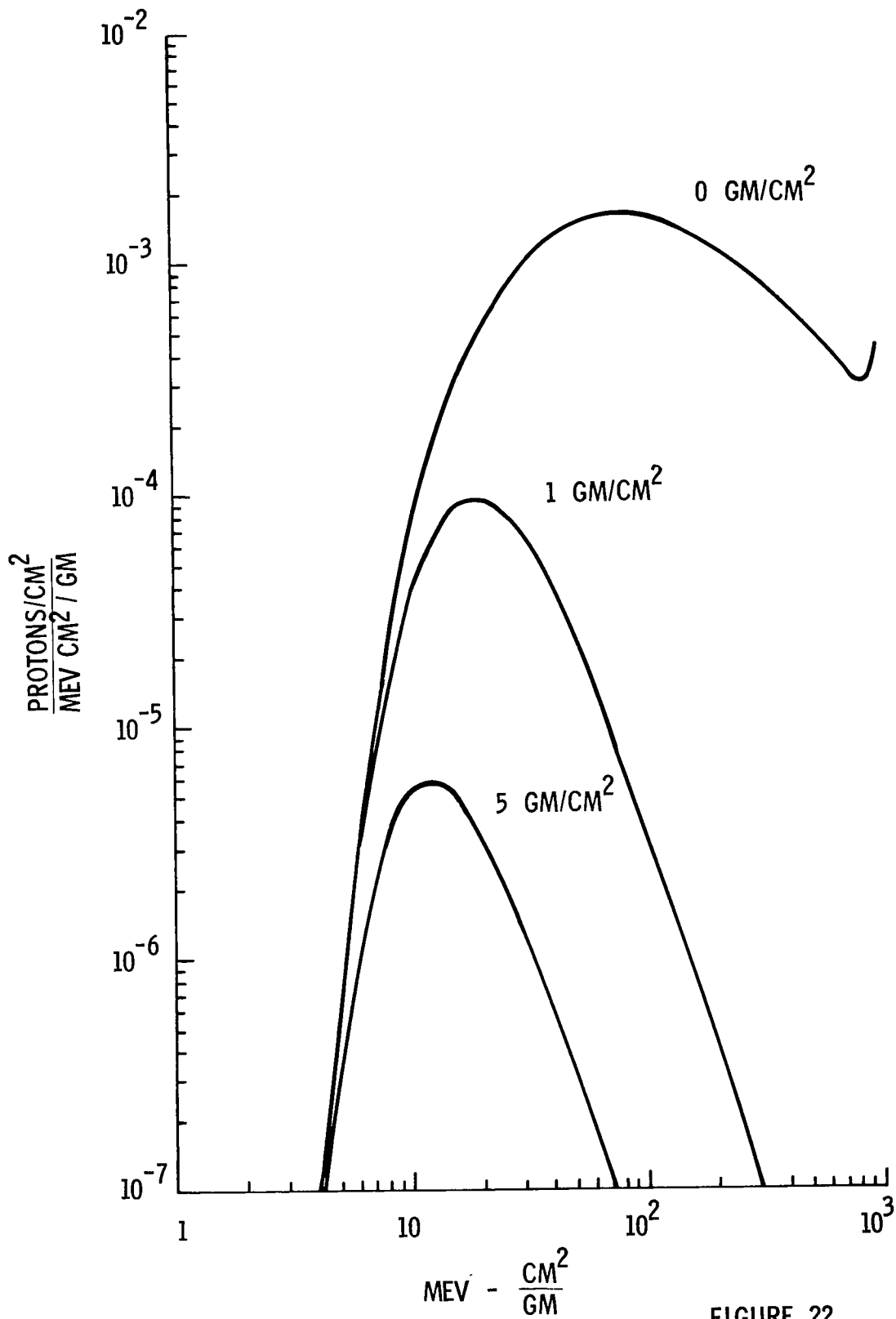


FIGURE 22

PENETRATION PROTON NUMBER - LET SPECTRUM
160 MV SPECTRUM INCIDENT

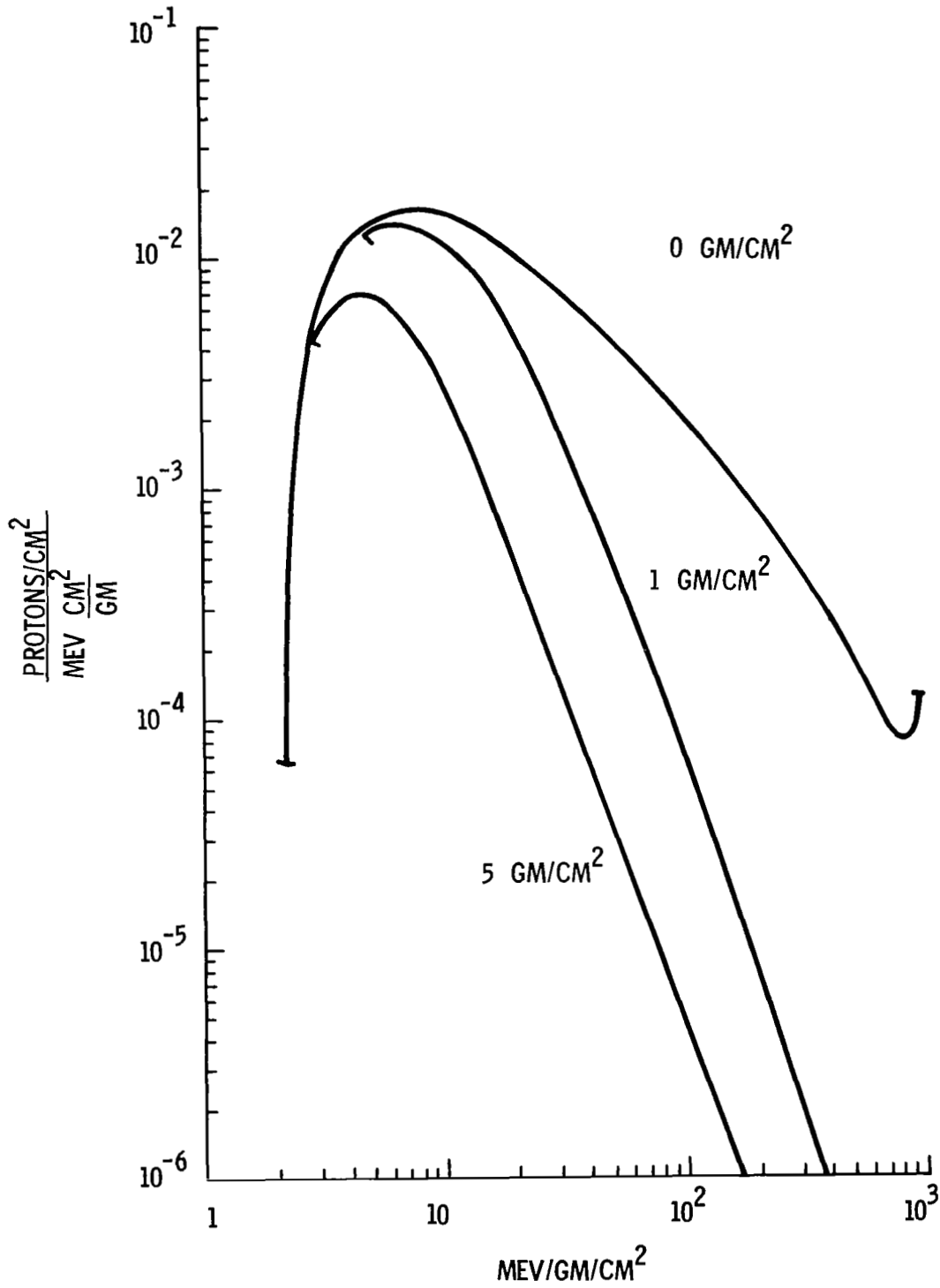


FIGURE 23

NUMBER - LET SPECTRUM
100 MV ALPHA SPECTRUM

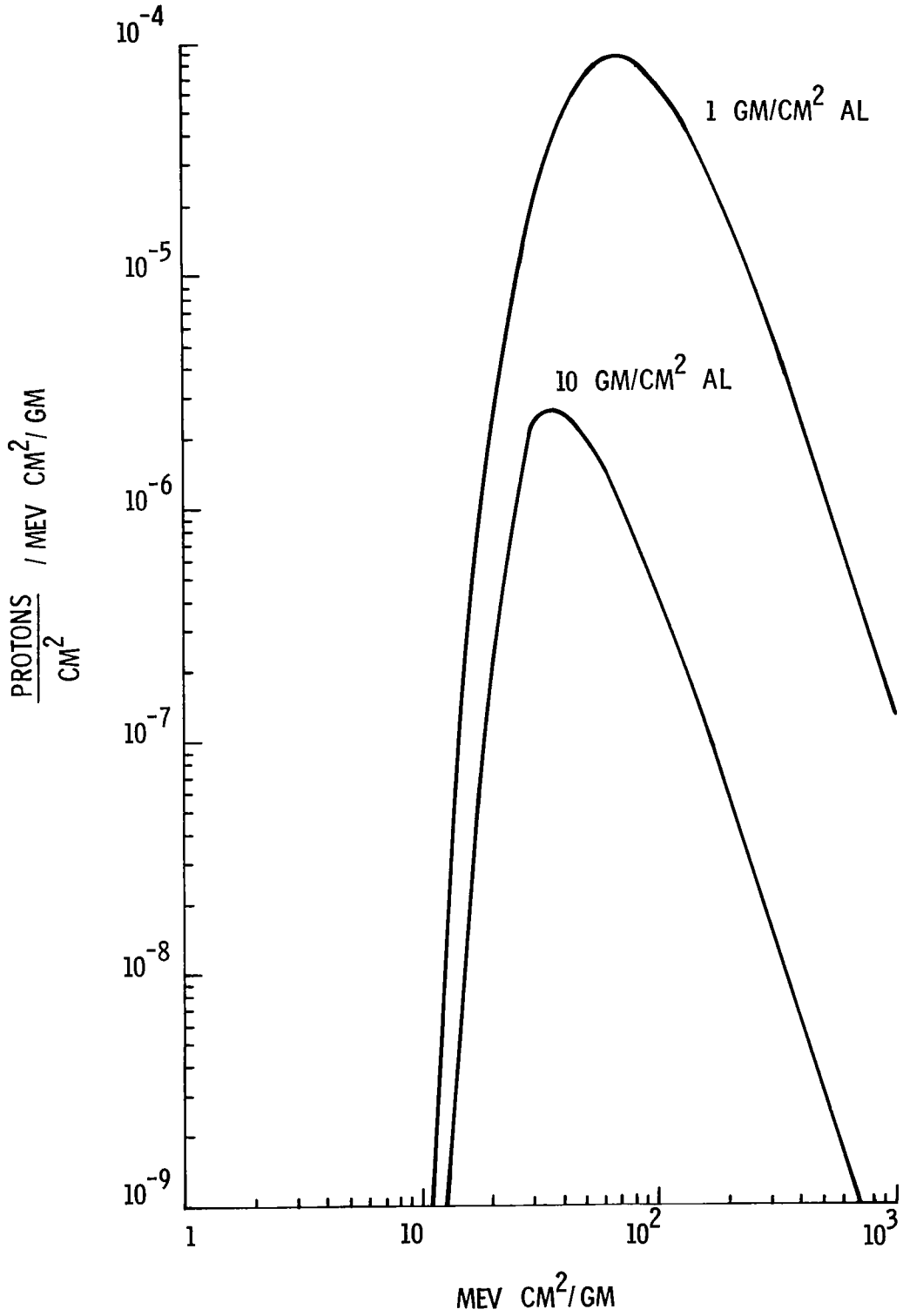


FIGURE 24

NUMBER - LET SPECTRUM
160 MV ALPHA SPECTRUM

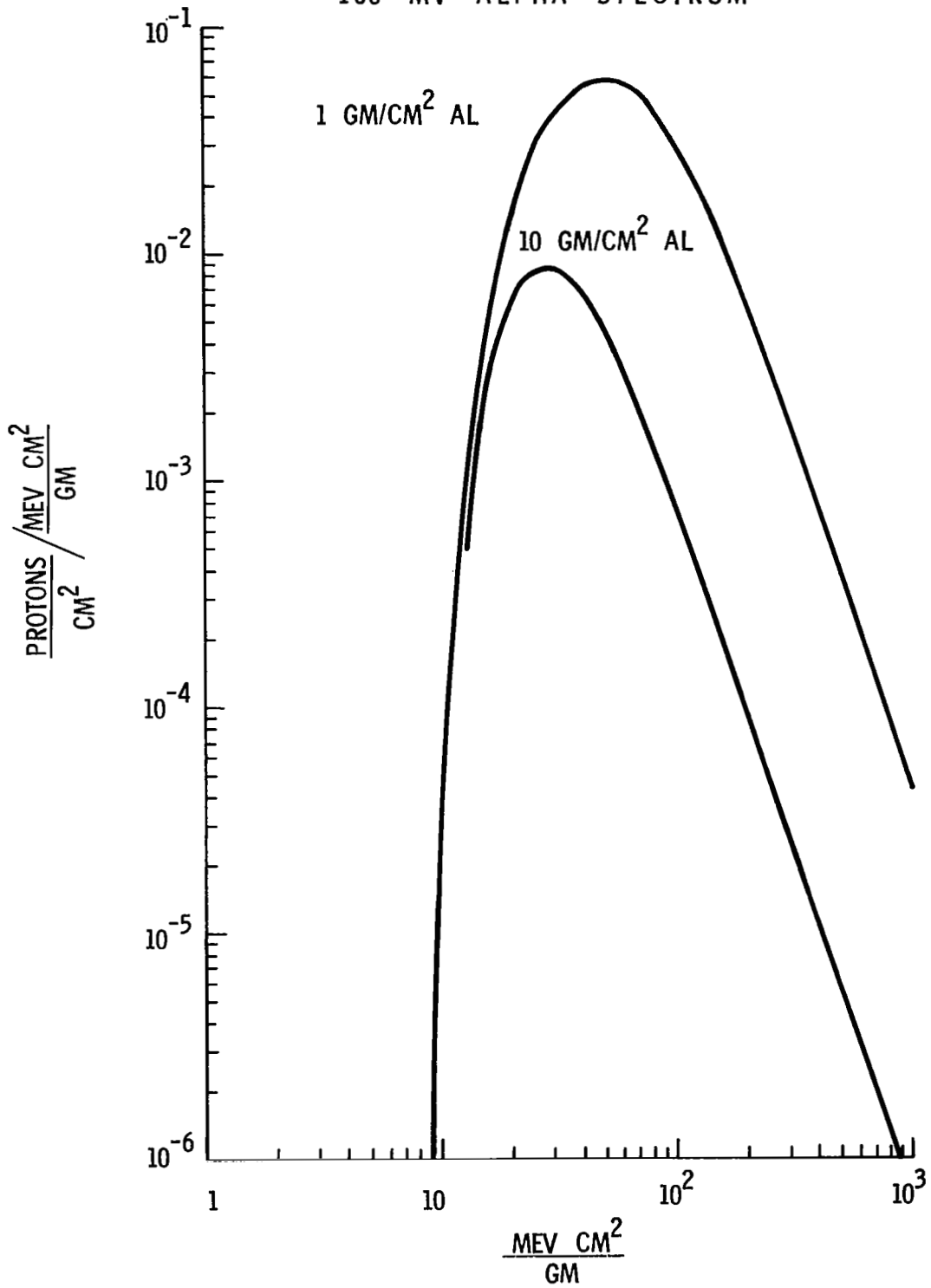
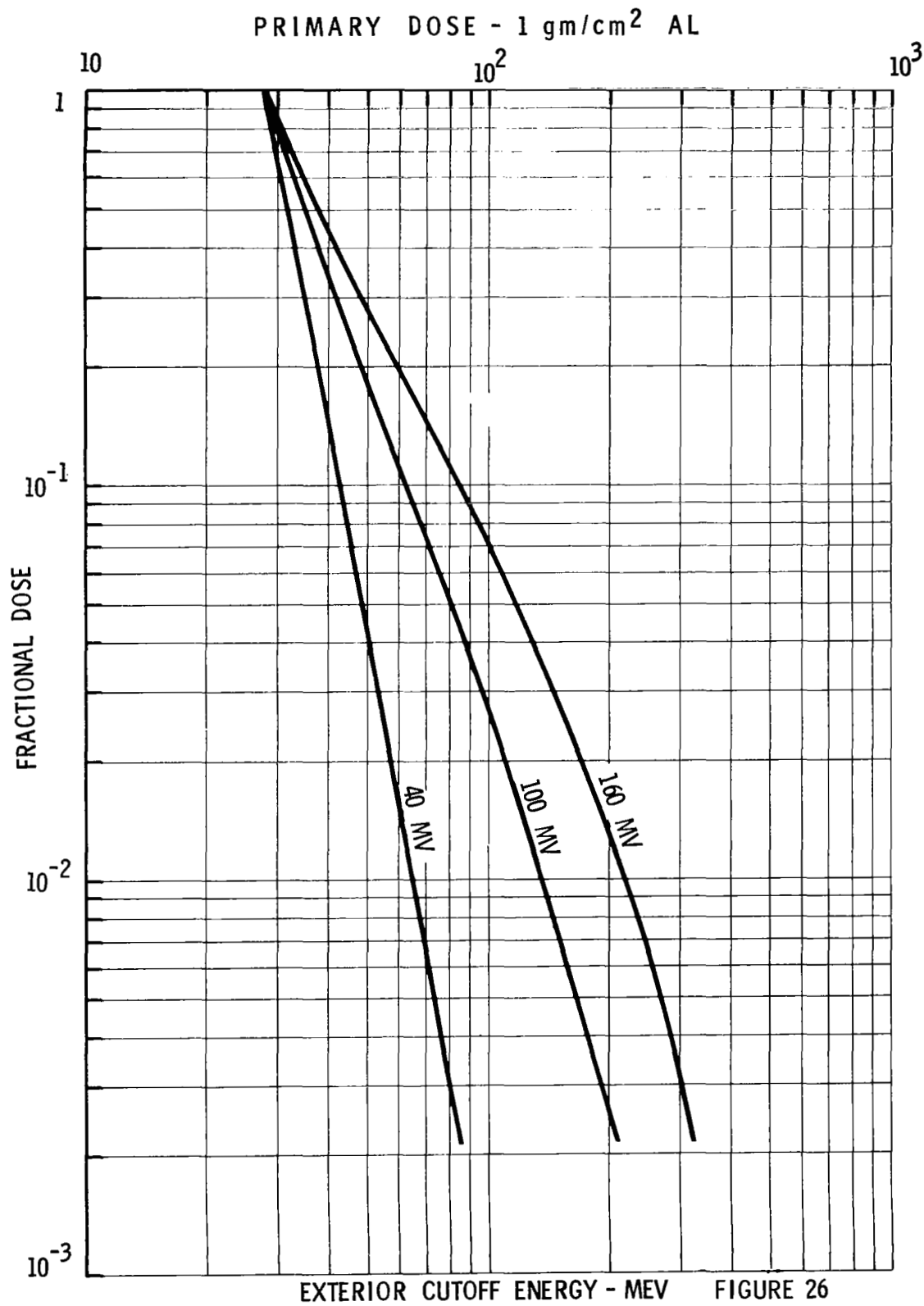


FIGURE 25



PRIMARY PROTON DOSE - 5 gm/cm² AL

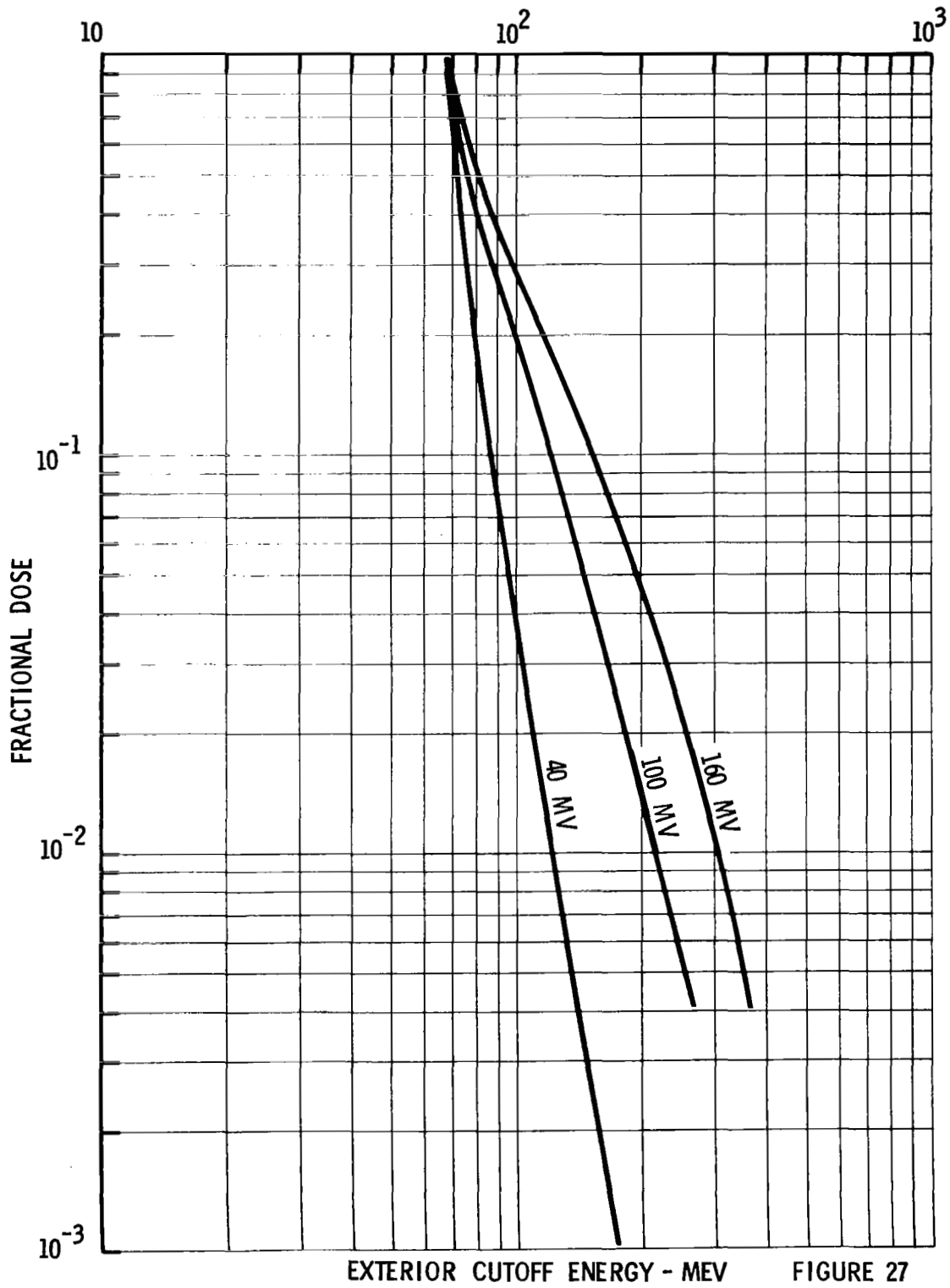
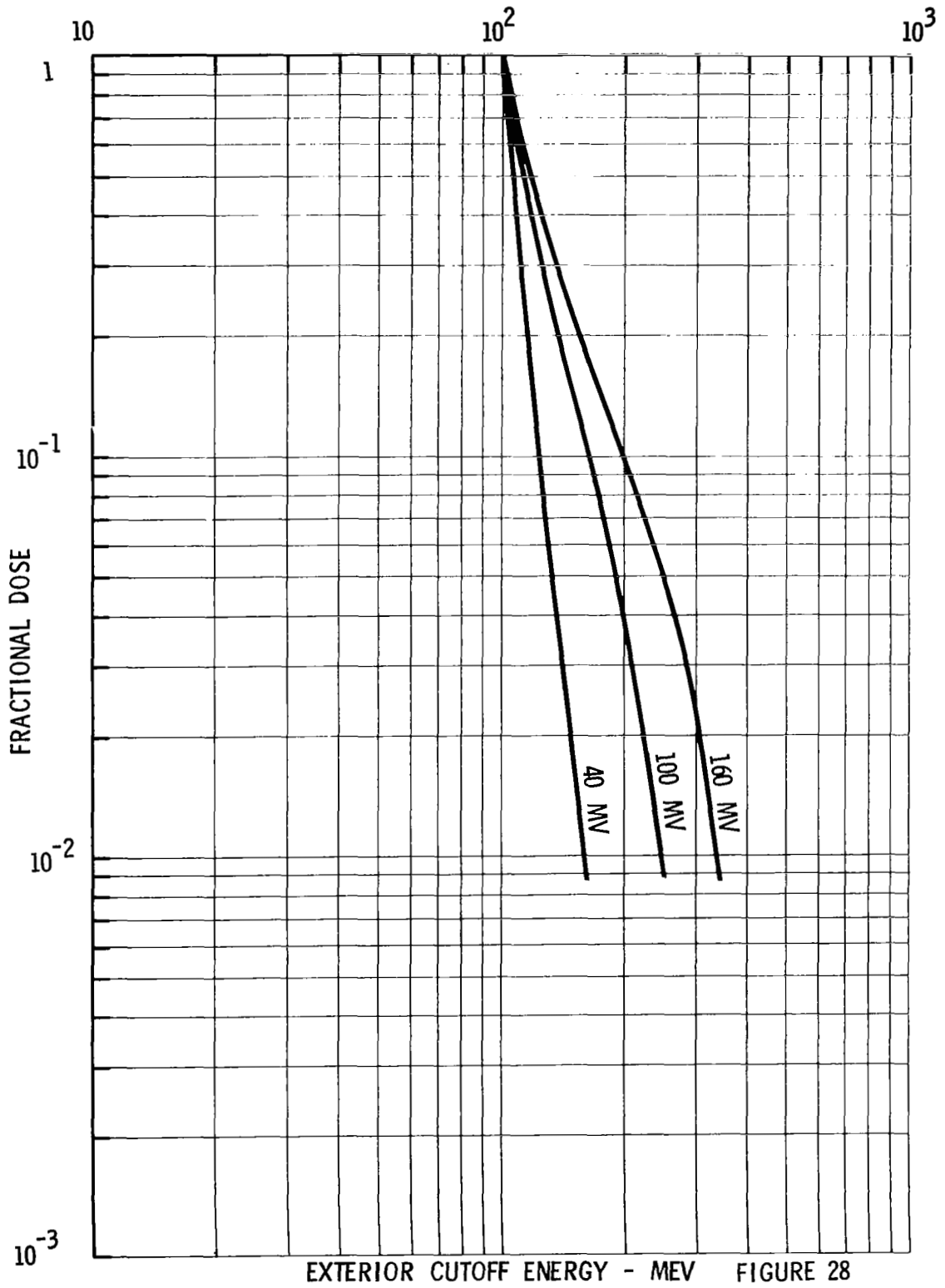
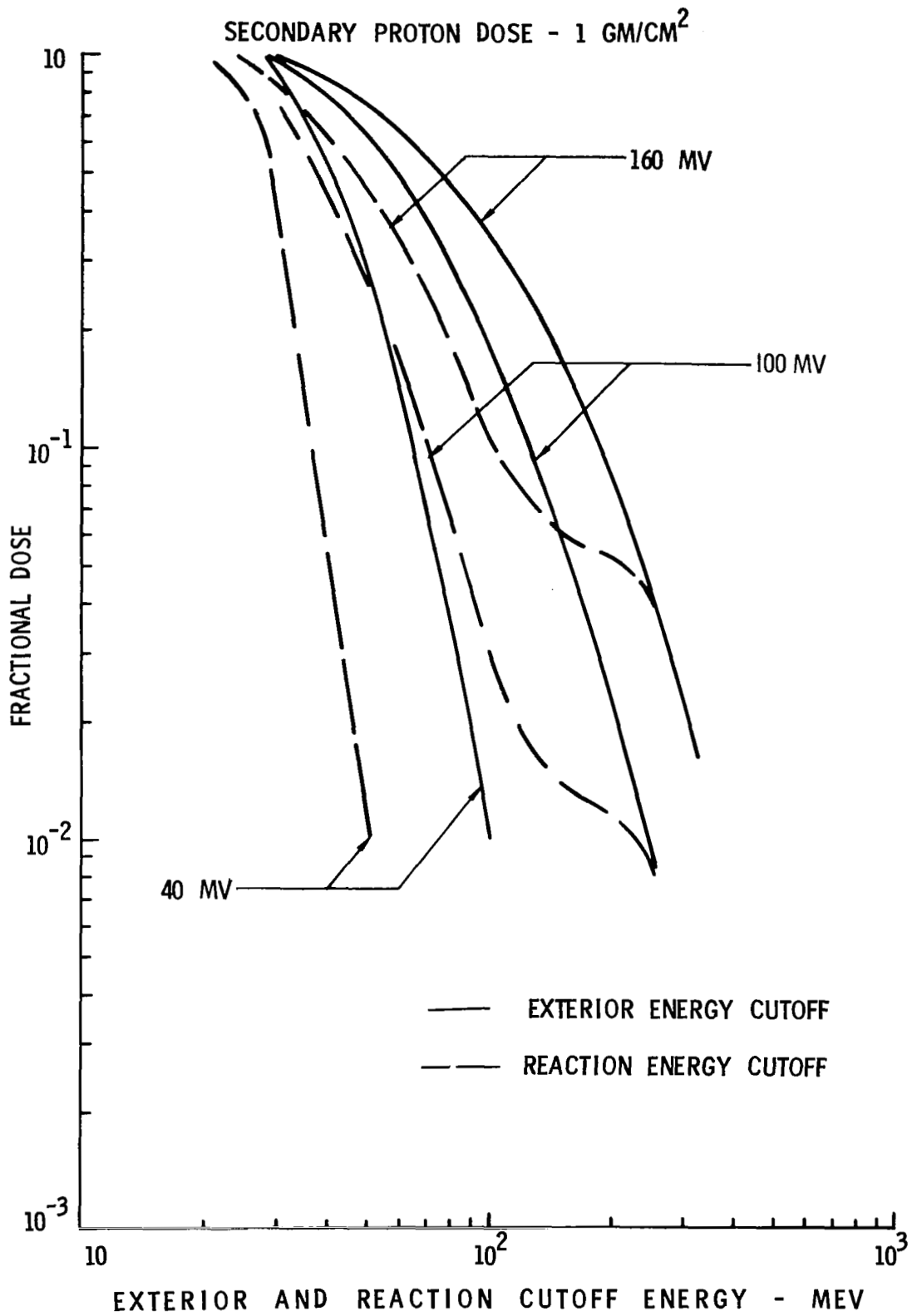


FIGURE 27

PRIMARY PROTON DOSE - 10 gm/cm²



EXTERIOR CUTOFF ENERGY - MEV FIGURE 28



SECONDARY PROTON DOSE - 5 GM/CM²

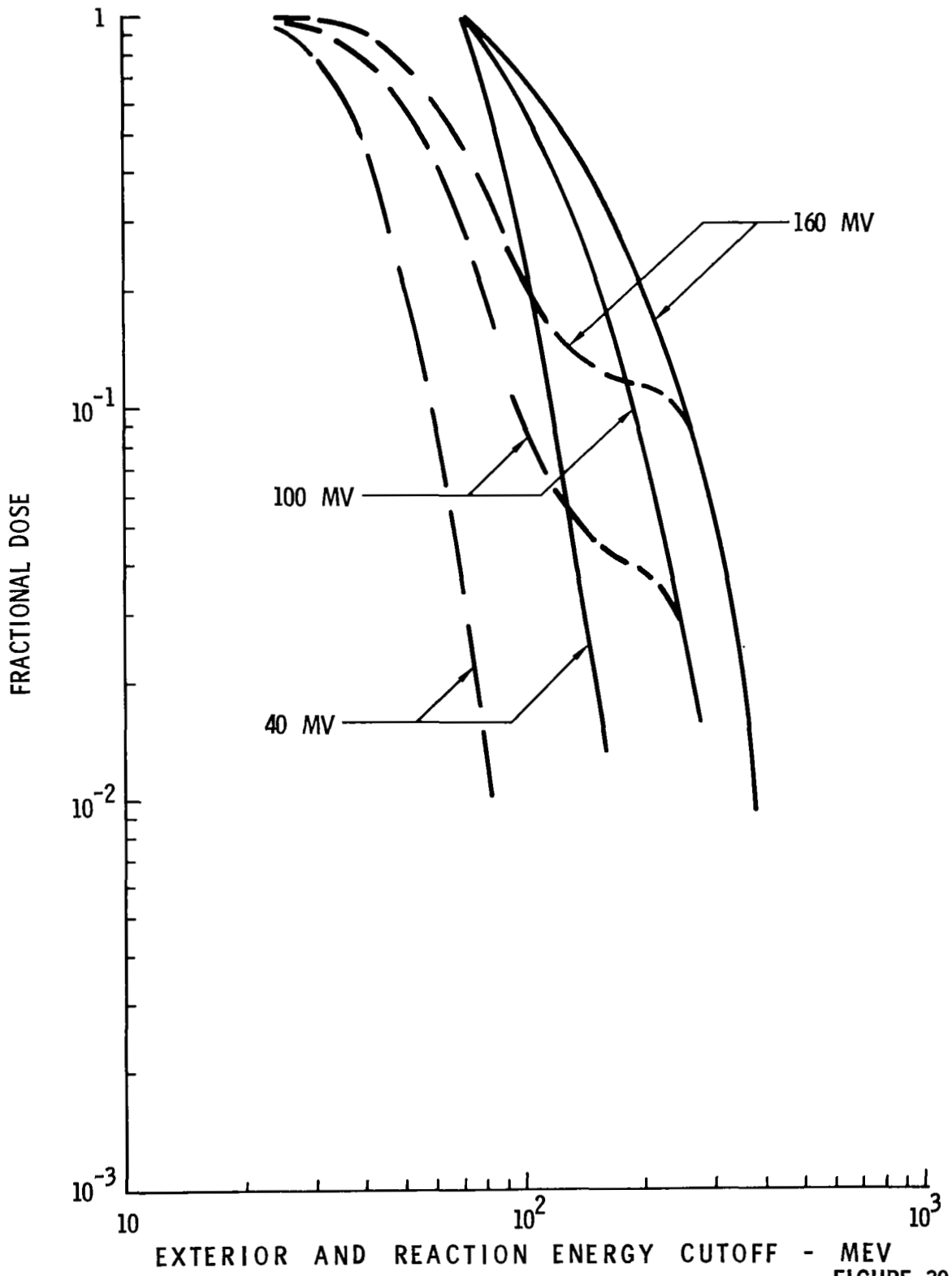


FIGURE 30

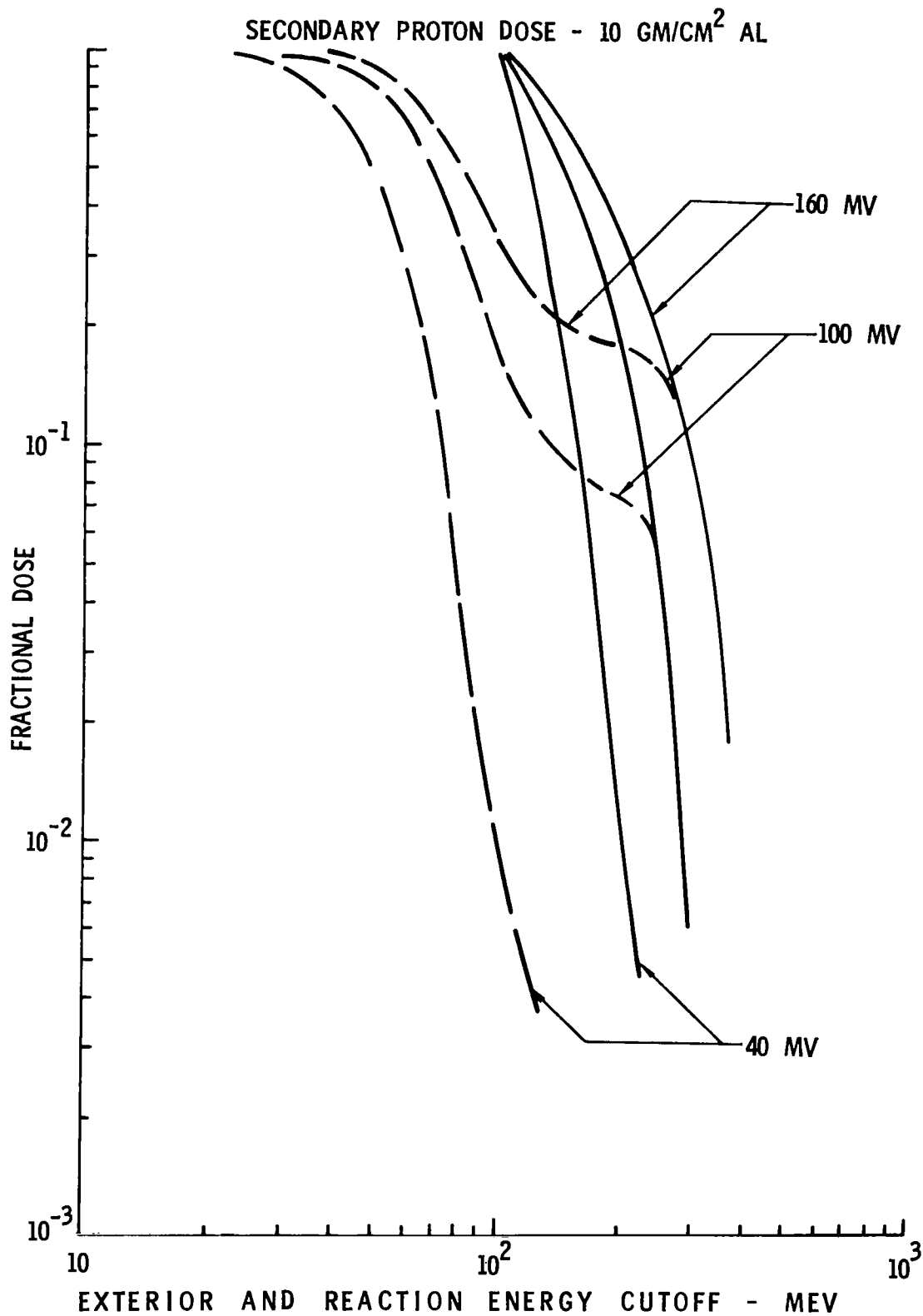


FIGURE 31

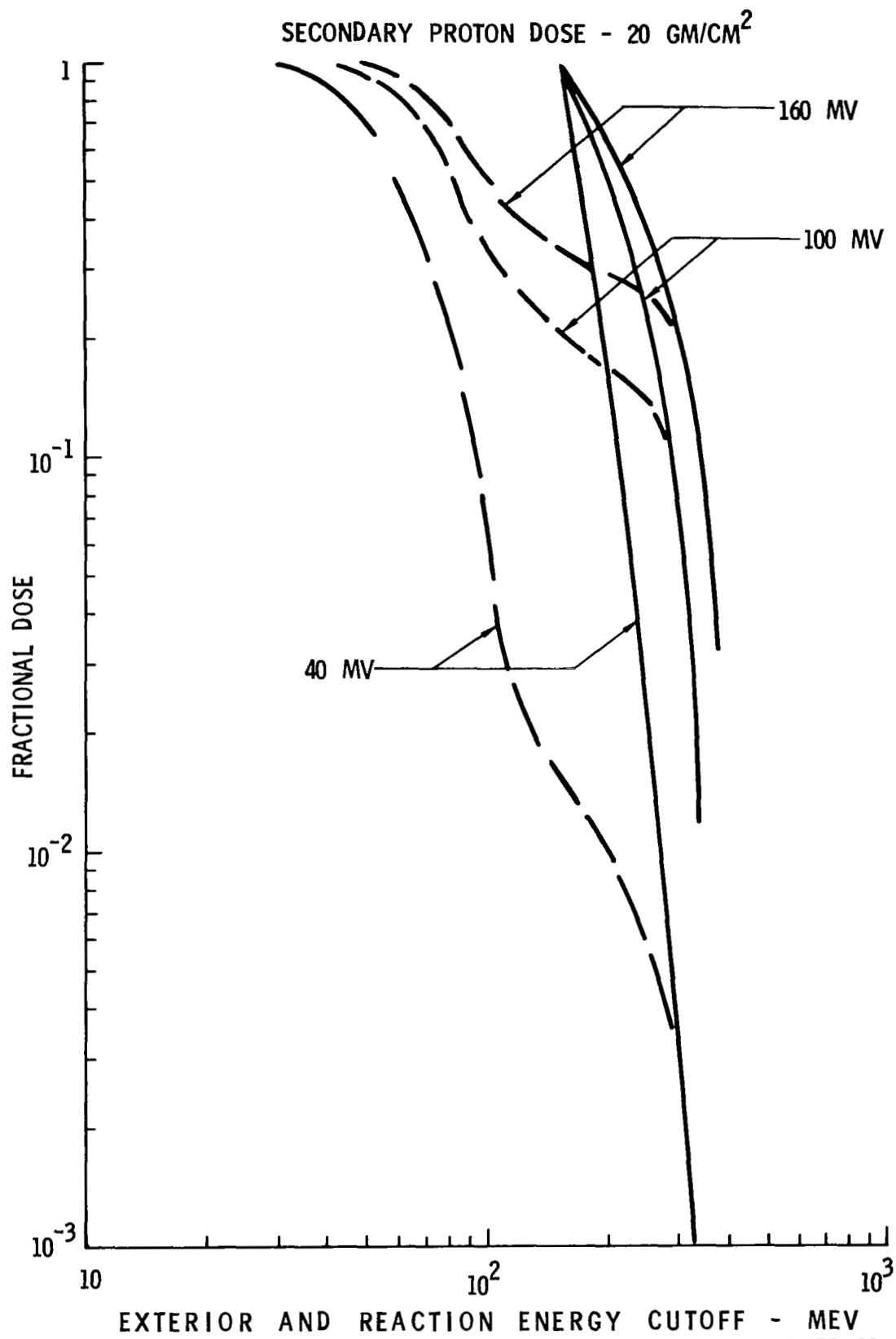


FIGURE 32

NEUTRON DOSE - 1 GM/CM²

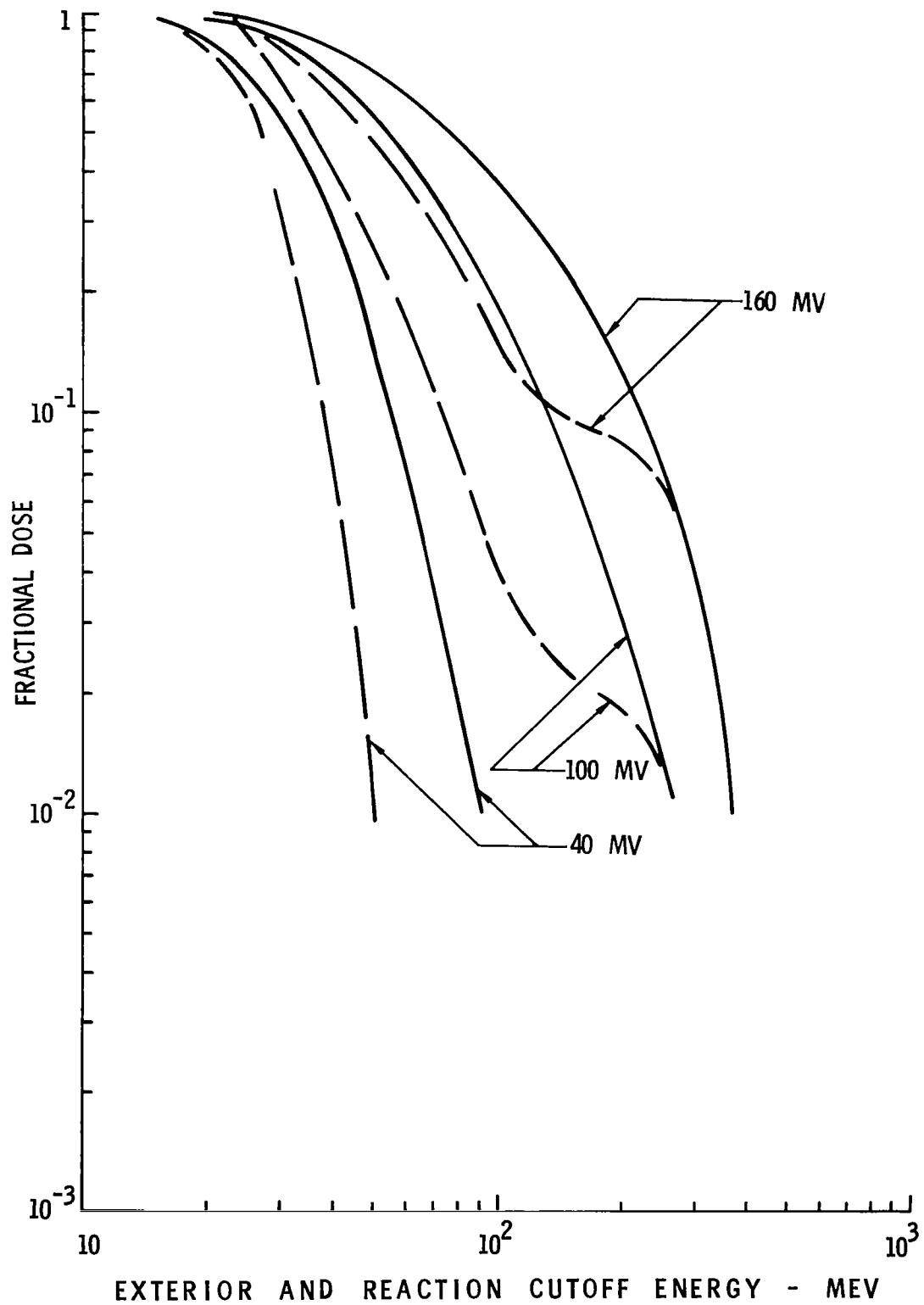


FIGURE 33

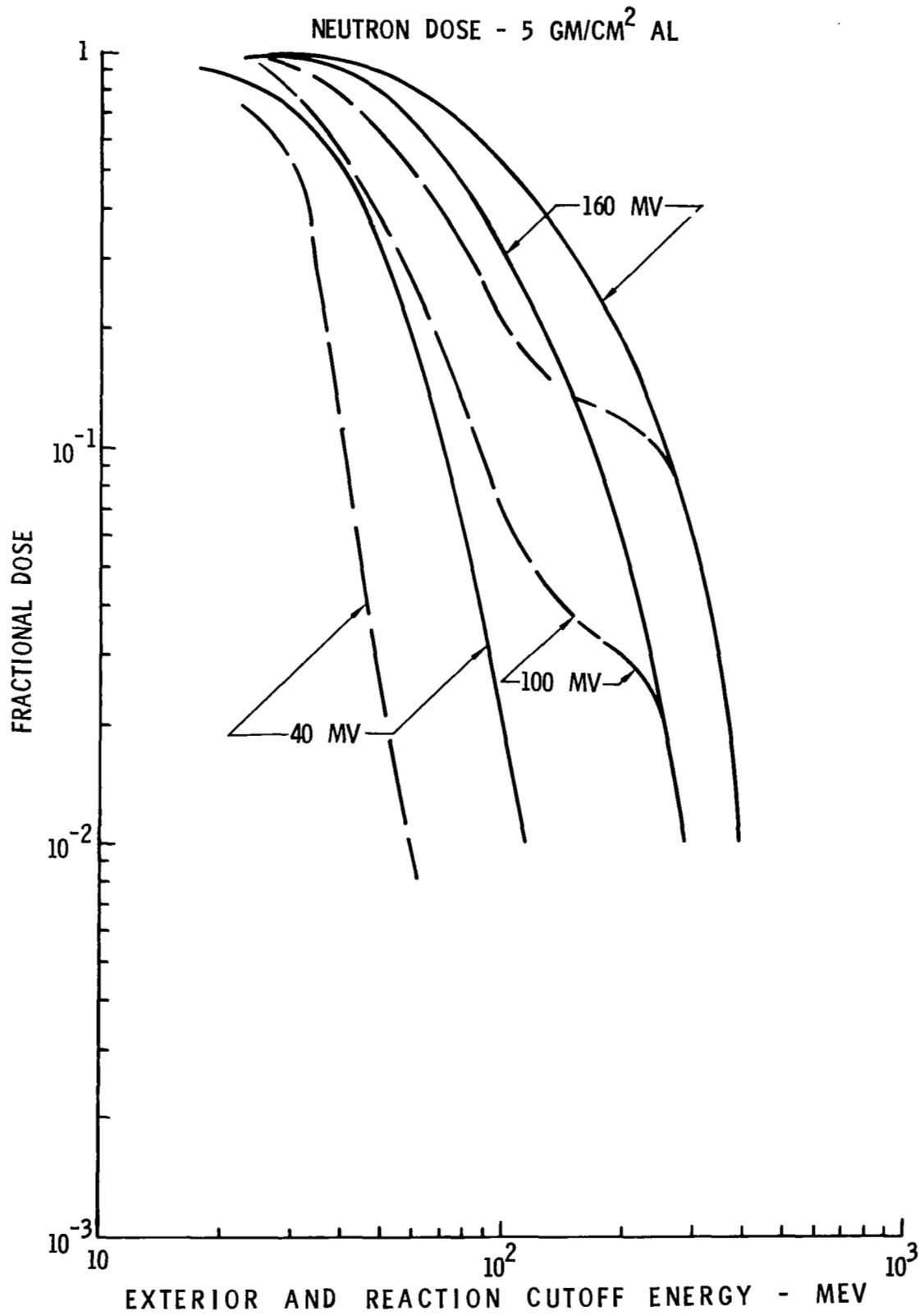


FIGURE 34

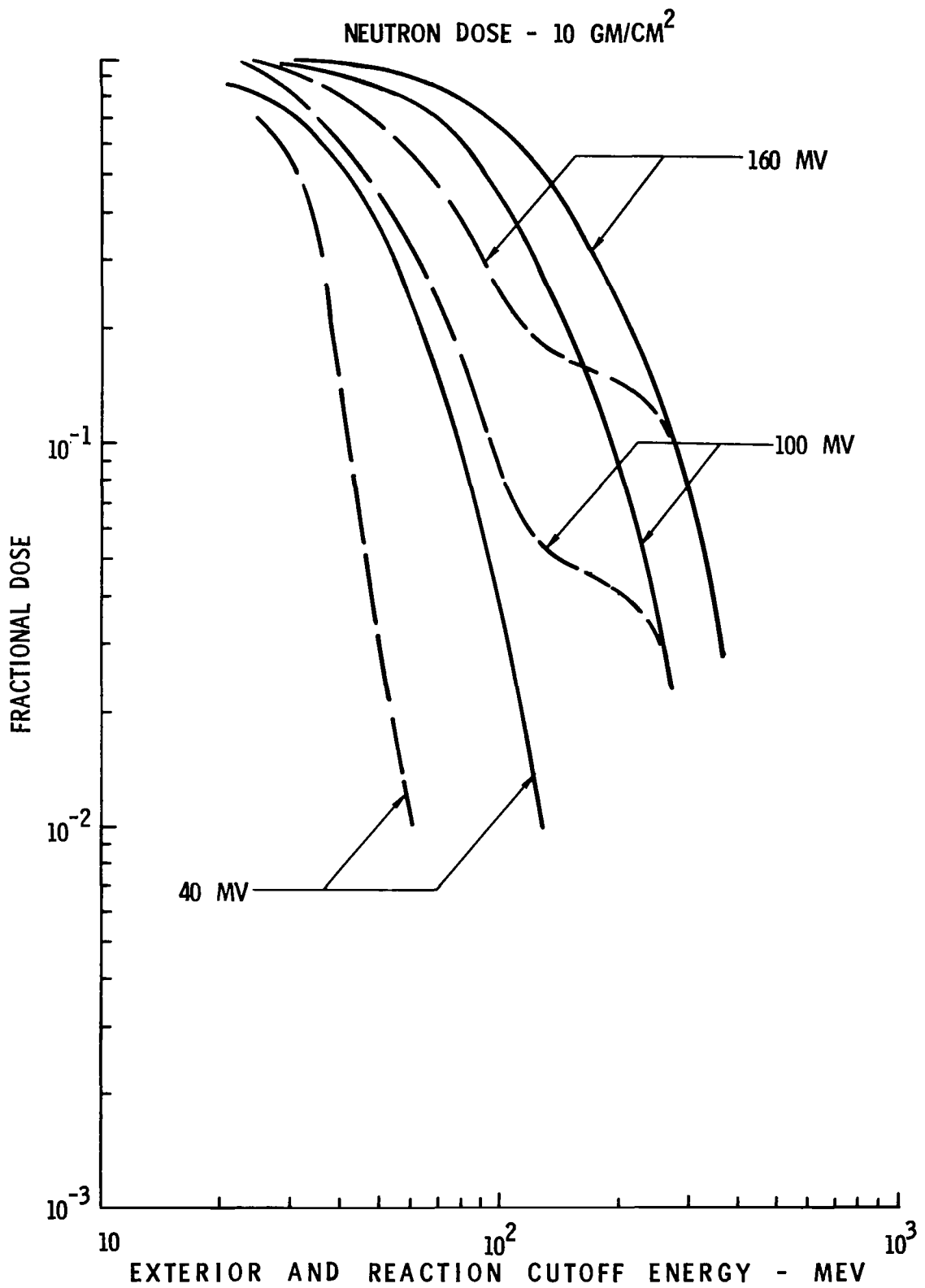


FIGURE 35

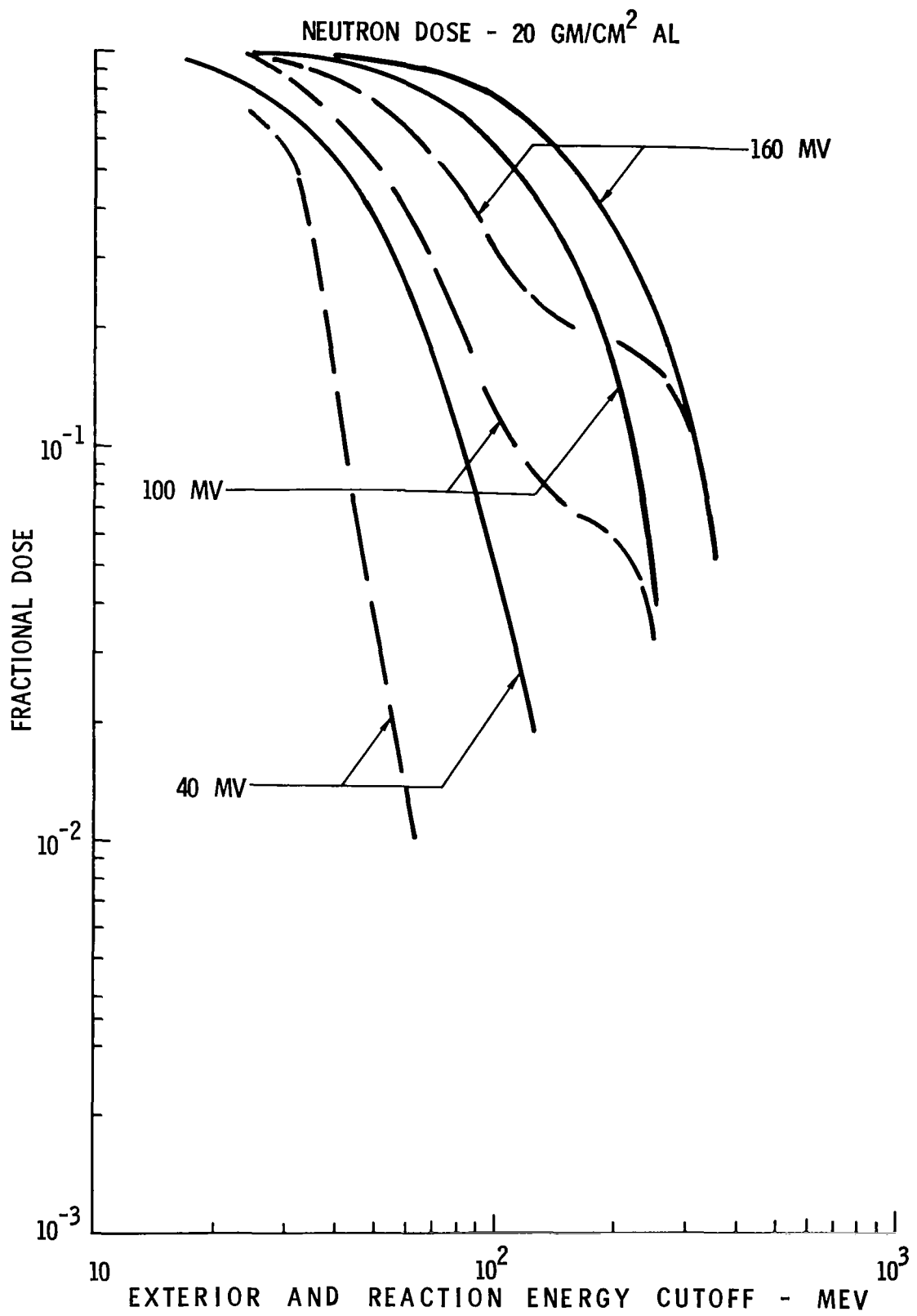


FIGURE 36

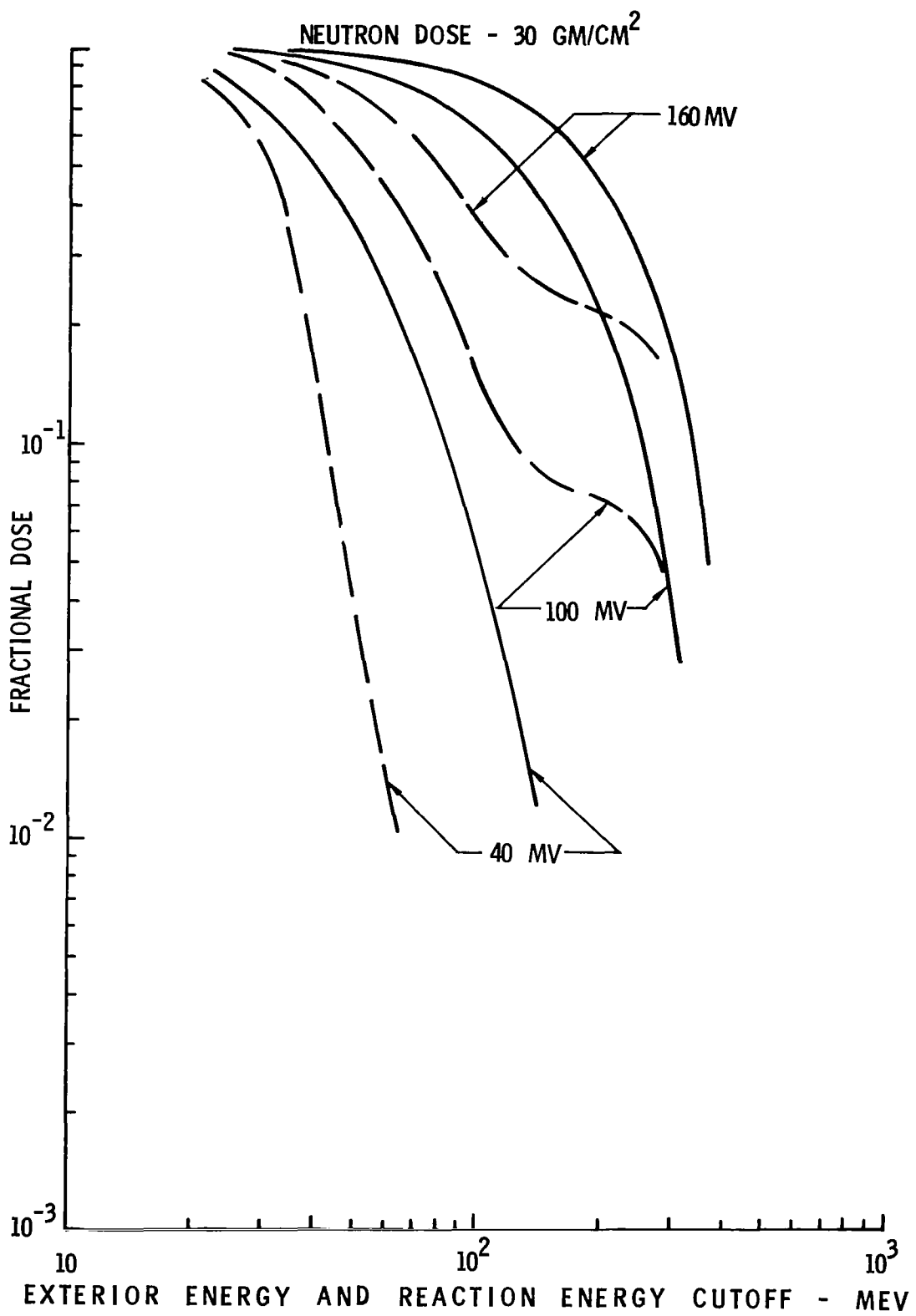


FIGURE 37

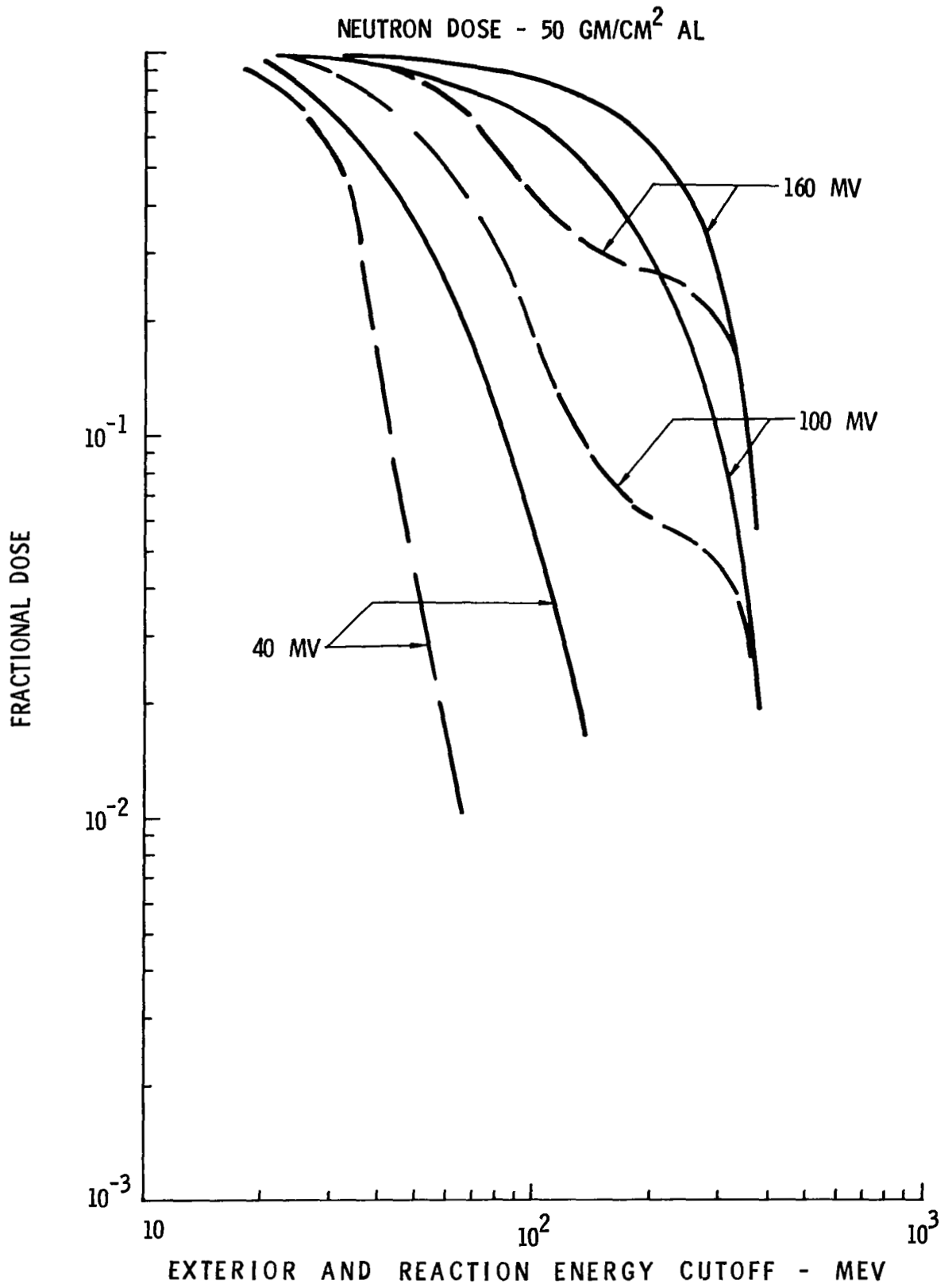


FIGURE 38

DIFFERENTIAL SECONDARY PROTON DOSE PER
UNIT INCIDENT PROTON ENERGY 10 gm/cm² AL

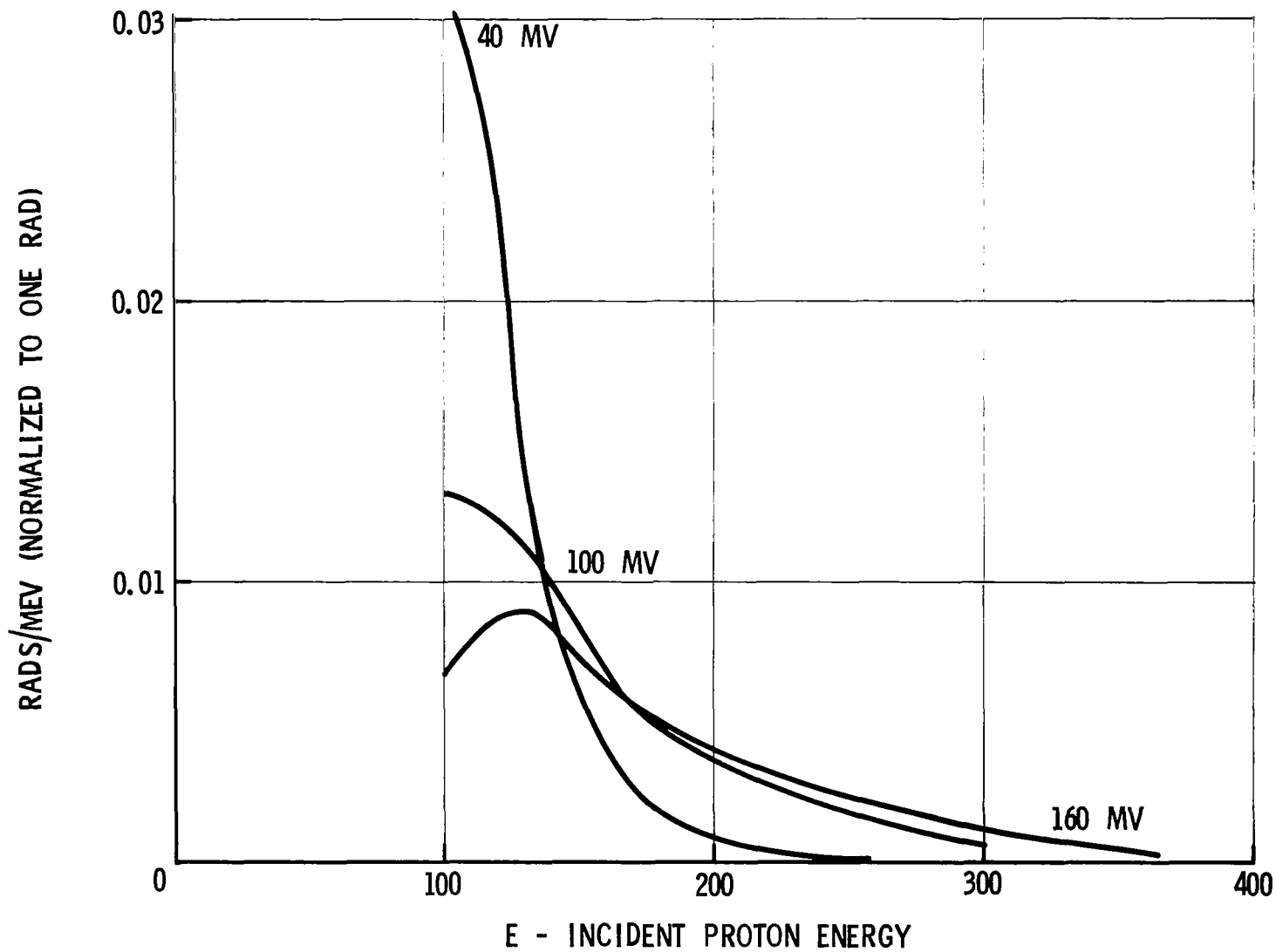


FIGURE 39

DIFFERENTIAL NEUTRON DOSE PER UNIT INCIDENT PROTON ENERGY
40, 100, 160 MV PROTON SPECTRUM INCIDENT

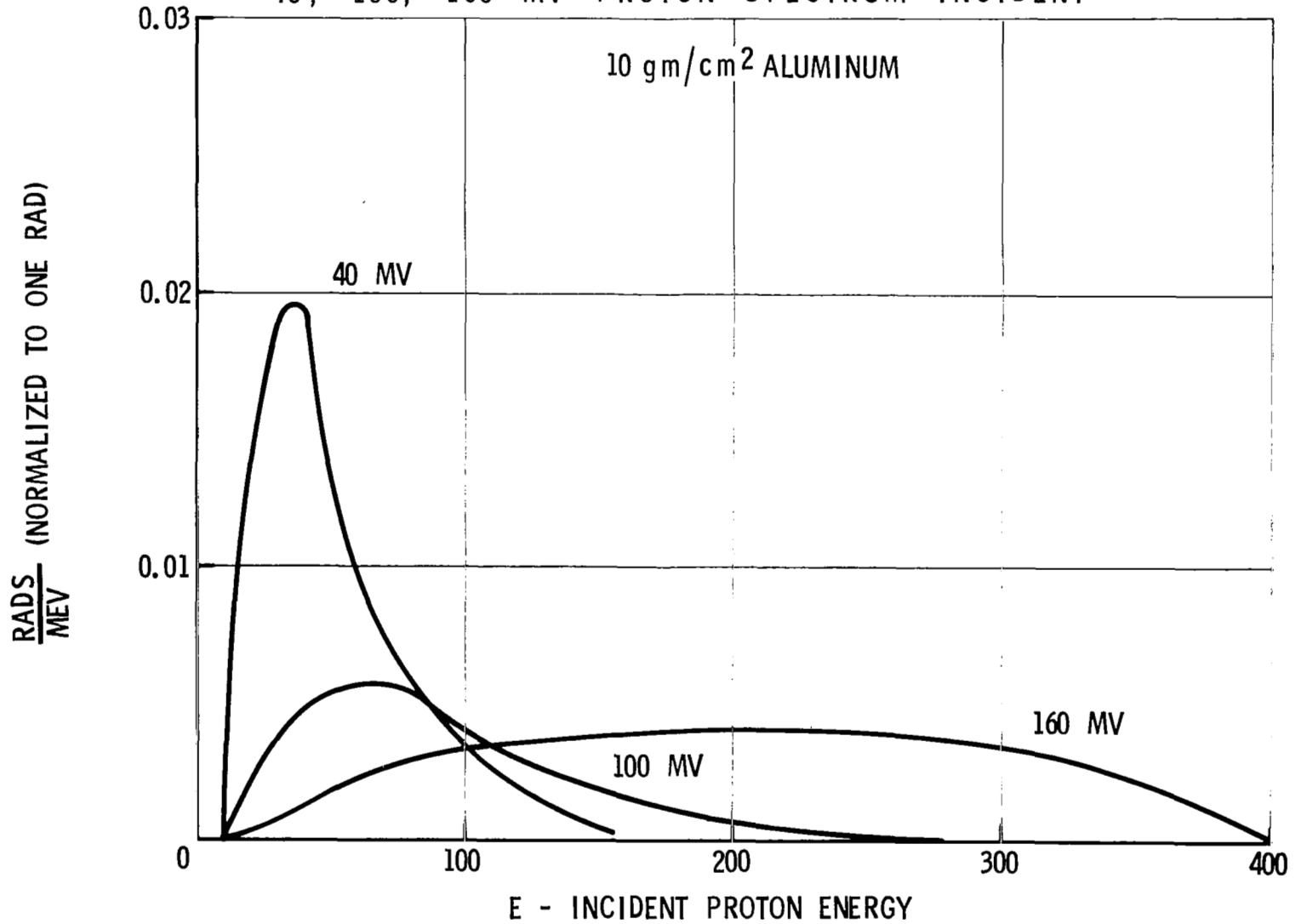
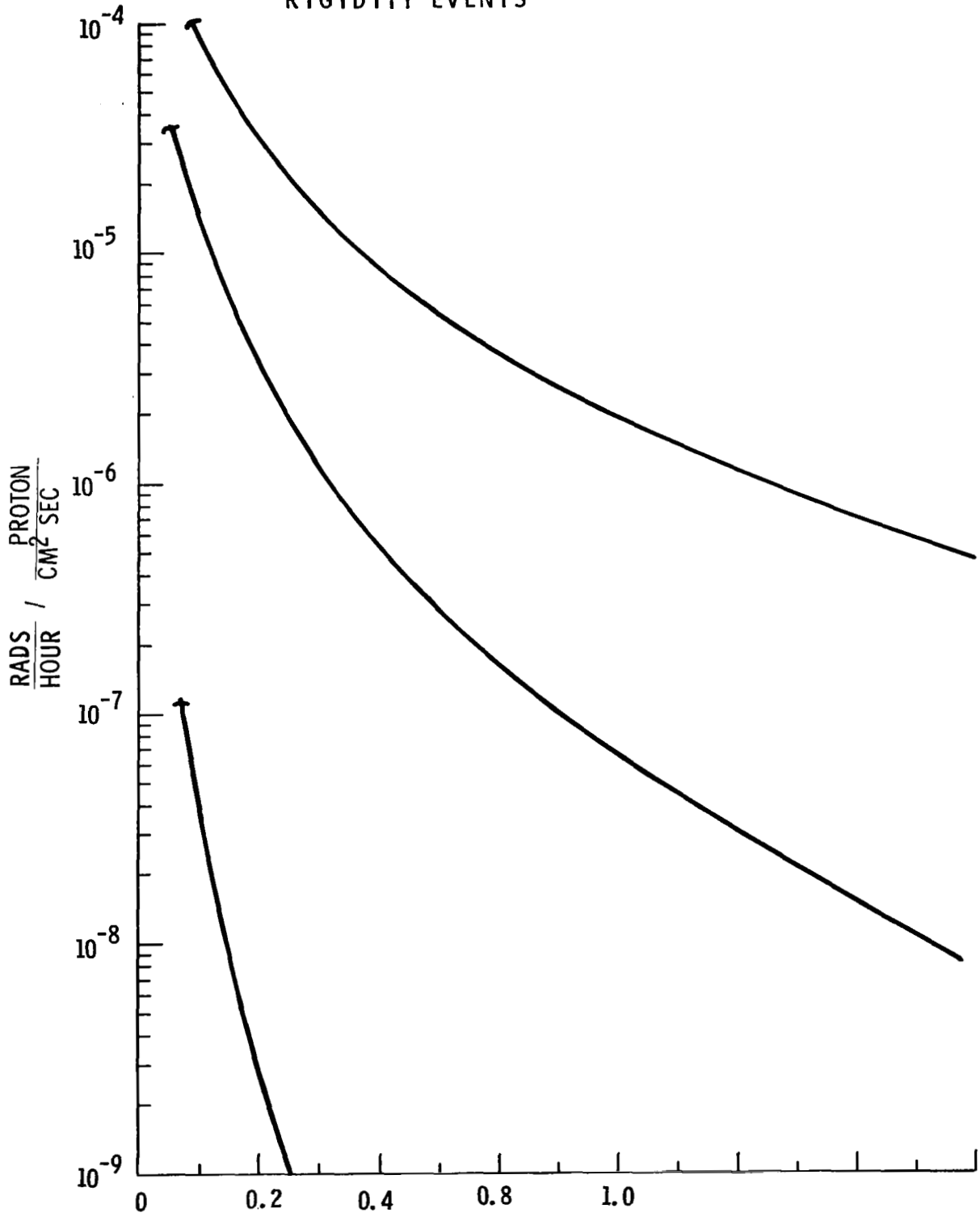


FIGURE 40

DEPTH - DOSE PROFILES FOR 10, 20, AND 30 MV RIGIDITY EVENTS



GM/CM² AL
FIGURE 41

PENETRATING PROTON NUMBER - LET SPECTRUM
20 MV SPECTRUM INCIDENT

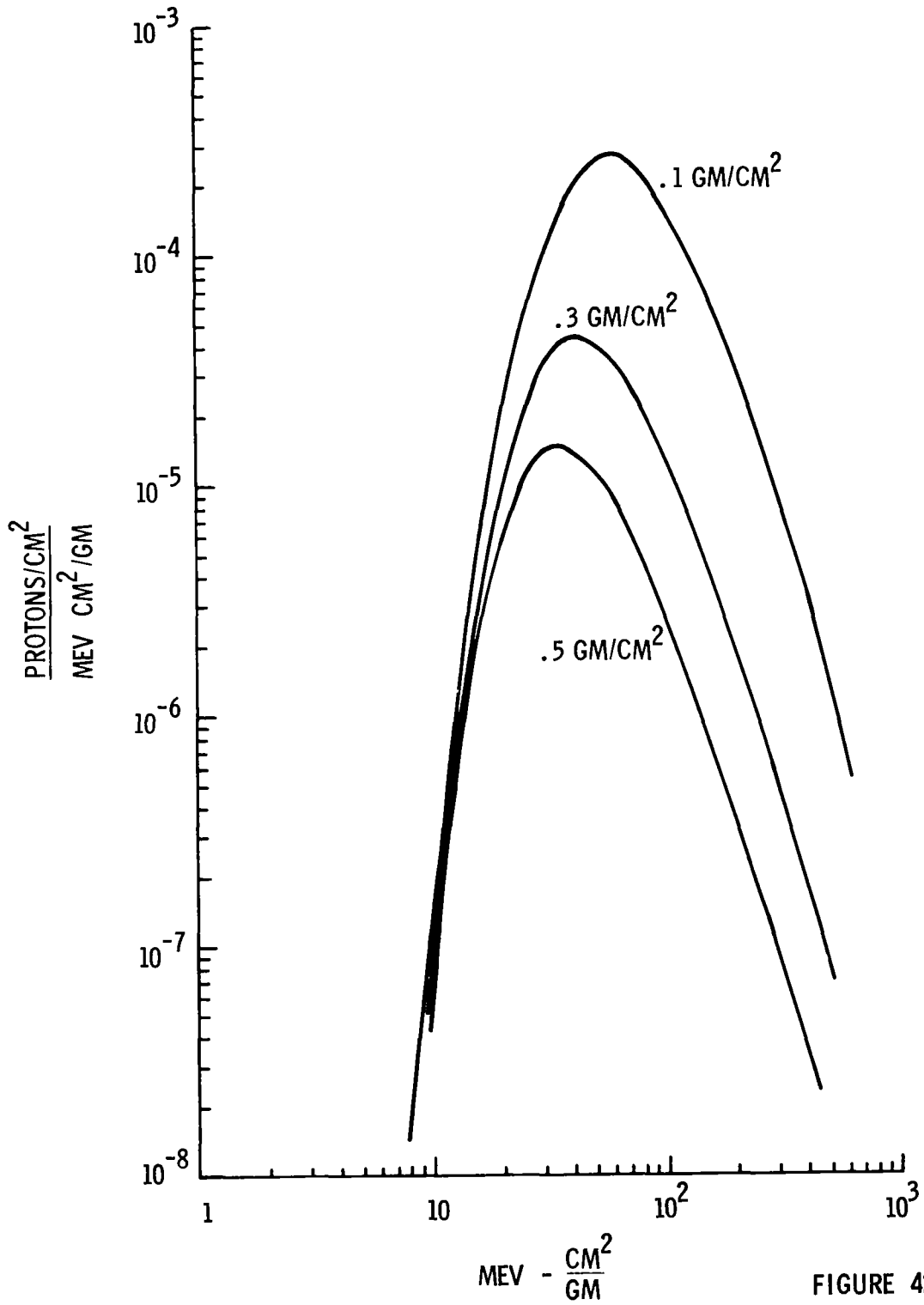
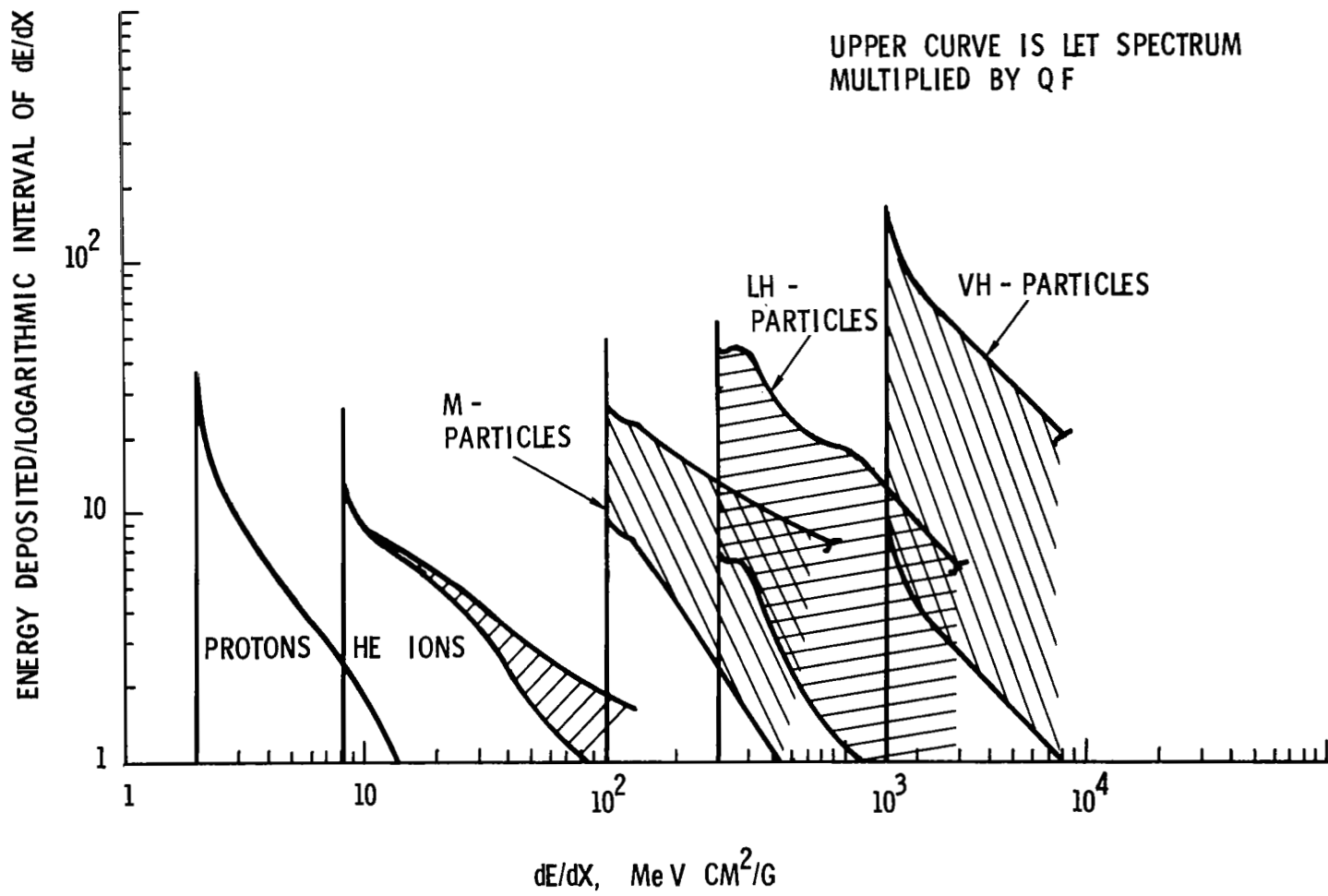


FIGURE 42

LET SPECTRUM FOR GALACTIC COSMIC RAYS UNDER
0.2 G/CM² WATER SHIELDING



77

FIGURE 43

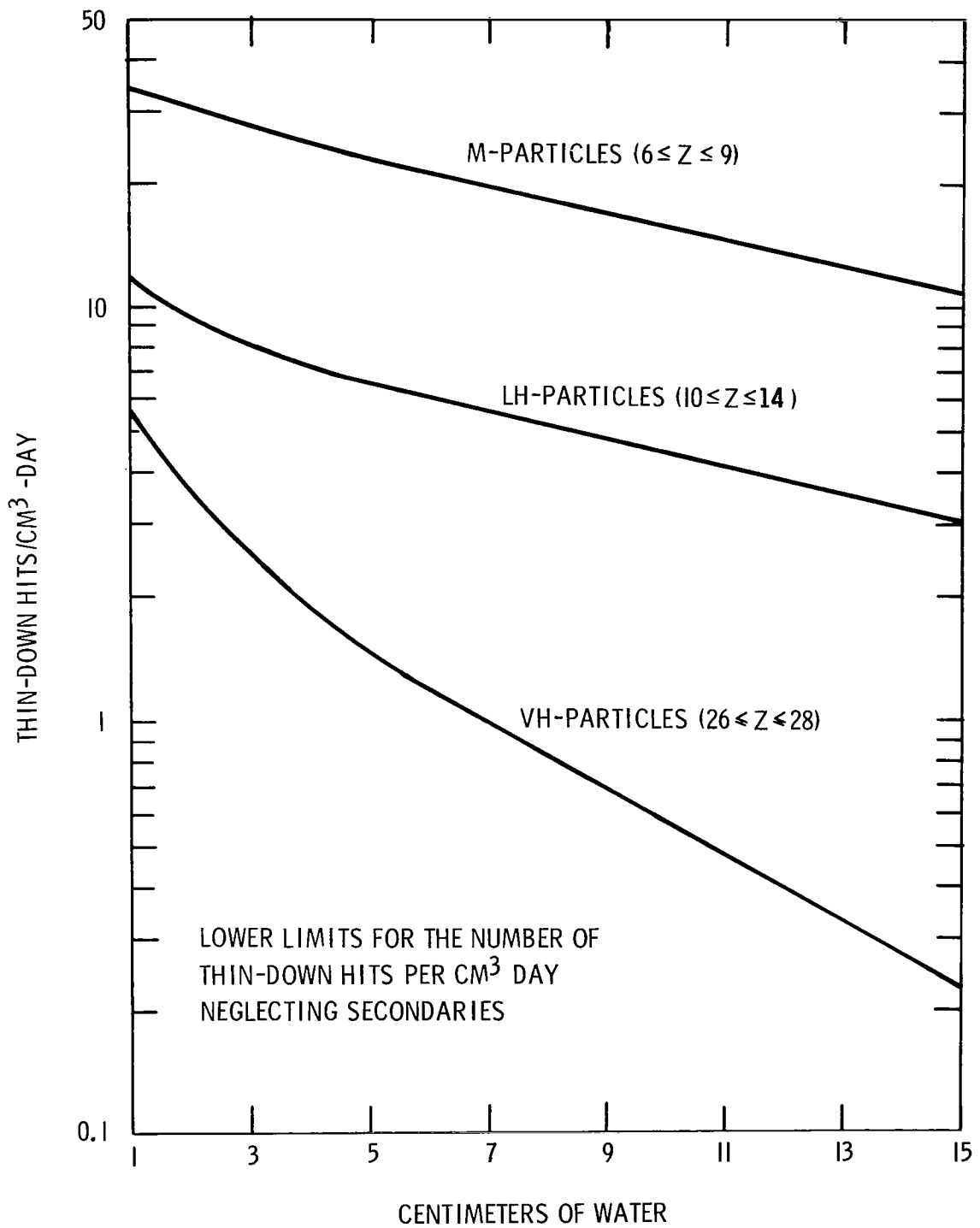


FIGURE 44

SOLAR PARTICLE EVENT LET SPECTRUM FOR PENETRATING PROTONS $P_0 = 20$ MV FOR VARIOUS THICKNESSES OF ALUMINUM

UPPER CURVE FOR EACH THICKNESS IS LET SPECTRUM MULTIPLIED BY QF

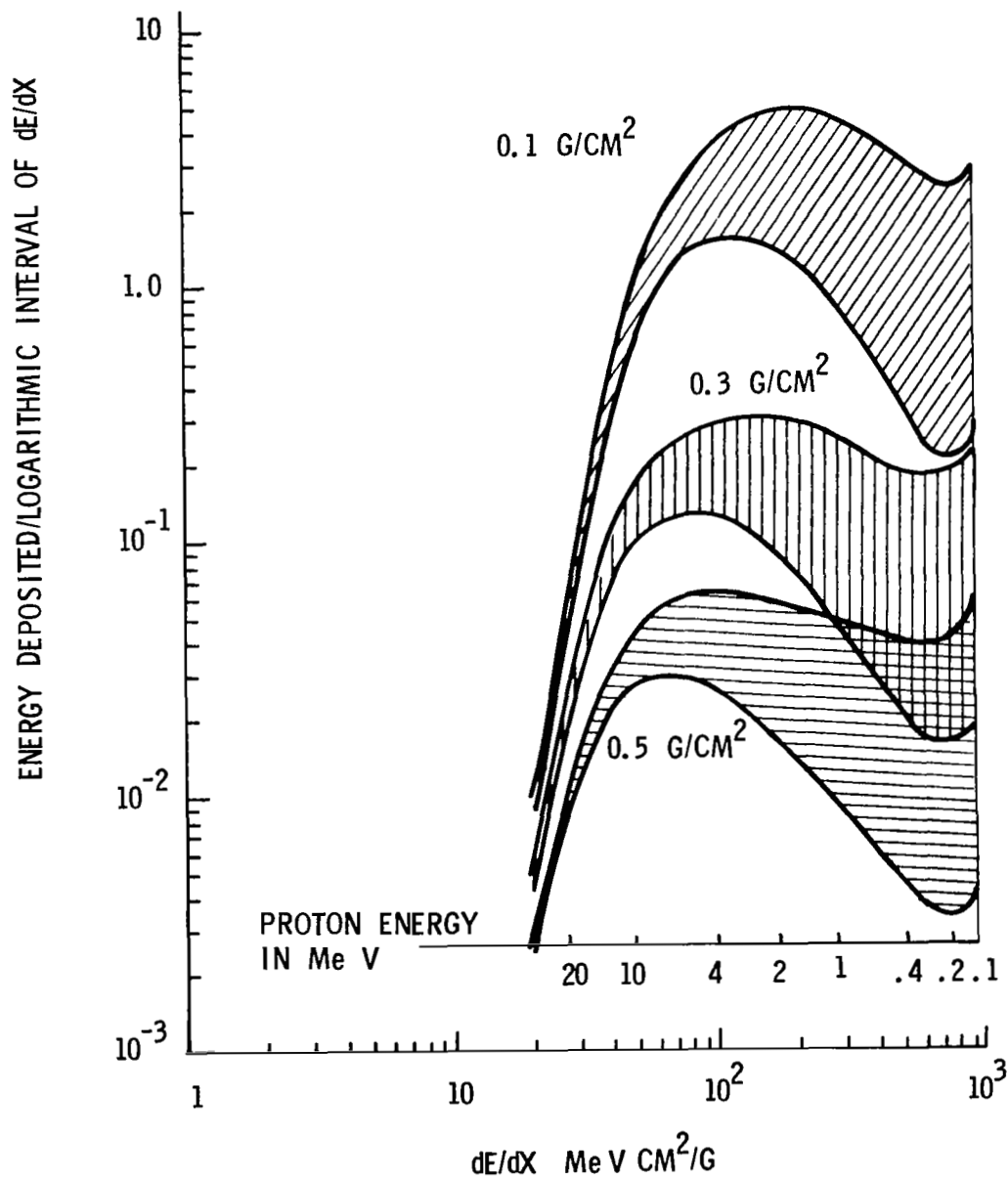


FIGURE 45

SOLAR PARTICLE EVENT LET SPECTRUM FOR
 PENETRATING PROTONS $P_0 = 160$ MV FOR VARIOUS

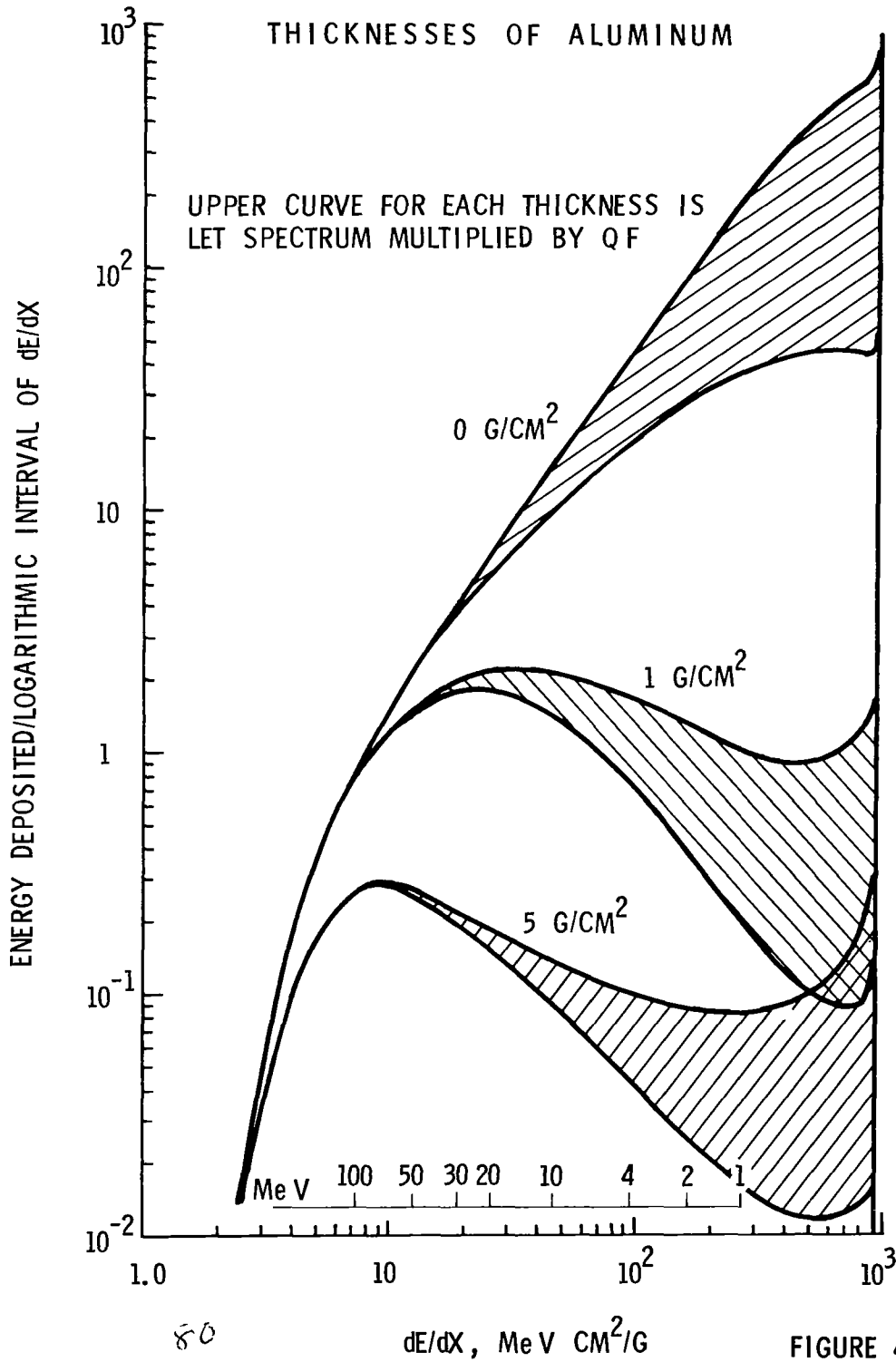


FIGURE 46

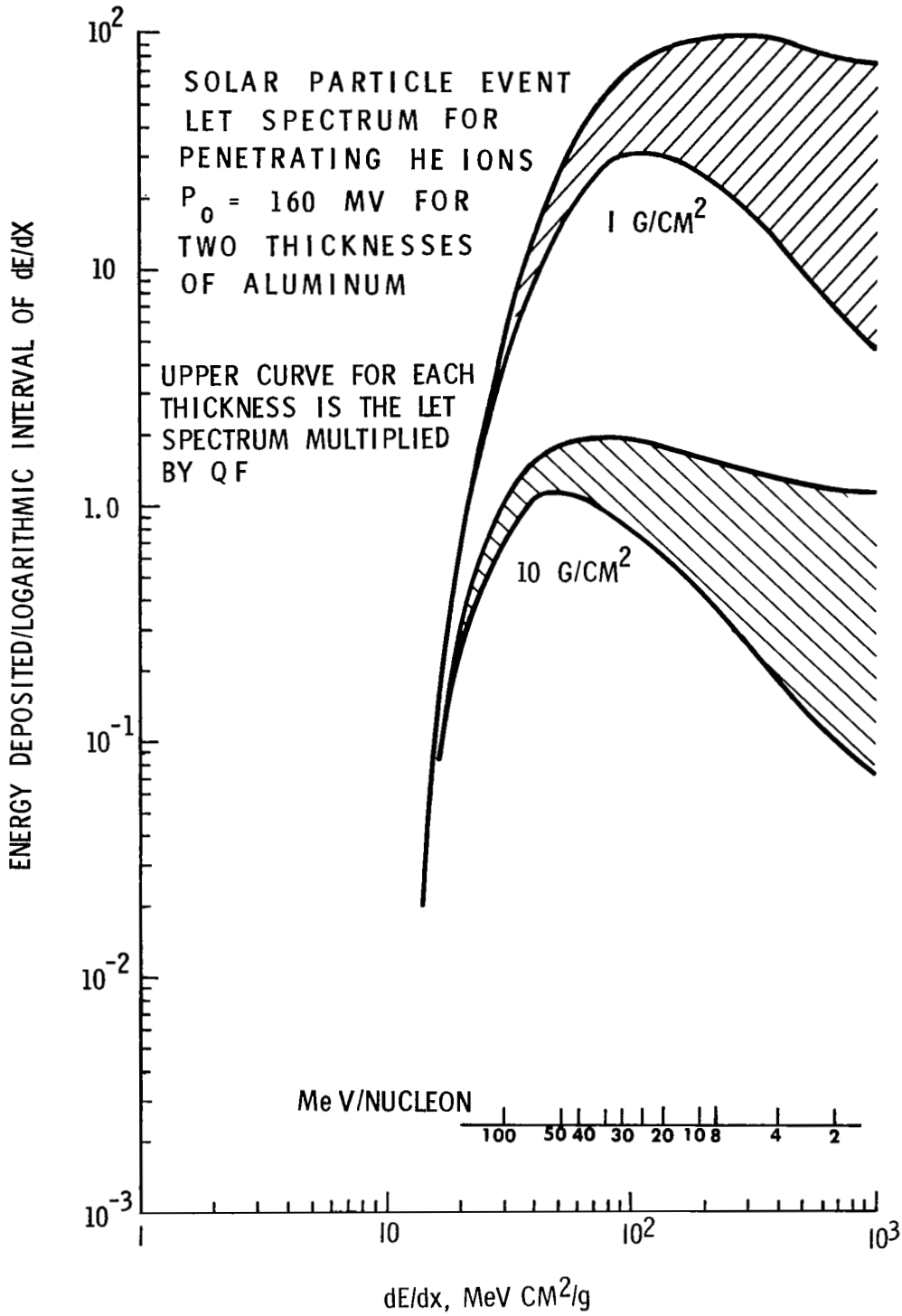


FIGURE 47

SOLAR PARTICLE EVENT LET SPECTRUM FOR PENETRATING He IONS
 $P_0 = 100$ MV FOR TWO THICKNESSES OF ALUMINUM

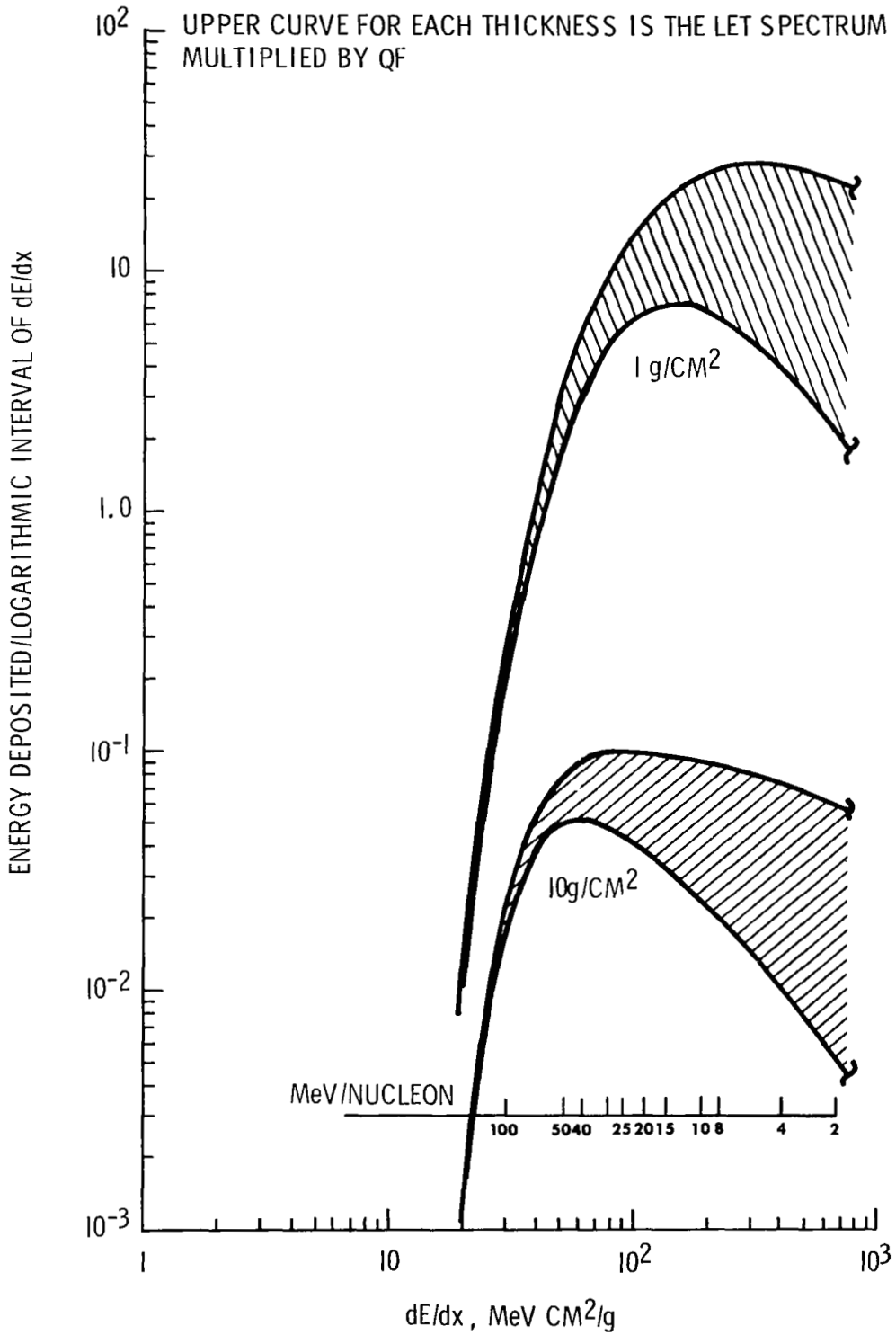


FIGURE 48